VTT PUBLICATIONS 325

The evaluation of integrity and elasticity of thermally sprayed ceramic coatings by ultrasonics

Pentti Kauppinen

VTT Manufacturing Technology

Dissertation for the degree of Doctor of Technology
to be presented with due permission for public examination and debate
in Auditorium V4 at Helsinki University of Technology (Espoo, Finland)
on the 14th of November, 1997, at 12 o'clock noon

TECHNICAL RESEARCH CENTRE OF FINLAND
ESPOO 1997

ISBN 951–38–5078–1 (soft back ed.)
ISSN 1235–0621 (soft back ed.)

ISBN 951–38–5079–X (URL: http://www.inf.vtt.fi/pdf/)
ISSN 1455–0849 (URL: http://www.inf.vtt.fi/pdf/)

JULKAISIJA – UTGIVARE – PUBLISHER

Valtion teknillinen tutkimuskeskus (VTT), Vuorimiehentie 5, PL 2000, 02044 VTT
puh. vaihde (09) 4561, faksi 456 4374

Statens tekniska forskningscentral (VTT), Bergsmansvägen 5, PB 2000, 02044 VTT
tel. växel (09) 4561, fax 456 4374

Technical Research Centre of Finland (VTT), Vuorimiehentie 5, P.O.Box 2000, FIN–02044 VTT, Finland
phone internat. + 358 9 4561, fax + 358 9 456 4374

VTT Valmistustekniikka, Ydinvoimalaitosten materiaalitekniikka, Kemistintie 3, PL 1704, 02044 VTT
puh. vaihde (09) 4561, faksi (09) 456 7002

VTT Tillverkningsteknik, Material och strukturell integritet, Kemistvägen 3, PB 1704, 02044 VTT
tel. växel (09) 4561, fax (09) 456 7002

VTT Manufacturing Technology, Materials and Structural Integrity,
Kemistintie 3, P.O.Box 1704, FIN–02044 VTT, Finland
phone internat. + 358 9 4561, fax + 358 9 456 7002

Technical editing Leena Ukskoski

Oy EDITA Ab, ESPOO 1997

Kauppinen, Pentti. The evaluation of integrity and elasticity of thermally sprayed ceramic coatings by ultrasonics. Espoo 1997, Technical Research Centre of Finland, VTT Publications 325. 130 p.

UDC 666.3:620.179.16:621.383.3
Keywords ceramic coatings, sprayed coatings, ultrasonic tests, elastic properties, piezoelectric transducers, acoustic velocity

Abstract

Thermally sprayed ceramic coatings are widely used in industrial applications where the coated component is subject to, e.g., high thermal loads or mechanical wear. The mechanical properties of the coating are finally created in the coating process and the chemical composition of the powder used as raw material can only give some hints about the properties of the final coating. Several non-destructive testing techniques are available for the detection of defects in ceramic materials or for the evaluation of density and density variations. In addition to this, ultrasonic techniques can be used for quantitative evaluation of elastic properties of materials. This evaluation is based on the measurement of sound velocities of different wave modes in the material and is normally applied only to relatively simple-shaped specimens having parallel surfaces. Acoustic microscopy operating at very high (> 100 MHz) frequencies has been used to measure the sound velocities in homogeneous and thin coatings. With this type of equipment, reliable and accurate results have been achieved in laboratory measurements. A lot of development work has been carried out world-wide to develop the measurement techniques and acoustic lenses (transducers) used in acoustic microscopy. However, less attention has been paid on the development of techniques for industrial applications on-site. The present work was focused on the development of measurement techniques for industrial applications.

A new type of large-aperture low-frequency transducer was designed and constructed for the measurement of sound velocities in thermally sprayed ceramic coatings. The major difference to the lenses used in acoustic microscopy is that in the new transducer no separate lens is needed for focusing the sound beam. The piezoelectric element in the new transducer is a plastic (PVDF) -film that can be shaped to create the required focus. The practical measurement of the sound velocity is based on a modification of the V(z)-technique known from acoustic microscopy. The measurements carried out with

specimens having different types of ceramic coatings and variable coating thickness show that the accuracy of the technique is sufficient for most industrial applications.

For industrial measurements the technique can be simplified and the measurement performed directly on-site. This technique was tested by measuring the sound velocity at different levels of strain in connection with an instrumented tensile testing of coated specimen.

The detection of cracking caused by bending loads was experimentally tested. The cracks could be reliably detected both by using a transmitter-receiver probe arrangement and by pulse-echo technique where only one transducer is used. This technique can also be applied in industrial conditions where access to the component to be measured is limited.

Preface

This work has been carried out in the Technical Research Centre of Finland (VTT) in connection with several national research projects where the use of ceramic materials for various industrial applications has been studied.

The financial support of the Jenny and Antti Wihuri Foundation, as well as the Technical Research Centre of Finland is gratefully acknowledged.

The work was supervised by Professor Antti Korhonen, to whom I would like to express my sincere gratitude for advice and encouragement.

One of the cornerstones of this work has been the development of a new type of ultrasonic transducer. The innovative work of Mr. Harri Jeskanen and Mr. Ensio Hosia in the design and construction of the new probe is gratefully acknowledged. To Mr. Harri Jeskanen I also express my gratitude for the excellent co-operation during the whole experimental part of this work.

I am deeply indebted to my friend Mr. Pertti Auerkari for valuable discussions and ideas in planning the experimental program of this work.

Among the staff of VTT Manufacturing Technology I want to thank especially Mrs. Seija Änkö for the continuous encouragement, Mr. Tuomo Hokkanen for preparing the figures and Ms. Åsa Åvall for typing the final manuscript.

I want to thank Professor Sakari Heiskanen, the former research director of VTT Manufacturing Technology, for the encouraging words that were the starting point for this work for almost 10 years ago.

Finally, I want to thank my parents for the continuous support and encouragement through all the years spent in this work. I thank my wife Sirkka and my children Eveliina and Aki for their patience during the course of this work.

Espoo, September 1997

Pentti Kauppinen

Contents

List of symbols

a, c	Coefficients
B	Bulk modulus
B_1 , B_2	First, second back-wall echo
b	Empirical constant
D_C	Average diameter of cracks
D_L	Diameter of the acoustic lens
D_R	Diameter of the entry circle of ultrasonic pulse
d	Volume concentration
E	Young's modulus
E_L	Young's modulus in through thickness direction
E_S	Young's modulus of the substrate material
E_T	Young's modulus in direction parallel to the surface
E_{loss}	Energy loss
E_0	Young's modulus of fully dense material
$E_c(\varepsilon)$	Young's modulus of the coating material
f	Frequency
F	Focal distance
G	Shear modulus
I	Incident amplitude
k	Wave number
k^{in}	Incident wave vector

k^{re}	Reflected wave-field
L	Longitudinal modulus
M	Volume fraction
N	Microcrack density
P	Porosity fraction
P_M	Porosity determined from dimensional measurement and weight
P_c	Porosity calculated from ultrasonic measurements
R	Reflected amplitude
$R(\theta)$	Reflection coefficient
R_L	Radius of the pupil function of the lens
S_1, S_2, S_3	Sound paths
s	Sample thickness
s_s	Thickness of the substrate
T	Round trip time delay between echoes
t	Travel time of an ultrasonic pulse
u	Displacement
V	Velocity of ultrasonic wave
V_F	Velocity in fluid
V_I	Velocity of interface waves
V_L	Velocity of longitudinal waves
V_{L0}	Sound velocity in non-cracked material
V_R	Velocity of Rayleigh waves

V_r	Velocity of reflected wave
V_S	Velocity of shear waves
V_{SAW}	Velocity of surface acoustic wave
V_{SO}	Velocity in solid
V_{ST}	Velocity of Stoneley wave
V_T	Velocity of refracted wave
V_{TA}	Axial transverse wave velocity
V_0	Velocity in fully dense material
Z	Acoustic impedance
z	Defocus distance
β_{ST}	Propagation angle of Stoneley waves
Δt	Time difference
ε	Strain
θ_c	Critical angle
θ_{c1}	First critical angle
θ_{c2}	Second critical angle
θ_{cr}	Angle of crack
θ_i	Incident angle of waves
θ_L	Lens angle
θ_p	Angle of leaky Rayleigh wave
θ_R	Rayleigh angle
θ_r	Angle of reflected waves

θ_{RL}	Angle of reflected longitudinal wave
θ_{RS}	Angle of reflected shear wave
θ_{T}	Angle of refracted wave
θ_{TL}	Angle of refracted longitudinal wave
θ_{TS}	Angle of refracted shear wave
Λ	Lame's constant
λ	Wave length
λ_{F}	Wave length in liquid
λ_{R}	Rayleigh wavelength
ν	Poisson's ratio
ρ	Density
ρ_{F}	Density of liquid
ρ_{S}	Density of solid
τ	Fundamental radio frequency of a transducer
φ	Shape factor
ω	Angular frequency of the acoustic wave

1. Introduction

Thermal spraying, because of its effectiveness and versatility, is a widely used surfacing process. Its attractiveness has led to numerous applications in which the quality of the sprayed coating has become critical to the functioning of the coated component. In such cases there is an urgent need for an effective non-destructive evaluation (NDE) technique to provide assurance of coating quality and integrity. Separate procedures are available to visually detect and measure voids, oxides, non-melted spray particles, and contamination/delamination along the coating/base material interface in thermally sprayed coatings. The procedures are based on image processing and analysis functions. Careful specimen preparation is necessary to minimize specimen variability for reproducible results.

Thermal NDE techniques have been successfully used to detect nonbonded (delaminated) areas of coatings and discontinuities below the surface. Other NDE methods, like acoustic emission, radiography and penetrant testing have also been used in some applications. Ultrasonic techniques have been widely applied to the inspection of bulk ceramics and have showed promise for the evaluation of sprayed coatings. These techniques have the unique potential of not only revealing the structural discontinuities of the coating but also giving quantitative data on the elasticity and porosity of the coating.

In this work, the applicability of ultrasonic testing techniques to the evaluation of elastic properties, porosity and adhesion of thermally sprayed ceramic coatings has been studied.

1.1 Elastic properties of materials

1.1.1 Young's modulus (E) and Poisson's ratio (ν)

The elastic properties govern the behaviour of a material subjected to stress over a region of strain where the material behaves elastically. The proportionality constant relating stress and strain in the region of elastic behaviour is the elastic constant, or more precisely, elastic modulus. Among the most elementary notions in considering the strength of a material is Young's modulus which

relates a unidirectional stress to the resultant strain. In an experimental stress-strain curve this modulus is the slope of the elastic portion of the curve. When a sample is elongated in the direction of the axially applied stress it also simultaneously narrows. This behaviour is described by another elastic modulus, Poisson's ratio, which is defined as the ratio of change in the lateral direction to the change in length.

Many technological problems are often adequately handled with a knowledge of Young's modulus and Poisson's ratio alone. These are only useful, however, if the material is both homogeneous and isotropic as most engineering materials are (Schreiber et al. 1973). This is not the case of ceramic coatings.

1.1.2 The Bulk modulus (B) and the Shear modulus (G)

Young's modulus and Poisson's ratio are not the simplest concepts even for isotropic materials. For isotropic materials, two fundamental properties arise as a result of subjecting the material to two different states of stress. These are the bulk modulus (B), where the strains perpendicular to the stress directions are all equal, and shear modulus (G), where the strains perpendicular to the directions of stress are everywhere zero.

1.2 Ultrasonic measurement of elastic constants

Although B and G are fundamental elastic constants which arise from very basic considerations, they do not always coincide with those elastic constants which are simplest to measure. When elastic properties are determined from the measurement of acoustic wave propagation through a material, other modulus are involved. For isotropic bodies, geometric considerations appropriate to the direction of wave propagation result in a reduction to two simple equations. The first equation is given by the condition that the displacements perpendicular to the wave-front direction are zero, and this yields the longitudinal wave equation. The second equation is given by the condition that the displacement along the direction of the wave-front is zero, which yields the shear wave equation for the isotropic case (Schreiber et al. 1973). In one dimension these reduce to

$$\frac{d^2u}{dt^2} = L\frac{d^2u}{\rho dx^2} \tag{1}$$

and

$$\frac{d^2u}{dt^2} = G\frac{d^2u}{\rho dx^2}\,, \tag{2}$$

where ρ = density and u = displacement.

These two kinds of waves are easy to generate and therefore, from the experimental view, the constants L and G are of considerable importance. The constant of the shear wave is precisely the same G (shear modulus) discussed before. The longitudinal modulus L, determined from the velocity of a propagating longitudinal wave, is neither the bulk modulus B nor Young's modulus E, although it is often confused with these two constants. The former relates a volumetric strain to a hydrostatic stress, and Young's modulus a strain to a flexural stress, whereas the longitudinal modulus relates the strain to a longitudinally applied stress. The longitudinal modulus is most often expressed as

$$L = \Lambda + 2G = \rho V_L^{\ 2}\,, \tag{3}$$

where Λ = Lamé constant
G = shear modulus
V_L = longitudinal velocity.
In all, six elastic moduli, B, E, Λ, ν, L, and G, are defined.

Any two of these are sufficiently complete to describe elastic behaviour, and any elastic modulus may be expressed in terms of any other pair (Schreiber et al. 1973). Most of the polycrystalline materials exhibit an isotropic behaviour and therefore the measurement of two velocities, one longitudinal (V_L) and one shear (V_S), define the elastic behaviour of the material. Based on the measurement of propagation velocities, the different modulus can be determined from Formulae (4)–(9):

$$B = \rho\left(V_L^{\,2} - 0.75V_S^{\,2}\right) \tag{4}$$

$$E = \frac{3\left(V_S^{\,2}V_L^{\,2} - 0.75V_S^{\,2}\right)}{(V_L^{\,2} - V_S^{\,2})} \tag{5}$$

$$\Lambda = \rho(V_L^{\,2} - 2V_S^{\,2}) \tag{6}$$

$$\nu = \frac{(V_L^{\,2} - 2V_S^{\,2})}{2(V_L^{\,2} - V_S^{\,2})} \tag{7}$$

$$L = \rho V_L^{\,2} \tag{8}$$

$$G = \rho V_S^{\,2}\,. \tag{9}$$

Poisson's ratio and Young's modulus can also be calculated from Formulae (10) and (11) (Krautkrämer & Krautkrämer 1983)

$$\nu = \frac{0.5 - \left(\frac{V_S}{V_L}\right)^2}{1 - \left(\frac{V_S}{V_L}\right)^2} \tag{10}$$

$$E = 4\rho V_s^{\,2}\,\frac{0.75 - \left(\frac{V_S}{V_L}\right)^2}{1 - \left(\frac{V_S}{V_L}\right)^2}\,. \tag{11}$$

Bergmann (1954) has presented an approximation Formula (12) for surface (Rayleigh) waves:

$$V_R = \frac{0.87 + 1.12\nu}{1 + \nu}\sqrt{\frac{E}{2\rho(1+\nu)}}\,. \tag{12}$$

This approximation formula is based on following relation (13) of velocities V_R and V_S.

$$\frac{V_R}{V_S} = \frac{0.87 + 1.12\nu}{1 + \nu} \ . \tag{13}$$

The velocity of a Rayleigh wave is typically 0.93 of the shear wave velocity, the exact proportion depending on Poisson's ratio for the material (Briggs 1985). As Poisson's ratio varies from 0 to 0.5, the Rayleigh wave velocity varies monotically from 0.87 V_S to 0.96 V_S (Viktorov 1967).

1.3 Behaviour of ultrasonic waves at material interfaces

1.3.1 Longitudinal and shear waves

When an incident longitudinal sound beam hits the surface of a solid material immersed in water at the angle θ_i (Fig. 1), the behaviour of the incident beam is described by the Snell's law (14)

$$\frac{\sin\theta_i}{V_{L_1}} = \frac{\sin\theta_{RL}}{V_{L_1}} = \frac{\sin\theta_{RS}}{V_{S_1}} \ , \tag{14}$$

where θ_i and θ_{RL} are the angles of the incident and reflected longitudinal waves and θ_{RS} the reflection angle of the shear wave. The propagation velocities of the longitudinal and shear waves in material 1 are V_{L1} and V_{S1}. For the angle of reflection θ_{RL} and θ_{RS} the Equations (15) and (16) are valid:

$$\theta_i = \theta_{RL} \tag{15}$$

$$\frac{\sin\theta_i}{V_{L_1}} = \frac{\sin\theta_{RS}}{V_{S_1}} \tag{16}$$

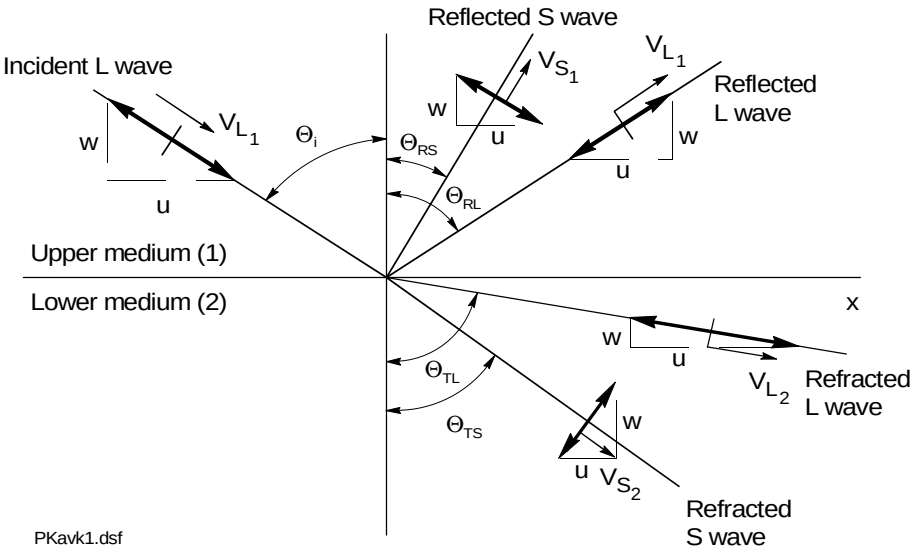

Figure 1. Reflection and refraction of a plane wave on the plane interface between two materials 1 and 2 at oblique incidence (Nickerson 1973).

As presented in Fig. 1, two reflected and refracted waves are formed from the incident longitudinal wave at the interface between materials 1 and 2. When the sample (material 1) is immersed in a liquid (material 2) the reflected shear wave will not be formed. By increasing the incident angle θ_i from 0, the first critical angle θ_{c1} will be reached. At this critical angle, the angle θ_{TL} of refracted longitudinal waves equals to 90° and the longitudinal waves will be completely reflected from the surface. In this case only shear waves will be propagating in material 2. When the incident angle is increased further, the second critical angle θ_{c2} will be reached. At this angle the shear wave will be totally reflected from the surface (θ_{TS} = 90°). The critical angles can be calculated from Equation (14) by setting $\sin\theta_{RL}$ or $\sin\theta_{RS}$ equal to 1 (Bergman 1954).

1.3.2 Rayleigh waves

When the incident angle θ_i is still increased further from the second critical angle, the reflected beam will be displaced 'downstream'. This displacement occurs only at the Rayleigh angle, θ_R, given by

$$\sin\theta_R = \frac{V_{L_1}}{V_R}, \tag{17}$$

where θ_R is the angle of incidence in the fluid, V_{L1} is the sound velocity in the fluid, and V_R is the Rayleigh velocity of the solid. Equation (17) is an extension of Snell's law, as usually applied to reflection and refraction phenomena at flat boundaries. In this case the 'refracted' wave travels with velocity V_R and the angle of refraction is 90°. Under these conditions the refracted wave is a Rayleigh wave whose velocity depends on the values of V_{L1}, the longitudinal wave velocity, and V_{S2}, the shear wave velocity of the solid. The value of V_R, which is always less than the shear wave velocity, must be greater than V_{L1} for θ_R in Equation (17) to be real and thus for the beam displacement to occur. Under these conditions a mode conversion from the incident longitudinal wave to a Rayleigh wave on the solid takes place (Plona et al. 1975).

It would thus appear possible to determine the Rayleigh wave velocity on a solid by observing at what angle of incidence, θ_R in Equation (17), the beam displacement occurs. The explanation of the beam displacement upon reflection at Rayleigh angle incidence implies that V_R in Equation (17) is the velocity of the Rayleigh wave on a free surface. However, the observation of a beam displacement along the interface requires that the surface of the solid not be free but loaded by a suitable liquid. The presence of the liquid changes the value of θ_R for a free surface as presented by Rayleigh (1885).

For a free solid surface, the Rayleigh equation can be written in the form (Plona et al. 1975)

$$4LS - \left(1 + S^2\right)^2 = 0, \tag{18}$$

where the quantities L and S are defined as (19), (20)

$$L = \sqrt{1 - \left(\frac{V}{V_L}\right)^2} \tag{19}$$

$$S = \sqrt{1 - \left(\frac{V}{V_S}\right)^2} \quad . \tag{20}$$

The desired value of the surface wave velocity, V_R, is the solution of Equation (18) for the quantity V. When the surface of the solid is bounded by a liquid, Equation (18) is no longer applicable. An additional term needs to be added, and the basic equation for this case can be written as

$$4LS - \left(1 + S^2\right)^2 = iX \,, \tag{21}$$

where

$$X = \frac{L\left(\frac{\rho_F V^4}{\rho_S V_S{}^4}\right)}{\sqrt{\left(\frac{V}{V_F}\right)^2 - 1}} \tag{22}$$

and ρ_F and ρ_S refer to the density of the liquid and the solid, respectively.

There are two physically meaningful solutions for V, the velocity of the surface disturbance. If both sides of Equation (21) are to be real, the square root in Equation (22) must be purely imaginary, making the entire right-hand side real. This will occur when the quantity V/V_F is less than unity. This particular solution for V represents the Stoneley wave solution. The other solution of Equation (21) is obtained when $V > V_F$, making the right-hand side of Equation (21) imaginary. This new solution differs from the Rayleigh wave solution of Equation (18) where the right-hand side equals zero and where V is real, equal to V_R and the phase velocity of the disturbance. The magnitude of the imaginary part of the velocity V depends on the ratio ρ_F/ρ_S in Equation (22). The imaginary part of V becomes very small when one considers liquid-metal boundaries where the density ratio is typically between 0.1 and 0.2. Consequently, the phase velocity differs from the true Rayleigh wave velocity by less than 1% for high-density solids. However, for low density solids, the difference becomes noticeable. Thus the Rayleigh wave velocity, as calculated

for free solids, is a very good approximation of the surface wave phase velocity on liquid-solid interfaces provided the solid has a density appreciably greater than the liquid density. When the two densities are equal, the free-surface Rayleigh wave velocity is less than the velocity of the actual surface wave (Plona et al. 1975). This modified Rayleigh wave is often called a leaky Rayleigh wave because it closely resembles a Rayleigh surface wave in the solid, but radiates energy into the liquid at the Rayleigh angle as it propagates along the interface (Bertoni & Tamir 1973). Owing to the presence of the propagating field in the liquid region, energy is continuously leaking away from the solid region as indicated by the flux oriented at the angle θ_P in Fig. 2.

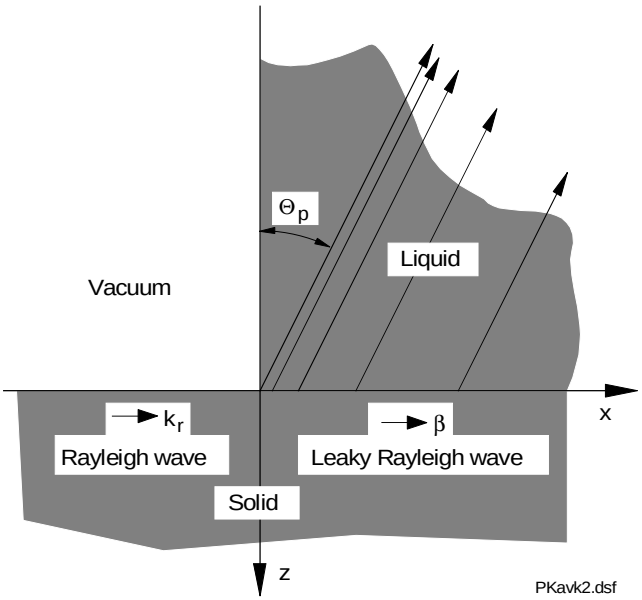

Figure 2. Excitation of a leaky Rayleigh wave along a liquid-solid interface by means of a Rayleigh wave incident from a vacuum-solid region (Bertoni & Tamir 1973).

Because of this energy leakage, the field along the liquid-solid interface must decrease with x so that the flux density diminishes along x and the wave attenuates. For most liquid-solid interfaces, the attenuation factor is a small quantity and the difference between the angles θ_P and θ_R (Rayleigh angle) is of the order of 0.1° or smaller (Bertoni & Tamir 1973). The major part of the attenuation arises from the radiation of an energy flux into the liquid.

Additionally, the attenuation is caused by the scattering of the wave from the microstructure or the roughness of the surface (Jagnoux & Vincent 1989).

In some cases it may be useful to use other low-density liquids than water as a coupling medium. Liquids in which the sound velocity is very low are, e.g., methyl alcohol (V_L = 1088 m/s (Kushibiki & Chubachi 1985) and iso-pentane (V_L = 1016 m/s) (Sinclair et al. 1984).

There are several methods for the determination of the velocity of Rayleigh waves. One of the oldest techniques is to use a Rayleigh wave interferometer. With this equipment the velocity of propagation of Rayleigh waves in a specific direction has been determined with an accuracy of 0.1 percent by Firestone & Frederick (1946). Other methods for determining the Rayleigh wave velocity have been presented by Kulik et al. (1989), Nomura et al. (1989), Yamanaka (1983), Liang et al. (1982) and Gilmore et al. (1989).

1.3.3 Lamb waves

A layered solid structure immersed in a liquid supports acoustic leaky interface waves in addition to the acoustic bulk waves. The leaky waves can be in the form of Rayleigh waves or layer waves such as general Lamb waves. The layer must be of a softer material than the substrate to be able to support the Lamb wave modes. In particular, the shear wave velocity of the layer must be less than that of the substrate. If this condition is not satisfied, only leaky Rayleigh waves are excited (Atalar et al. 1991).

When the thickness of the plate immersed in the liquid is small compared with all wavelength components of the ultrasonic pulse, disturbances on one surface do not decay in amplitude sufficiently rapidly to leave the opposite side undisturbed, and so surface waves such as the thick plate Rayleigh wave no longer exist. Instead, the separate surface and bulk waves are replaced by Lamb modes which affect both surfaces simultaneously, like standing waves, yet also travel along the length of the plate in the manner of surface waves. An approximate frequency f below which, for a given plate thickness s, Rayleigh waves cannot propagate has been proposed (Bushell et al. 1991).

$$f = \frac{8V_S}{s\pi} \ . \tag{23}$$

In the case of a thick layer on a base material modifying Rayleigh waves, so called Stoneley waves may exist. The velocity of these waves depends on the properties of both media. The existence of waves propagating along the interface of two solids is always theoretically possible, irrespectively of the material combination. But the non-attenuated, guided interface waves (Stoneley waves) exist only in cases satisfying the condition:

$$\max\left(V_{R_1}, V_{R_2}\right) \le V_{ST} \le \min\left(V_{S_1}, V_{S_2}\right), \tag{24}$$

where V_{ST} is the velocity of the Stoneley wave, V_{R1}, V_{S1} and V_{R2}, V_{S2} are the velocities of Rayleigh waves and shear waves in materials 1 and 2, respectively.

Attenuated waves propagate in the remaining material combinations. These waves are called interface waves. The attenuation is caused by the leaking to one of the media of elastic waves of a propagation velocity equal to the velocity of transverse waves in this medium. The propagation direction of these waves, together with the propagation direction of interface waves, forms an angle equal to

$$\beta_{ST} = \arccos\left(\frac{V_S}{V_I}\right), \tag{25}$$

where V_I is the interface velocity and V_S the shear wave velocity in the medium to which part of the energy of the interface wave is transferred (Pilarski 1986).

1.4 Measurement of ultrasonic velocities

1.4.1 Pulse-echo techniques

Measurement of ultrasonic wave propagation velocities are routinely used to determine elastic constants (Schreiber et al. 1973). A number of methods for measuring ultrasonic velocity have been described. Among these the methods

using broadband pulse-echo wave-forms are most frequently used. The basic problem with these methods is to determine the time delay between two successive echoes, each of which consists of only a few oscillations. In many instances it is fairly easy to find in the pulse-echo wave-forms some feature that can be used as a basis for measuring the time between the echoes. The pulse-echo overlap method is commonly used to make this type of measurement. The echoes must have similar wave-forms so that corresponding features can be readily identified and brought into coincidence (i.e. overlapped) either by analogic or digital manipulations. Because this condition is not always met and the pulse-echo signals are weak or distorted by attenuation and other factors, alternative methods like the phase-slope, cross-correlation, first-arrival-time and pulse-superposition methods are used (Hull et al. 1985, Papadakis 1972). From the different methods only the echo overlap, pulse-superposition and first-arrival-time methods are described here.

Echo overlap method

A typical transducer configuration for normal-incidence, contact, pulse-echo ultrasonic technique is presented in Figure 3. The broadband longitudinal ultrasonic wave produced by the transducer propagates through the quartz buffer to the front surface, where a portion of the wave's energy is transmitted into the specimen and a portion is reflected back to the piezoelectric crystal. The portion of the ultrasonic wave reflected from the front surface is the first echo, FS (Figure 3b). The wave transmitted into the specimen is reflected by the surface to the front surface where a portion is reflected back into the specimen and a portion is transmitted through the quartz buffer to the piezoelectric crystal. This wave is shown as echo B1 in Figure 3b. Finally, a third ultrasonic wave, echo B2, occurring from a second back-surface reflection is received at the piezoelectric crystal, as shown in Figure 3b. Time T in Figure 3b is required for ultrasonic pulses to travel twice the thickness s of the sample.

The initial step in the procedure for signal analysis requires digitization of echoes B1 and B2. Both echoes can be displayed simultaneously on one CRT trace or the echoes can be individually "windowed" in two separate time gates as presented in Figure 4 (Hull et al. 1985).

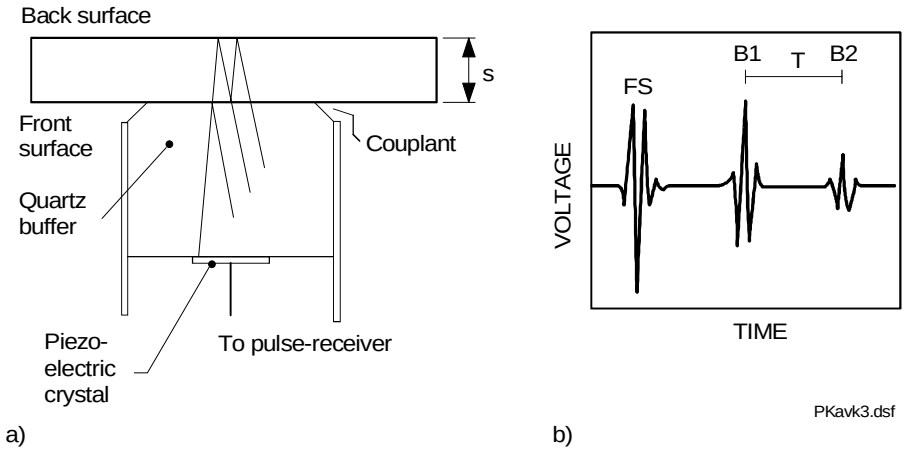

Figure 3. Specimen-transducer configuration for pulse-echo velocity measurements and principal echoes. Echo FS is returned by the front surface of specimen, and B1 and B2 are successive echoes returned by the back surface. Time T is the round-trip time delay between echoes B1 and B2 (Hull et al. 1985).

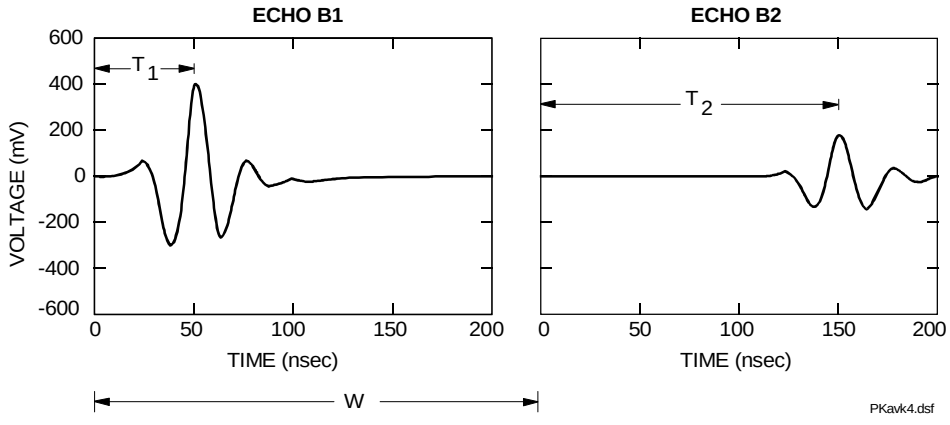

Figure 4. Backwall echoes B1 and B2 separately windowed shown in digitized form. Time delay, W, between windows is known and time delay T between echoes B1 and B2 is calculated from $T = W + (T_2 - T_1)$ (Hull et al. 1985).

First, signal B1 is digitized and the delay time read. The second echo (B2) from the backwall is then time-shifted to overlap with the digitized signal of B1. The delay time is then read again. From the two delay times and the thickness of the sample, the velocity can be calculated (Mak & Steinfl 1989). Because, except for amplitude, the echoes have similar wave-forms, the peak value criterion is adequate to overlap the echoes. It is apparent that the overlap is imperfect, e.g., the zero crossings are not all coincident. Effects of wave distortions, due to noise, dispersion, and other factors that operate the successive echoes, are present (Hull et al. 1985). For acoustically dispersive materials, the pulse shape is often distorted as it travels through the material, resulting in uncertainty in establishing the best overlap of the two signals. Therefore, the technique is accurate only if the ultrasonic pulse shape is not distorted as it traverses the sample (Mak & Steinfl 1989). Papadakis (1972) has estimated that the errors in the absolute values of measured delay times in the pulse echo overlap method can be less than 0.015τ, where τ is the period of the fundamental radio frequency of the transducer used. If broad-band pulses are used, the error is larger but still less than $0.10\tau_c$ at the center frequency. Translated into fractional errors in the single round-trip delay time, the errors may be as small as a few parts per million (Papadakis 1972). The technique has been successfully used, e.g., for measuring the ultrasonic velocity in green ceramic (Jones et al. 1986) and for estimating changes in sound velocity caused by the micro-cracking of alumina (Quinten & Arnold 1989).

Pulse superposition method

The pulse-superposition method uses a repetition rate equal to the audio frequency. If the audio frequency is set to be the reciprocal of the travel time for two round trips, then alternate echoes are overwhelmed by an input burst. The first, third, fifth, etc., echoes from one burst are superposed physically upon the third, fifth, seventh, etc., echoes from the previous burst as well as the fifth, seventh, ninth, etc., echoes from the next previous burst, etc. In this configuration, all odd echoes to infinity are superposed simultaneously. The pulse-superposition method is not as accurate as the pulse-echo overlap method and the error in the absolute values of measured delay times are estimated to be less than 0.027τ, where τ is the period of the fundamental radio frequency of the transducer used (Papadakis 1972). The method has been used by, e.g., Arons &

Kupperman (1982) to characterize the porosity reduction in local regions of ceramic solids after densification by hot isostatic pressing.

First-arrival time method

For materials with high ultrasonic attenuation, echo B2 may not be discernible on the screen. Only the first arrival time echo B1 can be measured. Together with the thickness of the material, the velocity can be calculated on this basis. When the signal-to-noise ratio is low for a certain echo, the measurement of the first arrival time can yield an error. The first arrival time method is considered to be less accurate than the other methods described here (Mak & Steinfl 1989). The measurement of sound velocity can easily be performed in immersion by measuring the time difference between the front surface echo and backwall echo of the sample. If the ultrasonic attenuation in the sample is very high, the measurement can be carried out by using separate transmitter and receiver probes in through-transmission mode. In this case the time-of-flight of ultrasonic waves from transmitter to receiver are measured with and without the sample between the probes. When the thickness of the sample is known the velocity can be calculated. This technique has been used to measure sound velocities in highly porous materials (Jungman et al. 1988).

1.4.2 Determination of ultrasonic velocities by measurement of angles of total reflection

The measurement of sound velocity is often complicated by various difficulties in transmitting longitudinal or shear waves into the sample. Bonding problems between the transducer and sample, as well as very high absorption coefficients, may limit the application of conventional methods. By measuring the angle of total reflection it is not necessary to transmit measurable quantities of ultrasonic energy into the sample. The method is based on the reflection properties of a liquid-solid boundary only, and not on the measurement of the propagation characteristics in the sample itself. The only requirement is that the sample has one flat surface (Mayer 1960).

If an ultrasonic beam in a liquid is incident on a liquid-solid boundary, part of the energy in the beam will be reflected. The remainder will be transmitted into the solid in the form of a longitudinal and shear wave. Snell's law (14) gives the

angles of reflection and refraction but does not give information about the amplitudes or energies of the various waves. If the energy of incident wave in the liquid is unity, the energy loss of the wave reflected at the boundary compared with the energy of the incident wave is given by

$$E_{loss} = 1 - \left(\frac{R}{I}\right)^2 . \tag{26}$$

The quantities R and I are the amplitudes of the reflected and the incident waves, respectively. The energy ratio of reflected to incident wave can be given as

$$\left(\frac{R}{I}\right)^2 = \left\{ \frac{\cos\theta_{TL} - \left(\frac{V_{L\rho}}{V_{f\,\rho_f}}\right)\cos\theta_i \left\{1 - 2\sin\theta_{TS}\sin 2\theta_{TS}\left[\cos\theta_{TS} - \left(\frac{V_S}{V_L}\right)\cos\theta_{TL}\right]\right\}}{\cos\theta_{TL} + \left(\frac{V_{L\rho}}{V_{f\rho\,f}}\right)\cos\theta_i \left\{1 - 2\sin\theta_{TS}\sin 2\theta_{TS}\left[\cos\theta_{TS} - \left(\frac{V_S}{V_L}\right)\cos\theta_{TL}\right]\right\}} \right\}^2 , \tag{27}$$

where V_f, V_L and V_S denote the velocities of the ultrasonic wave in the liquid and the longitudinal and shear wave velocities in the solid, respectively. The densities of the liquid and the solid are given by ρ_f and ρ. The angles θ_i, θ_{TL} and θ_{TS} are defined in Figure 5.

Applying Snell's law to the transmitted longitudinal and shear wave

$$\frac{V_L}{\sin\theta_{TL}} = \frac{V_f}{\sin\theta_i} \tag{28}$$

and

$$\frac{V_S}{\sin\theta_{TS}} = \frac{V_f}{\sin\theta_i} . \tag{29}$$

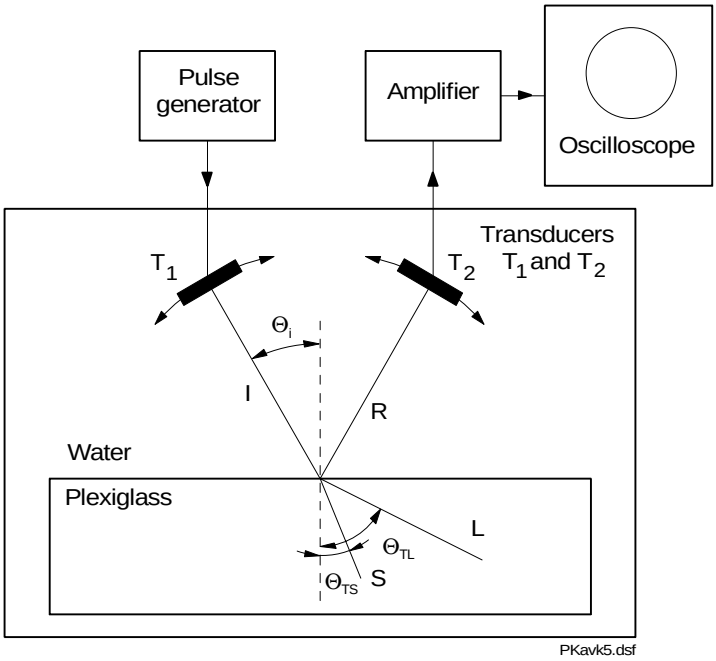

Figure 5. Diagram of setup for reflection measurements. S and L indicate the direction of propagation of the refracted shear and longitudinal waves (Mayer 1960).

The critical angle for these waves is reached when $\sin\theta_{TL} = 1$ and $\sin\theta_{TS} = 1$, respectively. In the first case $\cos\theta_{TL} = 0$ and the right-hand side of Equation (27) equals 1. It can be shown that Eq. (27) gives the value 1 again at the critical angle for shear wave. The incident energy is totally reflected in both cases according to Eq. (26).

Equation (27) shows that whenever $\sin\theta_{TL}$ or $\sin\theta_{TS}$ equals 1, no ultrasonic energy is transmitted into the solid sample. This means that there is a sharp rise in the amplitude of the reflected wave. The angle of incidence at which this sharp increase occurs can be located experimentally by using the setup shown in Fig. 5. Having found the critical angle (maximum reflection) and knowing the sound velocity in water, one can calculate the longitudinal velocity V_L from Eq. (28), since the only other term, $\sin\theta_{TL}$, equals 1 at the critical angle (Mayer 1960). The rise associated with the critical angle for the shear wave cannot be

observed if the sound velocity in water is greater than the shear velocity in solid, i.e., $\sin\theta_i > \sin\theta_{TL}$.

The general shape of the entire reflection curve depends on the ratio of the acoustic impedances of the two media used and on the ratio V_L/V_S. The peaks will become relatively higher as the ratio of the densities of the two media approaches unity. The ratio of the velocities does influence the relative height of the peaks to some extent. However, the exact shape of the entire curve is of little interest if only velocity measurements are to be made; the important feature is the location of the peaks associated with the critical angles, since only Snell's law is used for the calculation of the velocities (Mayer 1960).

Fountain (1967) has studied experimentally the accuracy and practical limitations of the angle-of-total-reflection method. The reflection curve measured on an aluminum sample in distilled water is presented in Fig. 6.

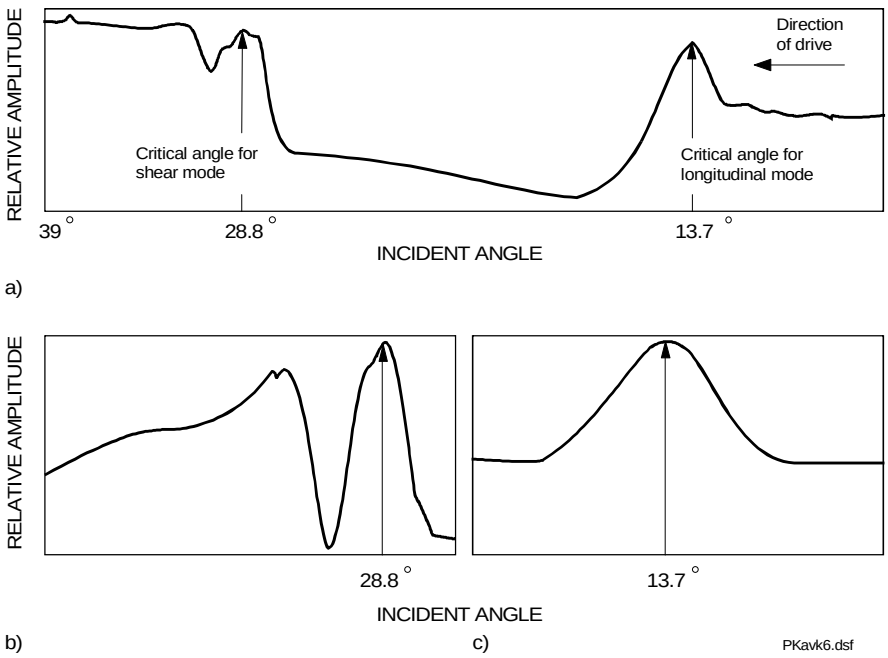

Figure 6. Reflected signal amplitude versus incident-beam angle at a distilled-water/aluminum boundary (Fountain 1967).

The amplitude of the reflected signal remains practically constant from an incident angle of 10° until a sudden increase in reflection occurs at 13.7°, the critical angle for longitudinal waves in aluminum. From this peak, the reflected signal drops below the level that preceded the peak and remains low, increasing only slightly until another sudden peak occurs at an incident angle of 28.8°. This peak indicates the critical angle for shear waves in the aluminum sample. The dip immediately following the shear wave peak is related to the lateral beam displacement that takes place close to the angle of total reflection. This shift is relatively large at the incident angle at which a Rayleigh wave is excited in the solid medium (Fountain 1967).

The angle-of-total-reflection method of measurement is dependent upon the unique occurrence of reflection peaks. This puts a limit on the minimum thickness of solid material on which it can be used. If the thickness of the solid material is only a few wavelengths of the incident sound, plate modes can be set up that will cause other reflection peaks, in addition to the desired critical angle effects. Based on the experimental measurements, Fountain (1967) has evaluated that the method is applicable on solids whose thickness is more than 15 wavelengths of the sound signal in the solid. The accuracy with which the incident angle can be resolved strongly depends on the transducer characteristics. Any amount of beam spreading prevents all parts of the incident beam from reaching the critical angle at the same time, thus causing a spreading of the maximum reflection peak (Fountain 1967).

The measurement of critical angle for reflection from the liquid-solid interface has been used to measure phase velocities along the surface and based on these measurements the elastic constants of the material have been determined. Henneke & Jones (1976) have shown, however, that this technique can not be used in general for anisotropic solids and may lead to rather large errors.

In the isotropic case, Snell's law of refraction states that the phase velocities of the incident and refracted waves are related by the expression

$$\frac{V_I}{\sin\theta_I} = \frac{V_T}{\sin\theta_T}, \tag{30}$$

where θ_I and θ_T are the angles between the incident and refracted wave vectors and the normal to the reflecting surface, respectively. Then, the critical angle of incidence, θ_C, is assumed to occur when θ_T becomes equal to 90°, and hence by this definition, the critical angle is given by

$$\sin\theta_C = \frac{V_I}{V_T}. \tag{31}$$

Since the direction of the refracted wave at the critical angle is assumed to correspond to the direction of a body wave propagating along the boundary, Eq. 30 can be used to calculate V_T for this known direction and a sufficient number of independent measurements will yield data from which the elastic constants can be determined. It has been pointed out, however, that in general, the critical angle occurs when the energy flux associated with the refracted wave becomes parallel to the interface of the two media and not when $\theta_T = 90°$. For this general definition of the critical angle, the governing equations have too many unknowns to allow for the determination of the elastic constants by the critical angle technique, if one considers the full statement of Snell's law (Henneke & Jones 1976).

Rokhlin & Wang (1989) have shown that the limitation presented by the above does not hold for two-dimensional composite materials. It is shown that, for two-dimensional composite materials at the critical angle, both phase and group velocities are oriented parallel to the sample surface and, therefore, Snell's law can be used for phase velocity extraction from critical angle measurements. Using this technique in combination with the double-through-transmission method, the full matrix of elastic constants for an orthotropic material can be reconstructed. The through-transmission method has also been used by Papadakis et al. (1991) to measure the elastic modulus of thick composites. The basic assumption in this work was that small sections of the composite could be treated as a homogeneous body analogous to a crystal for ultrasonic propagation.

1.4.3 Reflectometry

Saurel et al. (1989) have used the combination of reflectometry and acoustic microscopy to measure shear and longitudinal wave velocities of SiC CVD films. Based on the velocities measured, the elastic constants have been determined on the basis of homogeneous and isotropic solid theory. For thin and deposited materials having high acoustic velocities, echoes reflected by the surface and the interface interfere with each other and make it impossible to determine the time of propagation in the material directly from the interface echo. The velocity measurement is also difficult when the coating material has an impedance close to that of the substrate.

The technique used by Saurel et al. (1989) requires the use of a sensor whose aperture is less than the critical longitudinal angle. In this domain the reflection coefficient could be considered constant and equal to that at normal incidence:

$$R(\theta) \approx R(\theta = 0) = \frac{Z_{sample} - Z_{liquid}}{Z_{sample} + Z_{liquid}}, \tag{32}$$

where $Z = \rho V_L$, ρ being the density.

In this case, the signal reflected by the sample surface is proportional to V_L. A standard sample allows the elimination of the acoustic transfer function of the lens and of the liquid. The surfaces of the samples must be well polished to avoid diffusion phenomena. The measurement accuracy of V_L is estimated to be 5%. For the measurement of Rayleigh wave velocity, acoustic microscopy and the V(z) technique has been used. The calculated elastic constants were in agreement with those in the literature (Saurel et al. 1989).

1.4.4 The measurement of sound velocities based on V(z) curves

In Fig. 7, a plane compression wave is incident in the fluid at the critical angle for surface wave generation in the solid. At this angle, the variation in phase in the x_1 direction of the incident plane wave matches the variation in phase of a Rayleigh surface wave in the solid. The spatially periodic pressure that is applied to the surface upon reflection of the incident plane wave induces a

surface wave which propagates in the same direction as the x_1 component of the incident wave vector k^{in}. The spatially periodic motion of the surface arising from the propagation of the induced surface wave in turn generates a compression wave-field in the fluid which propagates in the direction of the reflected wave-field k^{re}. Therefore, unlike a true Rayleigh surface wave, which propagates freely on the surface of a free solid, the induced surface wave is damped by coupling to a propagating compression wave in the fluid. This damping due to coupling is commonly referred to as leakage, and the induced surface wave is referred to as a leaky surface wave (Roberts 1989).

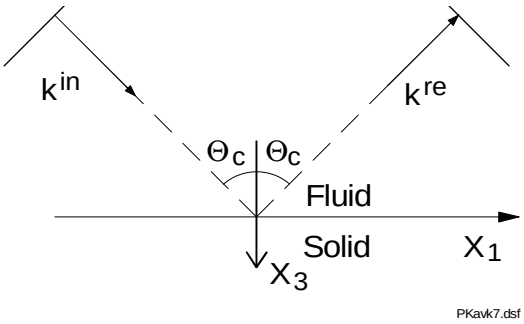

Figure 7. Plane wave reflection at a fluid-solid boundary at the critical angle for surface wave generation (Roberts 1989).

Figure 8 shows the incident pulse as originating at a highly focused lens which is used both as transmitter and receiver.

The pulse is incident perpendicular to the surface. A simplified description of the interaction of the incident pulse with the surface is provided by the ray theory. Rays are seen to emerge from the lens over a range of incident angles. A ray emerging from the lens at the critical angle for surface wave generation, θ_R , and hitting the surface at point (3) will generate a leaky surface wave. As this surface wave propagates, it will generate a compression wave in the fluid which emerges at the critical angle. Leaky surface waves are exploited by defocusing the lens, as shown in Fig. 8. Only the leaky ray emanating from point (4) on the surface, i.e., ray (4)–(5), will be accurately collimated by the lens. Leaky rays emanating from other points along the surface will be refracted by the lens in directions non-perpendicular to the plane of the transducer, and hence will not significantly contribute to the transducer output signal. The ray path (2)–(3) – (4)–(5) represents a transmission path that will provide a significant

contribution to the transducer output signal. The transmitted energy is propagating over segment (3)–(4) of this transmission path as a surface wave (Roberts 1989).

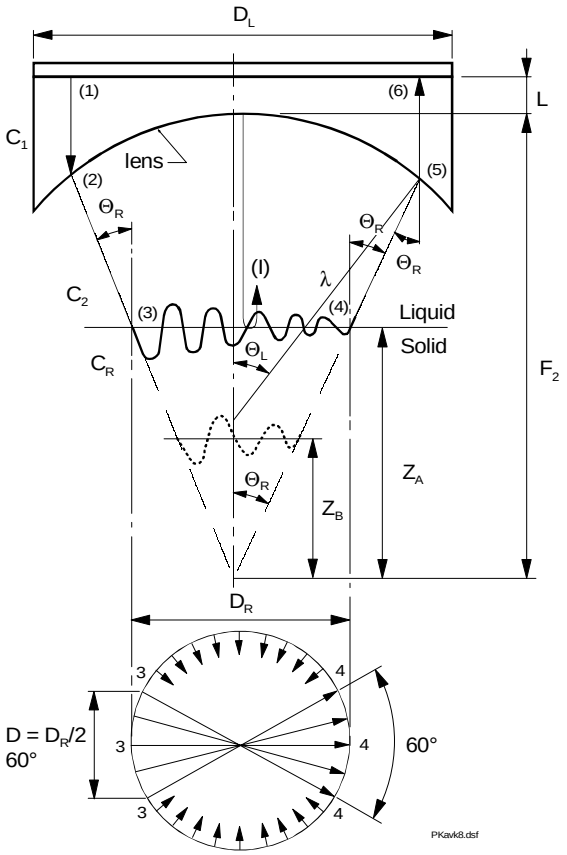

Figure 8. Transducer-lens configuration for acoustic microscope (Gilmore et al. 1989).

A common approach to surface wave velocity measurement with acoustic microscopy is to monitor the difference in arrival times of pulses propagating along ray paths (2)–(3) − (4)–(5) and the pulse directly reflected from the surface back to the transducer (I) in Fig. 8. This time difference is calculated by a simple consideration of difference in path lengths and wave velocities (Gilmore et al. 1989).

Let the velocity of longitudinal waves propagating in the lens be V_1 and the propagation velocity in the coupling liquid V_2.

The time t_1 required for the directly reflected pulse following the ray path on the lens axis to travel from the piezoelectric element and return is:

$$t_1 = \frac{2L}{V_1} + \frac{2\left(F - z_A\right)}{V_2}. \tag{33}$$

The round-trip travel time (t_2) for the pulse travelling along the ray incident at the Rayleigh critical angle is:

$$t_2 = \frac{2L}{V_1} + \frac{2\left(1-\cos\theta_L\right)}{V_1}K + \frac{2\left(F - z_A\right) - 2K\left(1-\cos\theta_L\right)}{V_2\cos\theta_R} + \frac{2z_A\tan\theta_R}{V_R}, \tag{34}$$

where θ_L, θ_R and V_R are the lens angle, the Rayleigh critical angle, and the velocity of Rayleigh waves. From Fig. 8 and Snell's law, the diameter (D_R) of the entry circle, where the incident pulse in the liquid is mode-converted into a leaky Rayleigh wave and (θ_R) are:

$$D_R = 2z_A\tan\theta_R \tag{35}$$

$$\theta_R = \arcsin\frac{V_2}{V_R}\ . \tag{36}$$

Writing the differences in round-trip travel time for the direct reflection (Δt_1) and the surface wave (Δt_2) at the two defocus distances z_A and z_B and combining Formulas (33)–(36) Gilmore et al. (1989) gives for V_R

$$V_R = \sqrt{\frac{\left(V_2\right)^2}{1-\left(\frac{\Delta t_2}{\Delta t_1}\right)^2}} \tag{37}$$

Formula (37) permits the Rayleigh velocity to be determined from the time measurements at two water path settings.

In acoustic microscopy Δt is normally measured by determining the value of z for which $\Delta t = n / f$, where f is the center frequency of a narrow-band pulse and n is an integer. At this depth of defocus, the signals from the two different ray paths are out of phase, and the result is a minimum in the total output signal. Thus, the surface wave velocity is obtained by noting the position of the minima in the plot of the total received signal amplitude versus the defocus distance z (Roberts 1989).

It was first experimentally observed that the contrast of a micrograph periodically changed with the axial distance between the lens and the object (Atalar et al. 1977, Weglein and Wilson 1977). Since then this technique has come to be known as acoustic material signature (AMS) or as the V(z) technique, representing the variation of the output voltage of the transducer V with distance z (Nikoonahad 1984).

1.5 The contrast of the acoustic microscope

The contrast theory for the acoustic microscope is well developed for a specimen whose properties are uniform across the surface. If the surface of the specimen is at the focal plane of the lens, then the returned signal from the transducer, due to the reflected acoustic wave, is the sum over the area of the acoustic wave incident on it. In two dimensions this is:

$$V(0) = \int_{-k}^{k} P(k_x) R(k_x) dk_x , \qquad (38)$$

where k is the wave number in the coupling fluid and k_x is the component of the wave vector parallel to the specimen surface. $P(k_x)$ is the two-way pupil function of the lens for waves passing through the focus and $R(k_x)$ is the reflectance function of the specimen surface. If the specimen is moved towards the lens so that the surface is at distance -z from the focal plane, then a phase shift Δ is

introduced for each wave, where k_z is the component of the wave vector normal to the specimen surface.

The signal on the transducer, expressed as a function of the defocus, z, is then:

$$V(z) = P(k_x)R(k_x)e^{-2ik_z z}dk_x \ . \tag{39}$$

This can be expressed as a Fourier transform, with z and $2k_z$ as the transform pair. This means that V(z) can be regarded as a Fourier transform of the pupil function of the lens and the reflectance function of the specimen. The pupil function may be regarded as a constant for an instrument with a given lens, and if it is well behaved the interest is in the reflectance function of the specimen. This is a complex function, because there are phase changes associated with it, and for an isotropic half-space the dominant phase change occurs around $k_x = k_R$, the Rayleigh wave vector. In the Fourier transform this would be expected to lead to oscillations of periodicity:

$$\Delta z = \frac{2\pi}{2k_{z_1} - 2k_{z_2}}, \tag{40}$$

where k_{z1} and k_{z2} correspond to $k_x = 0$ and k_R respectively. If θ is the angle of incidence, and θ_R is the angle that corresponds to $k_x = k_R$, then this may be written as:

$$\Delta z = \frac{\lambda}{2(1 - \cos\theta_R)}, \tag{41}$$

where $\lambda = 2\pi/k$ is the wavelength in the fluid (Briggs & Somekh 1987, Briggs 1985).

1.5.1 Experimental ray model for V(z) curves

Weglein (1979) has presented a model for a V(z) curve based on the interference between two components re-radiated into the immersion fluid at the material's critical Rayleigh angle θ_R. One component is specularly reflected

from the solid, and the second component undergoes a lateral shift before re-radiating at θ_R. The characteristic period Δz of this interference signature varies as the square of the Rayleigh wave velocity and is empirically given by Equation (42):

$$\Delta z = \frac{\lambda_R}{\sin\theta_R}, \tag{42}$$

where λ_R is the Rayleigh wavelength.

Materials covering a greater than 3:1 velocity range agree well with this physical model. Substitution of the longitudinal wave velocity in the expression extends the range of measurable AMS to acoustically slower materials.

The highly convergent beam used in the acoustic microscope includes critical angles for total internal reflection of both longitudinal and shear waves in the substrate as well as Rayleigh critical angles. Yet these waves do not appear to influence the AMS in a significant manner. The excitation of leaky surface-skimming bulk waves is in most cases restricted and quite small. Unlike Rayleigh waves, the energy distribution of surface-skimming bulk waves is not confined to the solid surface, thus substantially reducing the intensity and consequently the periodic surface particle excursion that provides coupling to the liquid. The efficiency of surface-skimming bulk-wave excitation is further reduced because of the usually large acoustic impedance mismatch at the liquid-solid interface that permits little energy to be transmitted into the solid (Weglein 1979).

Interesting exceptions to these restrictions are materials where the velocity of Rayleigh waves is sufficiently slow to preclude phase matching to the incident acoustic beam ($\sin\theta_R = V_f / V_R > 1$), where V_W is the velocity of compression waves in the coupling water. In such cases, a leaky surface-skimming compression wave is excited in the solid and it behaves in an analogous manner to the leaky Rayleigh wave in forming the interference phenomena. The conditions for this phenomena are: (a) the absence of strong Rayleigh wave interaction, (b) a low acoustic reflection coefficient at the liquid-solid interface, and (c) a large Poisson ratio rendering the material elastically very deformable

(Weglein 1979). The velocity of surface-skimming compression waves from V(z) curves has been experimentally measured by Morsch et al. (1988).

For well-collimated beams obliquely incident to the interface, the phase shifts encountered upon reflection result in a reflected beam whose position is translated laterally along the reflecting surface. The lateral shift for acoustic beams is known as the Schoch displacement, and it is most pronounced when the acoustic beam is incident at the critical angle for Rayleigh-surface-wave excitation. When the incident beam is normally incident to the interface, there can be no lateral displacement for the entire beam. However, the phase shift experienced by each component does alter the wave front of the reflected beam in a manner that is unique for each reflecting surface. By measuring the shape of this reflected wave front we can, in principle, monitor the elastic properties of the surface (Atalar 1978).

In the model proposed by Weglein, the Schoch displacement is assumed to be proportional to the axial translation of the object from the focal plane. According to Atalar (1979) this has no justification. Moreover, in the suggested ray model, the phase shift between the specularly reflected and the displaced wave is related to the size of the displacement. Atalar has shown that this phase shift is independent of the displacement when the extra path in the liquid travelled by the specularly reflected wave is included.

The physical model presented by Atalar considers two cases depending on the velocities of Rayleigh waves in the solid and compression waves in the liquid. If the Rayleigh wave velocity in the solid medium is less than the sound velocity in the liquid, the reflectance function can be neglected. In this case the separation between the peaks of the V(z) curve is given by

$$\Delta z = \frac{\lambda_0 F^2}{R_L^{\,2}}, \tag{43}$$

where R_L is the radius of the pupil function of the lens and F is the focal distance (Figures 9 and 10). Thus Δz depends only on lens parameters and the wavelength in the liquid.

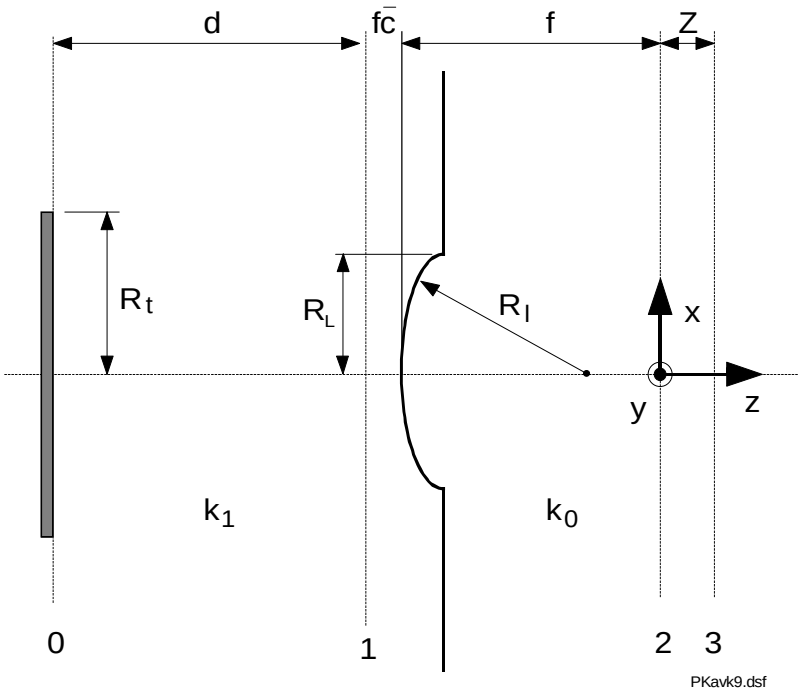

Figure 9. Geometry and coordinate system of the acoustic microscope used by Atalar (1979).

In the second case considered by Atalar, the Rayleigh velocity is high enough so that the critical angle is within the angles covered by the lens. This requires the Rayleigh velocity V_R to be at least

$$V_R \geq \frac{V_f F}{R_L}, \tag{44}$$

where V_f is the sound velocity in the liquid. Under these circumstances, the phase of the reflected wave is affected by two factors: the reflectance function phase and the exponential defocusing factor. When the object is located at the focal plane (z = 0), the exponential factor is unity and thus the wave fronts of the reflected wave take the shape of the reflectance phase function. This is demonstrated by curve A in Fig. 10.

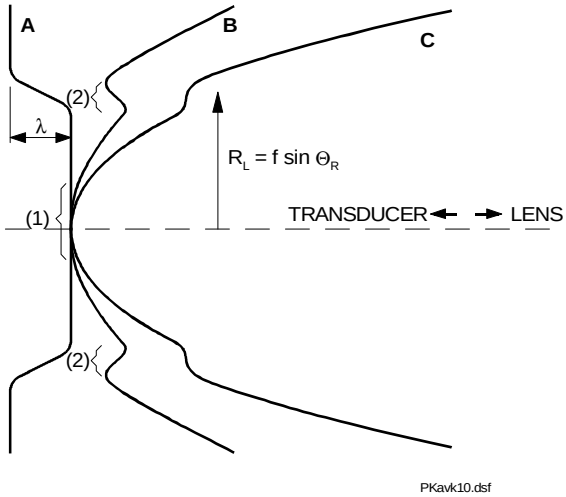

Figure 10. The shape of the reflected wave fronts at the back focal plane of the lens (plane 1) for a single-crystal reflector. Wave front A is for Z = 0. Wave fronts B and C are for increasingly negative values of Z (Atalar 1979).

The rays with large incident angles are reflected with a phase shift that approaches 2π corresponding to a whole wavelength λ (Atalar et al. 1977). In this case the output of the transducer is large since most of the wave front is parallel to the transducer. There is not an appreciable contribution to output from the region corresponding to the transition. If the object is brought closer to the lens ($z < 0$), the exponential factor comes into play and adds a curvature to the wave fronts as illustrated in Fig. 10 by wave front B. For this case the main contribution to the output comes from the region where the wave fronts are more or less parallel to the transducer. There are two contributions: one is around $r \approx 0$, and the other around $r \approx f\sin\theta_R$. The phase relationship between these two quantities must be considered. If they are in phase, they will add up to give a peak, but if they are out of phase there will be a dip. To have a peak, the phase difference between these two should be $2n\pi$ ($n = 1,2,..$). For the position of the peaks Atalar derives

$$z = \frac{-n\lambda_f}{2\left(1-\cos\theta_R\right)} \qquad n = 1,2,\ldots . \tag{45}$$

Therefore the distance between the successive peaks (or nulls) is predicted as

$$\Delta z \approx \frac{\lambda_f}{2\left(1-\cos\theta_R\right)} \quad V_R > \frac{V_f F}{R_L}. \tag{46}$$

Equation (46) is plotted as a solid line in Fig. 11 along with Weglein's experimental measurements. By adding that

$$\Delta z = \frac{\lambda_f}{2\left(1-\cos\theta_R\right)} \approx \frac{\lambda_f}{\sin^2\theta_R} = \frac{\lambda_R}{\sin\theta_R} \quad , \tag{47}$$

where the last result is the empirical formula quoted by Weglein. This is also plotted in Fig. 11 as a dashed line for comparison (Atalar 1979). The formula, which was first derived from ray considerations and also by an angular spectrum approach, has been extensively tested experimentally, and it is well established that oscillations do indeed occur in V(z) with a periodicity that is accurately described by this equation (Briggs & Somekh 1987, Vetters et al. 1989, Weglein 1985).

Ilett et al. (1984) have considered the effect of elastic discontinuities on the acoustic images and V(z) curves. The experimentally obtained images show that an enhanced contrast is found from surface-breaking cracks and from other discontinuities such as interfaces and grain boundaries. Subsurface oblique cracks are shown to generate interference fringes in acoustic images. An explanation of the fringes is illustrated in Fig. 12.

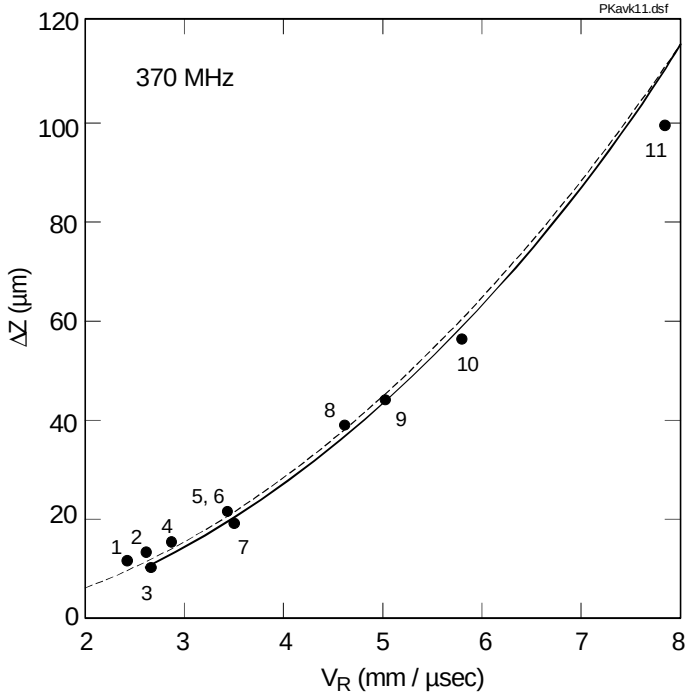

Figure 11. Periodicity of the acoustic signatures versus mean Rayleigh velocity of different materials (Atalar 1979).

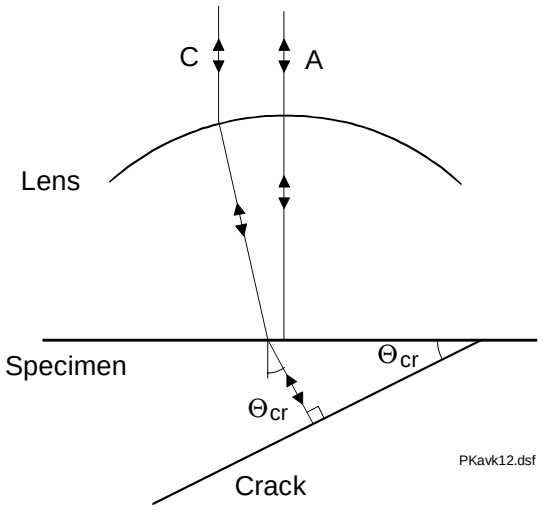

Figure 12. Schematic diagram of the beams that are important in bulk wave interference fringes from angled cracks (Ilett et al. 1984).

In this case two rays are important: ray A, which strikes the surface normally and is reflected to the lens, and ray C, which is refracted at the specimen surface so as to strike the crack normally, and is also reflected along its own path. As the lens is scanned parallel to the surface the path followed by ray A remains constant, but that of ray C varies. Since the transducer sums the amplitudes of the two contributions, periodic interference results, leading to the observed fringes. The periodicity is

$$\Delta x = \frac{\lambda}{2 \sin \theta_{Cr}} \ . \qquad (48)$$

A special case of the fringe pattern due to a crack in the specimen occurs when the crack runs normal to the surface, i.e. for $\theta = 90°$. Equation (48) then predicts a fringe periodicity of $\lambda/2$. Here the wavelength is the Rayleigh wavelength. The $\lambda_R/2$ spacing is actually the most common in acoustical images (Briggs 1985, Weaver et al. 1985).

The interference fringes around an inclined boundary are not symmetric on both sides of the boundary. The model presented by Kojima (1989) explains this asymmetry by considering the behaviour of three types of rays as shown in Fig. 13.

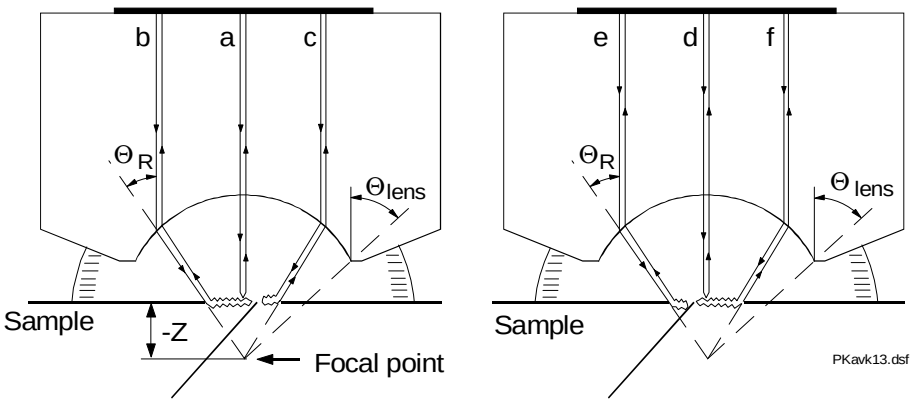

Figure 13. The schematic illustration of the reflection of leaky Rayleigh waves at the very thin domain which is inclined to the surface (Kojima 1989).

One ray is the geometrically reflected beam with the normal incidence (beam a, d). The two others with the incident angle θ_R (the Rayleigh critical angle) are converted to a leaky Rayleigh wave; they are then reflected at the boundary and reradiate the waves to the fluid with incident angle θ_R and finally reach the transducer (beam b, c, e, f). The asymmetry of the fringes is caused by the difference between the interference of two beams a, c and d, e. Asymmetric fringes are important sources for obtaining information about the subsurface inclination of any kind of boundary.

In the case of a straight line reflector, the interference fringe appears as parallel lines with the periodicity $\lambda/2$ as described previously. A small cylindrical or hemispherical hole reflects acoustic waves in all directions on a surface. The interference fringes will in this case appear around such a small hole and their spacing will vary with directions owing to elastic anisotropy. Elongated interference rings can therefore be of great importance in obtaining data about local elastic anisotropy (Kojima 1989).

If the properties of the reflecting material vary across the surface, the reflectance function $R(\theta)$ is no longer defined, since scattering will occur at discontinuities and there will no longer be a single, infinite reflected plane wave. This causes serious difficulties in applying the V(z) formalism in a case where there is an elastic discontinuity within the diffraction-limited spot on which waves are incident. Ilett et al. (1984) have shown that the effect of the crack on V(z) will be to change the position and amplitude of the nulls, but not their periodicity. Thus the velocity of Rayleigh waves in the material can be determined also when the material is not free from elastic discontinuities (Ilett et al. 1984).

1.6 Measurement of elastic anisotropy

The measurement of V(z) curves is normally performed by using a spherical lens with which a plane wave radiating from the transducer is circularly focused into a point. Because the point-focus beam excites leaky surface acoustic waves propagating in all directions, the acoustic properties are measured as a mean value around the beam axis. This means that the system cannot be applied appropriately for detecting the acoustic properties that reflect crystallographic

anisotropies (Kushibiki & Chubachi 1985). The directional acoustic microscope lens developed by Hildebrand & Lam (1983) uses two circular piezoelectric transducers, positioned with their centers above opposite edges of the spherical lens, as shown in Fig. 14. One transducer is used to generate the acoustic pulse while the other transducer is used to detect the reflected pulse. The orientation of the two transducers determines an azimuthal direction of propagation of the surface waves.

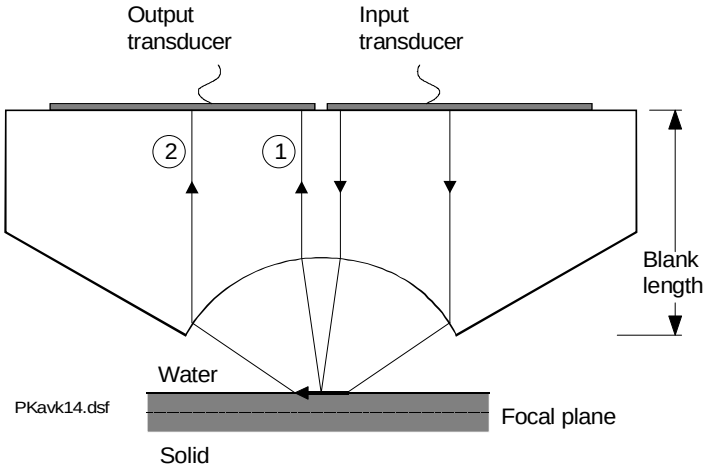

Figure 14. Schematic illustration of the directional acoustic microscope lens. Ray path (1) represents a low angle specular reflection while ray path (2) represents a re-radiated surface wave (Hildebrand & Lam 1983).

V(z) curves obtained with the directional acoustic lens exhibit periodic variations similar to those seen with the conventional acoustic lens. The spacing of the nulls (Δz) for the directional acoustic lens follow the same relation as for the conventional acoustic lens since the interference mechanisms are the same (Hildebrand & Lam 1983). Kushibiki & Chubachi (1985) have developed a sapphire lens with a cylindrical concave surface and line-focus beam. The lens structure, including the dimensions, is depicted in Fig. 15.

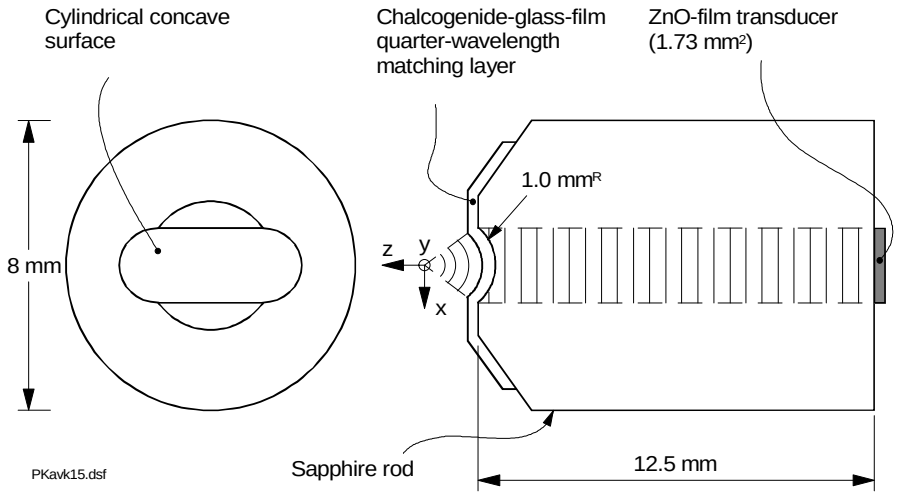

Figure 15. Structure of acoustic line-focus-beam sapphire lens with cylindrical concave surface (Kushibiki & Chubachi 1985).

The experimental results show, that the line-focus-beam acoustic microscope can be used for determining the physical constants, such as the elastic constants and the density. The system has been used with all sample configurations, such as semi-infinite, layered, or diffusion-layered, and thin-film structures. In very thin films two modes contribute to the V(z) curve. The shorter interval in V(z) curve corresponds to leaky surface acoustic wave (LSAW) mode, while the longer interval corresponds to leaky pseudo-surface acoustic wave (LPSAW) (Kushibiki et al. 1987). By employing leaky surface acoustic waves or leaky surface skimming compression waves (LSSCW) most of the characterization area for solid materials can be covered through the V(z) curve analysis. For materials that have homogeneous acoustic and structural properties, the velocity is by far the more significant acoustic property for characterization than attenuation is (Kushibiki & Chubachi 1985). The velocity of leaky surface acoustic waves mainly affects the interval of dips in V(z) curves, while the attenuation factor affects the shape of V(z) curves (Kushibiki et al. 1982).

Chubachi et al. (1991) have developed a directional acoustic microscope with high spatial and angular resolutions. A point-focus-beam lens with a simple rectangular transducer has been introduced to replace the cylindrical lens used in the line-focus-beam microscope. The line-focus-beam microscope is not

suitable for two-dimensional imaging because the spatial resolution along the cylindrical lens axis is not considered. The point-focus-beam lens with a rectangular transducer (dimensions 1.73 mm × 0.5 mm) has been successfully used to measure the anisotropic properties in each grain area of a polycrystalline sample.

The bulk acoustic wave method is advantageous for the direct evaluation of elastic modulus. In this method, longitudinal and shear wave velocities propagating in different directions are measured with the pulse-echo overlap technique. This method, however, gives only average values and requires a considerably large sample having two parallel surfaces (Yamanaka et al. 1985). Kupperman & Karplus (1984) have determined the elastic anisotropy of a green ceramic specimen from the change in sound velocity that occurs when a shear wave transducer is rotated with respect to the specimen, thus varying the polarization of the shear waves propagating in a particular direction. The velocity was measured by overlapping successive echoes in the pulse-echo mode and determining the time delay from the oscilloscope. Since the modulus of elasticity is related to the velocity of sound, variations in shear velocity with polarization can indicate variations of modulus with direction.

1.6.1 The effect of porosity on the propagation velocity of ultrasonic waves and on the elastic properties of the material

The formulae for empirical correlation between porosity fraction and ultrasonic velocity for polycrystalline materials have been reviewed by Roth et al. (1990). In general, the velocity of a longitudinal ultrasonic wave travelling in a solid is related to the elastic properties and density of the solid by:

$$V_L = \sqrt{\frac{E(1-\nu)}{\rho(1+\nu)(1-2\nu)}}, \tag{49}$$

where V_L, E, ρ, and ν are the velocity, elastic modulus, bulk density, and Poisson's ratio, respectively, of the material. The velocity of a shear wave travelling in a solid is related to the elastic properties and density of the solid by:

$$V_S = \sqrt{\frac{E}{2\rho(1+\nu)}}\,. \tag{50}$$

According to Spriggs (1961) the effect of porosity on elastic modulus is of the type:

$$E = E_0 e^{-bP}\,, \tag{51}$$

where E_0 is the elastic modulus of a fully dense (nonporous) polycrystalline specimen, b is an empirical constant related to pore shape, pore distribution, and the ratio of open-to-closed pores, and P is the volume fraction porosity.

An alternative equation has been suggested by Phani et al. (1986) to describe the relationship between elastic modulus and porosity fraction:

$$E = E_0 (1-P)^{2n+1}\,, \tag{52}$$

where n, like b above, is an empirically-determined constant that depends on pore distribution and pore geometry factors. The porosity fraction, P, can be expressed as:

$$P = 1 - \left(\frac{\rho}{\rho_0}\right), \tag{53}$$

where ρ_0 is the theoretical (nonporous material) density. From Equation (53) the bulk density as a function of porosity fraction can be expressed:

$$\rho = \rho_0 (1-P) \tag{54}$$

Substituting Equations (52) and (53) into Equation (50) allows velocity to be expressed as:

$$V_L = V_0 (1-P)^n\,, \tag{55}$$

where V_0 is a constant for a given material equal to :

$$V_0 = \sqrt{E_0(1-\nu)\rho_0(1+\nu)(1-2\nu)}\,, \tag{56}$$

V_0 is the velocity in a fully dense (nonporous) material, i.e. the "theoretical" velocity.

Setting n = 1 in Equations (52) and (55) results in good agreement for a number of materials over a wide porosity fraction range ($0.1 < P < 0.7$) (Phani et al. 1986). In this case, the Equation (55) is reduced so that:

$$V = V_0(1-P)\ . \tag{57}$$

Based on Equation (57), Roth et al. have used linear regression to analyse the empirical results relating ultrasonic velocities to the porosity fraction. The longitudinal and shear wave velocities versus percent porosity for Al_2O_3 are presented in Figures 16 and 17. The experimental results of different studies are presented with symbols.

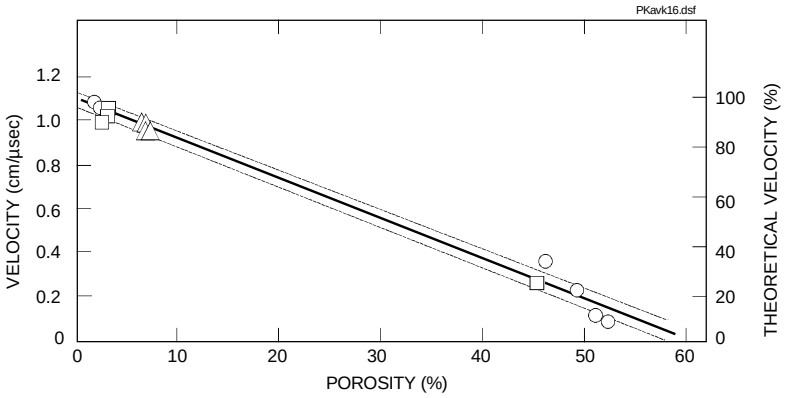

Figure 16. Longitudinal velocity versus percent porosity for Al_2O_3. Velocity = -0.018 × percent velocity + 1.11. Percent theoretical velocity = -1.63 × percent porosity + 100. Correlation coefficient = -0.995 (Roth et al. 1990).

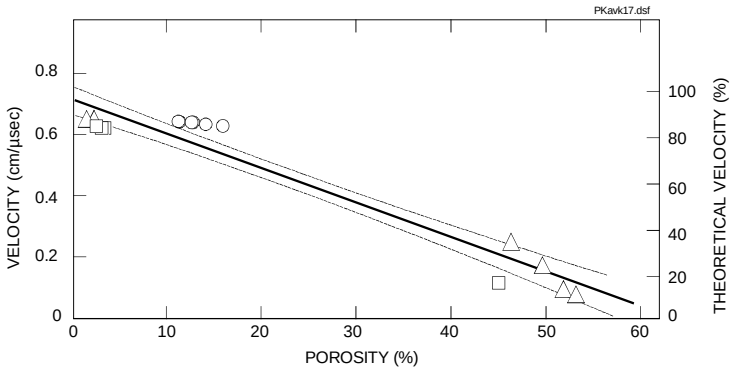

Figure 17. Shear velocity versus percent porosity for Al_2O_3. Velocity = -0.011 x percent porosity + 0.703. Percent theoretical velocity = -1.56 x percent porosity + 100. Correlation coefficient = -0.960 (Roth et al. 1990).

Arons & Kupperman (1982) have evaluated the effects of hot isostatic pressing (HIP) on the porosity of alumina. An increase in velocity of 1.5% was observed after HIP. The technique proved to have high sensitivity, and data about local porosity variations was obtained.

Both the shear and longitudinal velocities decrease with increasing porosity, even though the rate of decrement is slightly different for the two. The models proposed to explain the elasticity of porous solids are derived from the composites by treating the pores as a second phase with vanishing small elastic constants. According to these models there is a linear dependence of the composite elastic constants on the fraction pore volume and a linear decrease of Poisson's ratio with porosity. Nagarajan (1971) has studied the validity of these models and has observed experimentally greater values than those predicted by the model. Further, Nagarajan did not find a linear decrease of Poisson's ratio.

Wang (1984a) has studied theoretically Young's modulus of porous materials and compared the theoretical results with the empirical Spriggs' equation. At high densities (low porosity) the theoretical analysis supports Spriggs' correlation, however, for correlating data over a wider range of porosity, the b value in Spriggs' equation cannot be treated as a constant, and the exponent in the equation cannot be considered a linear function of porosity. This is especially evident at high porosity. The approximated solution proposed by Wang is:

$$E = E_0 e^{-aP+cP^2} \tag{58}$$

This is quite satisfactory over a wide porosity range. The coefficients a and c are nonnegative numbers.

Nielsen (1982) has studied the elastic properties of two-phase materials. If phase 2 in the material is much softer or much stiffer than phase 1, the extreme elastic modulus (k^x_0) have been expressed by

$$\kappa^{x}{}_{0} = \frac{1-d}{1+\dfrac{d}{\kappa_0}} \approx 1-\left(1+\frac{1}{\varphi\kappa_1}\right)d\,, \tag{59}$$

where φ is a shape factor and κ_1 is a function of Poisson's ratio ν_1 for the matrix in the following way:

$$\kappa_1 = \frac{2(1-2\nu_1)}{1+\nu_1} \tag{60}$$

and d is the volume concentration of the phase given by

$$d = \frac{M_2}{M_1 + M_2} \tag{61}$$

Wang (1984b) has studied Young's modulus of porous alumina in situations where the porosity percentage not only changes, but changes also occur from interconnected to disconnected pore structure. The experimental study was carried out with porous Al_2O_3 rods with a the density of 57 to 95% of the theoretical density. Young's modulus was determined both by a sonic-velocity technique and by three-point bending test. The results from both measurements are presented in Figure 18. At $P < 0.4$, the bending modulus has a smaller value than the sonic modulus. This is due to the high porosity, causing local deformation and specimen damage under loading points.

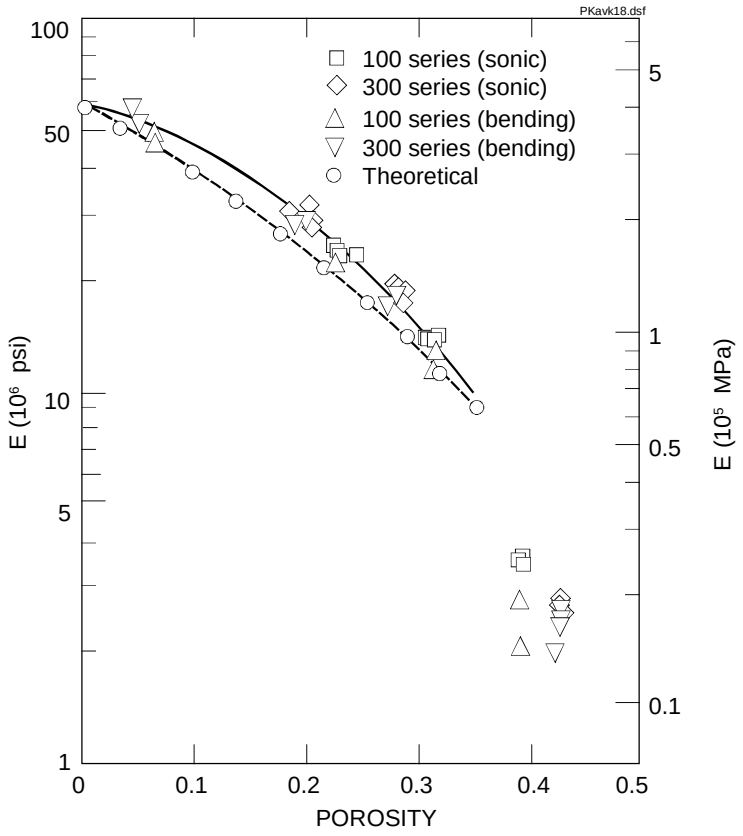

Figure 18. Young's modulus of alumina as a function of porosity. The solid curve is Equation (62) with an applicable porosity range from zero to 0.32. The dotted curve is a portion of the theoretical curve (Wang 1984b).

The solid line in Figure 18 has been determined from experimental data by a least-squares method using Spriggs' formula in form:

$$E = 4.01 \cdot 10^5 e^{-\left(1.46P + 9.82P^2\right)}. \qquad (62)$$

The dotted curve is a portion of the theoretical curve presented by Wang (1984a). The close agreement between the theoretical curve and the experimental results shows that the present model is realistic. Especially Spriggs' equation can be applied for both open and closed pores and for relatively small porosity ranges. It can also be applied to non-spherical particles (Wang 1984b). The effect of spherical pores on ultrasonic velocity has been

considered by Sayers & Smith (1982). At high concentrations the pores become interconnected and a model containing parallel cylindrical pores is recommended in this case. An additional model taking into account the shape of pores have been presented by Nielsen (1982).

1.6.2 Effect of pore shape on elasticity

Ledbetter et al. (1989) have studied the effect of the pore shape on the elastic constants. In the study, besides spherical pores, both randomly-oriented rod-shaped and disc-shaped pores are considered. The results show that the elastic properties depend strongly on the pore shape. Disc-shaped pores reduce elastic stiffness more than rod-shaped pores. Theoretical calculations suggest that porous alumina contains disc-shaped and ellipsoid-shaped pores instead of the cylindrical pores frequently suggested in the studies.

Ranachowski (1975) has shown experimentally that the porosity of samples of various compositions can be determined based on the measurement of the longitudinal ultrasonic wave propagation velocity. A diagram showing the relationships between the compositions of the materials and velocities at a given porosity will be necessary for this determination.

1.6.3 The effect of microcracking

The effects of micro-cracking on the propagation parameters are a strong increase of attenuation and a decrease in velocity. Numerous models have been proposed for the calculation of the average Young's modulus of a microcracked isotropic material. From Hasselman's equation (Hasselman & Singh 1979) for Young's modulus, the longitudinal wave velocity in a micro-cracked material may be written (Gault 1989):

$$V_L = \frac{V_{L_0}}{\sqrt{1+\frac{16ND_c^{\,3}}{9}}}, \tag{63}$$

where V_{L0} is the velocity in the non-cracked body assumed to be isotropic, N is the micro-crack density, and D_c the average diameter of the cracks.

A comparison of different formulae used for the calculation of the elastic properties of a solid containing voids or soft inclusions has been presented by Shin et al. (1993). The same type of formulae have been reported by several authors and therefore only two of the formulae for the calculation of the bulk modulus are presented here. Formula (64) originally presented by Okano (1960) and Formula (65) presented by Mackenzie (1950) are:

$$B = B_0\left(1 - \frac{3B_0 + 4G_0}{4G_0} P\right) \tag{64}$$

and

$$B = B_0\left(\frac{4G_0(1-P)}{4G_0 + 3B_0 P}\right). \tag{65}$$

In both these formulae B is the bulk modulus, G the shear modulus and P the volume fraction of voids in the material made up of a dispersion of voids in a homogeneous matrix. The corresponding modulus values for the matrix are B_0, and G_0. In both formulae it has been assumed that the shear and bulk modulus of inclusions are negligible in comparison with those of the substrate. Formula (64) is reported to be valid only for volume fractions < 0.3, and Formula (65) also for higher volume fractions.

1.7 Characterization of surface coatings and multilayer materials

Waves excited in a layered solid structure will be either bulk waves or leaky interface waves. The leaky waves can be in the form of leaky Rayleigh waves or layer waves, such as general Lamb waves. The reflection coefficient at the liquid-layered-solid interface has phase transitions corresponding to these modes. A leaky Rayleigh wave has a wave speed close to that of a Rayleigh wave in the substrate material when the layer is very thin. As the layer thickness is increased, the phase velocity decreases rapidly, and it reaches a minimum with a value lower than that of the Rayleigh wave in the layer material. As the

layer thickness is further increased, the wave gets faster and it approaches the speed of the Rayleigh wave in the layer material. When the layer material has a higher transverse speed than that of the substrate, only a single-mode leaky Rayleigh wave can exist. These layers will not support general Lamb wave modes (Atalar et al. 1990).

Atalar et al. (1991) have developed a technique for measuring the elastic parameters of layers supporting Lamb wave modes. The technique is based on using a bulk wave transducer with a varying angle to generate the incident wave in the liquid and another wedge transducer at a distance acting as a receiver. The separation of the transducers is such that the specularly reflected beam will not be intercepted by the receiver, but only those waves which couple to a mode traveling in the layers will cause an output in the receiver. By recording the detected signal amplitude, V as a function of incidence angle, θ_i, a characteristic curve, $V(\theta)$ is obtained. This curve has peaks corresponding to the phase transitions of the reflection coefficient at the liquid-layered-solid interface. The shape of the curve is highly dependent on the elastic parameters and thickness of the layers. If the shear wave velocity of the layer is higher than that of the substrate, only leaky Rayleigh waves are excited. In this case, $V(\theta_i)$ curves will have a single peak corresponding to the leaky Rayleigh wave (Atalar et al. 1991).

For layered media, there may be several transitions in the reflectance function phase. The number of transitions increase as the layer thickness increases. These fast phase variations arise from various modes excited in the layer. For a layer thicker than a few Rayleigh wavelengths, the substrate has a negligible effect on the microscope output. The layer thickness plays an important role for the generation and propagation of acoustic surface wave modes in investigations of the acoustic material signature of coatings. Therefore, three cases can be distinguished (Vetters et al. 1989).

(1) The layer thickness is very small in comparison with the wavelength of the Rayleigh wave in the substrate. In this case the layer causes a shift of the minima in the V(z) curve of the bulk material, due to surface acoustic wave dispersion dependent on layer thickness. The corresponding surface acoustic wave velocities can be determined by equation:

$$\Delta z = \frac{V_0}{2f\left(1-\sqrt{1-\frac{{V_f}^2}{{V_R}^2}}\right)}\ , \qquad (66)$$

where f is the ultrasonic frequency, V_R the Rayleigh wave velocity and V_f the sound velocity within the coupling medium. In very thin layers a linear correlation between the sound velocity and layer thickness is obtained.

(2) The layer thickness is greater than the wavelength of Rayleigh waves in the layer material. Then the periodicity of V(z) curve is mainly determined by the layer material.

(3) Intermediate layer thickness cause generation of higher SAW modes. Then the evaluation of the V(z) minima is not straightforward.

The definition of the penetration depth of the acoustic microscope has been given by Atalar (1985). According to this definition the acoustic microscope can penetrate a certain distance in a solid, if an inhomogenity of that distance below the surface gives a noticeable contrast change. The contrast behaviour of the microscope for objects with no lateral variation can be deduced from V(z) curves. By comparing the V(z) curve of the layer material with that of a similar layer of known thickness on a substrate, the penetration depth can be determined experimentally. It is important to observe that the difference between V(z) curves is negligible for a small value of z. The presence of the substrate through the layer is sensed because the surface waves that are mainly in the layer region are perturbed due to the skirts of waves extending into the substrate region. The perturbation of the surface waves becomes more pronounced when the interaction distance increases. However, the magnitude of the leaking surface waves will decrease as the surface waves travel longer distances in the solid medium. This will reduce the perturbation contribution at the transducer output. For most cases, the maximum difference between the V(z) curves stays more or less the same for a range of z values. The value of z should not be increased indefinitely because the resolution criterion must also be taken into account. The resolution can not be ignored in a penetration argument and therefore one should limit /z/ to a maximum value (Atalar 1985). Experimental studies by e.g.

Vetters et al. (1989), Matthaei et al. (1989) and Saurel et al. (1989) have shown that the Rayleigh wave penetration in the material is about one wavelength. When the layer is thicker than one wavelength, the substrate may not influence the results.

As the layer thickness is much smaller than the penetration depth of the surface wave, the velocity is a function not only of the layer quality but also of the layer thickness. Yamanaka et al. (1985) have shown that in samples having thin (< 2 μm) TiN coatings on steel, a linear relationship exists between the velocity increase ΔV_R and the thickness of the coating s. In this case a dimensionless parameter $\Delta V_R/s\omega$ provides a good measure of the film quality, where ω is the angular frequency of the acoustic wave. The experimental results show a good correlation between this parameter and the hardness of the coating. Thus the velocity of leaky surface waves provides a good measure of the hardness of the coating, if the thickness of the coating is known (Yamanaka et al. 1985).

The limited penetration depth of Rayleigh waves has been used to evaluate the depth of surface-opening cracks. The crack acts as a low-pass filter for the deeper portions of Rayleigh surface waves and the cut-off point for the "filter" can be related to the crack depth. The maximum reflection from a surface-opening crack is measured when the depth of the crack corresponds to the wavelength and the length of the crack is approximately the effective diameter of the ultrasonic beam (Fahr et al. 1984).

1.8 Integrity evaluation of the ceramic-metal interface

Conventional ultrasonic techniques can be used for evaluation of discontinuities on ceramic-metal interface. Both the pulse-echo and through-transmission technique can be used to reveal the presence of subsurface defects in thermally sprayed ceramic coatings. Many thermally sprayed coatings have a rather non-homogeneous layered structure, which strongly attenuates ultrasonic waves. The attenuation ultimately limits the thickness of coatings that can be successfully tested using ultrasonic techniques. The attenuation increases with frequency which determines the resolution of the ultrasonic imaging system. Hence, it is desirable to use the highest possible frequency ultrasonic waves to produce high resolution examinations of coatings. The very high attenuation of coating

material may, in some cases, be an advantage. Because the coating attenuation is very high, any variation in the signal found in an ultrasonic test is invariably caused by a change in the properties of the coating rather than by the substrate. Ultrasonic techniques are capable of detecting the presence of adhesion defects, porosity and thickness variations in thermally sprayed coatings (Almond 1982).

Ultrasonic techniques have been widely used to evaluate the integrity of joints consisting of ceramics bonded to ceramics or to metals. High-frequency ultrasonic technique using broadband excitation has been successfully used to detect discontinuities in brazed ceramic-metal joints (Kauppinen & Kivilahti 1991). If required, the lateral resolution can be improved by using narrow-band excitation (Pangraz et al. 1989). If the ceramic material will support elastic waves of a sufficiently high frequency, the signal from the opposite faces of the braze layer can be resolved, and it is then possible to determine directly whether the non-bond occurs at the ceramic-braze or braze-metal interface. The measurement of the transmission coefficient of Lamb waves has been used for evaluating the bond quality in butt-joint specimens (Simpson & McClung 1989). In this technique a Lamb wave is excited on one side of the joint and the amplitude of the wave on the second side is measured after propagation through the bond. The quantity determined by this measurement is the relative area of the bonded region, which is related to the prediction of shear strength.

2. Experimental investigations

2.1 Introduction

Based on the literature survey performed in connection of this work and earlier (Kauppinen 1991) it can be summarized that ultrasonic testing of ceramics has mainly been used as a quality control tool during the manufacturing of ceramic products and in the electronics industry to detect structural discontinuities in ceramic-metal joints in microcircuits. Acoustic microscopy has been mainly applied to thin ceramic films on various substrates to detect possible disbonding and to measure the elasticity or thickness of the coating. In relatively few studies ultrasonic techniques have been applied to thick ceramic coatings even though the industrial interest in using these types of coatings as thermal barriers or as protective layers in aggressive environments is increasing. As in thin coatings, the main interest in thick coatings is to assess the quality of bonding between the coating and the substrate, to detect structural discontinuities affecting the performance of the coating and to evaluate the elasticity. In principle the techniques applicable to thin coatings can be applied. However, the anisotropic structure of thermally sprayed coatings is not comparable, e.g., with the structure of CVD coatings and therefore the practical performance of measurements has to be totally modified.

2.2 Scope of experimental studies

The main target of the experimental work carried out was to study the applicability of different high-frequency ultrasonic techniques to the characterization of ceramic coatings of varying thickness and compositions. Several types of coating and substrate combinations were used in the experimental study because, from the point of view of the measurement technique, the problem is the same: how to characterize the brittle ceramic material bonded to a metallic surface?

For the evaluation of the integrity of ceramic materials different ultrasonic techniques were applied. The test materials were both bulk ceramics and thermally sprayed ceramic coatings with various thickness. The bulk ceramics

were used to study the ultrasonic evaluation of porosity. The main goal of the present work was the evaluation of the elastic properties and porosity of ceramic coatings. For this purpose, a new type of ultrasonic transducer was designed and constructed. The equipment, transducers and test materials used in the experimental work are described in the following section.

2.3 Equipment used in the measurements

2.3.1 C-mode scanning acoustic microscope (C-SAM)

The main part of the work was performed using a reflection-type high-frequency ultrasonic inspection system manufactured by Ultrasonic Sciences Ltd in the UK. The equipment used at VTT has been tailored according to the specifications given to the manufacturer, and therefore the equipment is not a pure commercial type.

The equipment shown in Figure 19 consists of 3 main parts: (1) an immersion tank with high-accuracy manipulators, (2) an ultrasonic unit with pulser-receiver cards and (3) a control and data acquisition unit.

The measurements are performed with the samples immersed in water and the ultrasonic transducer is moved to the area of interest with step motor driven X-Y-Z manipulators. One step of the motors corresponds to 7.5 μm which is the positional resolution of scanning movements. The scanning with transducer can be performed automatically by using the PC software included in the control unit. Scanning is possible both in the X-Y and the Y-Z planes. For preventing the corrosion of the samples, inhibitors are added to the water. During measurements the temperature of the water is +20°C. A single transducer or a frame carrying separate transmitter and receiver probes for through-transmission testing can be mounted to the probe holder of the manipulator. The probes used in the measurements were mainly commercial high-frequency probes manufactured by Panametrics (USA) or Krautkrämer GmbH (Germany). In order to reach the area of interest inside the samples, probes with different focusing distances were used. The position of the focus in the material was determined by adjusting the water path between the transducer and the sample

surface. The transducers used in each application are presented in connection with each particular measurement.

Kuva 1

Figure 19. C-mode scanning acoustic microscope C-SAM.

The ultrasonic unit contains two pulser-receiver cards; one for frequencies 0.5–20 MHz and the other one for frequencies 20–75 MHz. Additionally, the unit contains a gated-peak-detector, master-controller and A/D converter cards. If necessary, external ultrasonic equipment can also be connected to the system. In some applications a Krautkrämer USIP12 with a high-frequency unit USH100 was used. With this equipment combination frequencies up to 100 MHz can be used.

The control of the mechanical scanners as well as the adjustment of the ultrasonic equipment (attenuation control, damping, filtering, gating of signals etc.) is carried out using the control unit based on a 486 PC. The data acquisition software allows storage of full A-scan data (amplitude and time-of-flight) and enables presentation of results in conventional C-scan, B-scan or time-of-flight C-scan format. In C- and B-scan images, the echo amplitudes stored within the gate are presented in false colors. Thus the different colors seen on images correspond to echo amplitudes exceeding a certain height.

2.3.2 Acoustic microscope (SAM)

The measurement of Rayleigh wave velocities in thin ceramic coatings was performed in Fraunhofer Institute for Nondestructive Testing in Saarbrücken, Germany. The equipment used was a scanning acoustic microscope of type ELSAM, manufactured by Leica. The operating frequency of this device was 1 GHz and the measurements were performed by using the V(z) technique. Because the wave length, and thus the penetration depth of Rayleigh waves in ceramics, is with this frequency only a few microns the measurement of sound velocity in volumes of some hundreds of μm^3 can be performed. In the measurements a drop of distilled water (T = 21°C) between the acoustical lens and the specimen was used for coupling. The measurement principle is shown in Figure 20.

Based on the V(z) curves measured, the software of the equipment automatically calculates the corresponding Rayleigh wave velocities. The same technique can also be used for the measurement of the velocity of skimming longitudinal waves.

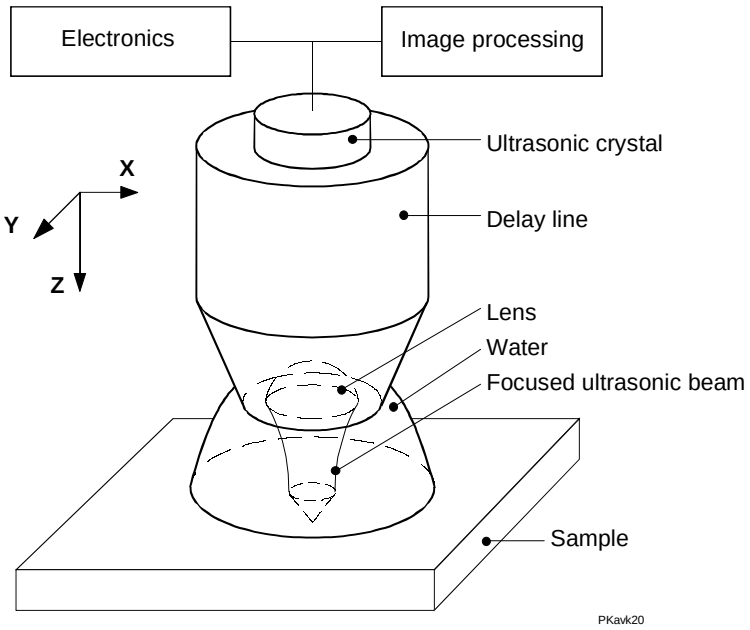

Figure 20. Scanning acoustic microscope ELSAM.

2.3.3 Conventional ultrasonic equipment

In some cases the measurements were performed using conventional laboratory ultrasonic equipment (Krautkrämer USIP12). The equipment was used, e.g., in cases where the immersion of samples was not possible due to the adverse effect of water penetration into the sample. In these cases a contact-type ultrasonic transducer was used with ultrasonic gel as couplant. This technique was mainly used in measurement of sound velocities in porous bulk ceramics.

2.4 Specimens used in the measurements

2.4.1 Bulk ceramics

In order to assess the applicability of ultrasonic techniques for the determination of porosity of bulk alumina, two samples with different porosity fractions were

used. The samples were received directly from the manufacturer of fine ceramics and, according to the material specification given, the composition was 99% pure Al_2O_3. The variation in porosity fraction was due to different level of sintering. Both samples were plates and therefore ideal for the measurement of sound velocities. The porosity of the samples was determined from dimensional measurements and by measuring the weight of the samples. The details of the samples are given in Table 3 summarizing the results of measurements.

2.4.2 Thick thermally sprayed coatings

Steel plates (185 × 50 mm) having thick (3000–5000 μm) thermally sprayed alumina coatings were used to study the integrity of the coating under bending loads. The exact composition of the coating material was not given by the manufacturer, but based on the EDS analysis the material was Al_2O_3+TiO_2 and some minor impurities. From the ultrasonic point of view the exact composition of the coating is of minor importance. Most of the specimens were delivered by the Finnish industry. Additionally some reference specimens were received from Osaka University, Japan. Altogether 15 samples were studied.

For the evaluation of porosity and elasticity of thick thermally sprayed coatings, samples with alumina, tungsten carbide or chromium carbide based cermet (80% Cr_3C_2, 15% Ni and 5%Cr) coatings were used. The details of these coatings are given in Table 1.

The thicknesses given in the table were measured using Förster Monimeter 2.094. As can be seen from the table, the thickness of the coating varied markedly in most of the specimens. The sound velocities in each specimen were measured in the central area where the thicknesses were close to the maximum values given in the Table 1.

Table 1. Specimen used in measurements.

Specimen code	Material	Thickness [μm]	Substrate material	Coating process	Manufacturer/ Supplier
AL4500	alumina	4500	steel plate	plasma	Osaka Univ.
AL500	alumina	320	steel plate	plasma	TTKK
AL1000	alumina	770	steel plate	plasma	TTKK
AL1500	alumina	1220	steel plate	plasma	TTKK
AL2000	alumina	1700	steel plate	plasma	TTKK
Cr-1	cermet	550-600	steel plate	HVOF	VTT
Cr-2	cermet	400-650	steel plate	HVOF	VTT
Cr-3	cermet	120-300	steel plate	HVOF	VTT
Cr-4	cermet	130-300	steel plate	HVOF	VTT
Cr-5	cermet	600-1650	steel plate	HVOF	VTT
Cr-6	cermet	150-2400	steel plate	HVOF	VTT
Cr-7	cermet	250-1600	steel plate	HVOF	VTT
P-1-55	cermet	55	steel tube	HVOF	VTT
P-1-60	cermet	60	steel tube	HVOF	VTT
P-1-120	cermet	120	steel tube	HVOF	VTT
P-1-180	cermet	180	steel tube	HVOF	VTT
P-1-270	cermet	270	steel tube	HVOF	VTT
P-1-330	cermet	330	steel tube	HVOF	VTT
P-1-370	cermet	370	steel tube	HVOF	VTT
P-1-400	cermet	400	steel tube	HVOF	VTT
P-1-470	cermet	470	steel tube	HVOF	VTT
CHR-V1	cermet	300	steel plate	HVOF	VTT
CHR-V2	cermet	150	steel plate	HVOF	VTT
CHR-V3	cermet	500	steel plate	HVOF	VTT
WC36-1	tungsten carbide	150-200	steel plate	HVOF	VTT
WC36-2	tungsten carbide	200-250	steel plate	HVOF	VTT
WC36-3	tungsten carbide	190-230	steel plate	HVOF	VTT
WC36-4	tungsten carbide	180-225	steel plate	HVOF	VTT

2.4.3 Thin thermally sprayed coatings

The thin alumina coatings (< 1000 μm) were produced by different techniques of thermal spraying: plasma spraying, detonation and the high-velocity-oxygen-fluid (HVOF) technique. The composition of most coatings was similar to the thick coatings: Al_2O_3 + TiO_2.. The details of the specimens are given in Table 4. In order to improve the bonding between the steel substrate and coating, the steel plates had been sandblasted before thermal spraying. In thin coatings (< 100 μm) the roughness of the surface after sandblasting was such that ultrasonic measurement was not possible due to the strong scatter of ultrasonic waves from the rough interface between the coating and the substrate.

2.5 Development of a line-focused low-frequency transducer

2.5.1 The principle of a line-focused transducer

The line-focused beam technique was originally developed by Kushibiki and Chubachi (1985). The structure of the acoustic line-focus-beam sapphire lens is presented earlier in Fig. 15. As can be seen from the dimensions, this lens produces a microscopic focal area and can therefore only be used for measurement of the sound velocity in a very small local area. As with the spherical lens of the acoustic microscope used here in the experimental measurements, the use of a line-focus-beam lens of this type for measurement of sound velocities in porous coatings would lead to a very large dispersion of results. One method to overcome this problem is to use an arrangement with separate transmitter and receiver probes. By adjusting the tilt angle of both probes, the angle of total reflection of sound energy emitted by the transmitter probe can be found. As described earlier, this method is based on the reflection properties of a liquid-solid boundary only, and not on the measurement of propagation characteristics in the sample itself (Mayer 1960). Also the probe arrangement is rather complicated and the construction of the probe frame clumsy in practical measurements as can be seen in Fig. 21 showing a two-probe frame constructed at VTT.

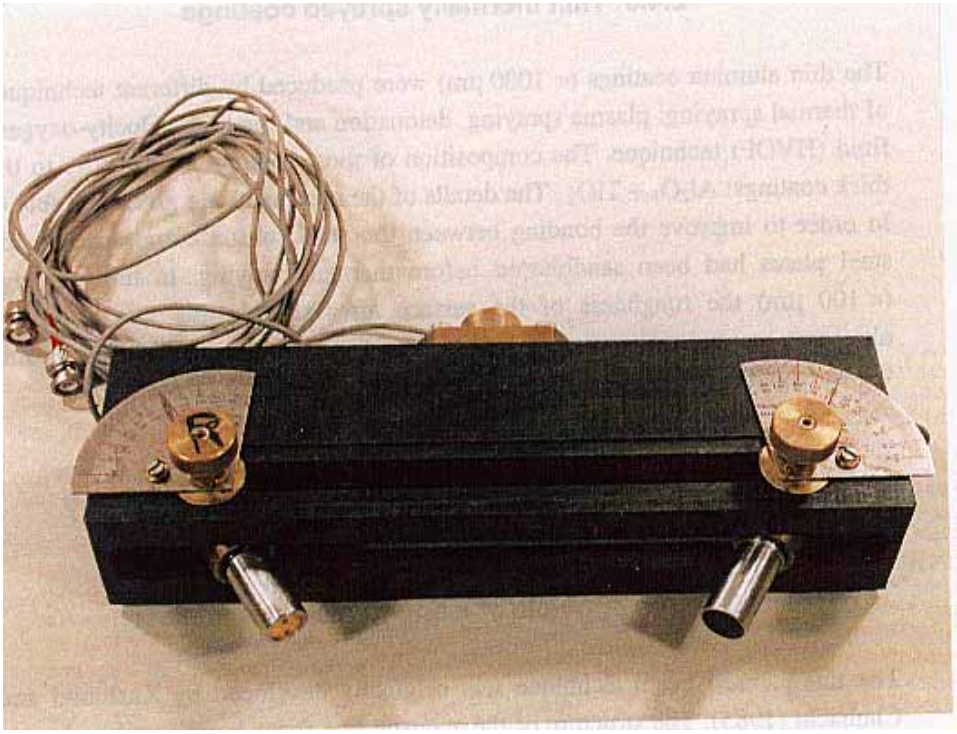

Figure 21. A two-probe frame constructed for the measurement of angle of total reflection.

2.5.2 The low-frequency large aperture transducer

In this work a totally new type of ultrasonic transducer was designed and constructed.

The structure of the line-focused transducer constructed is schematically shown in Fig. 22.

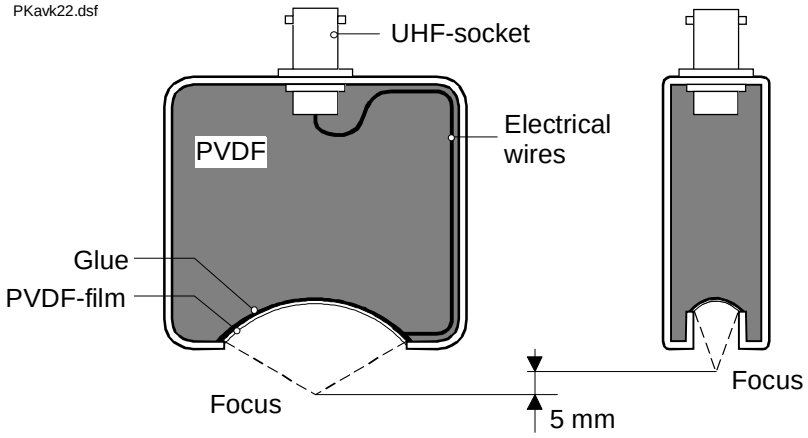

Figure 22. The construction of the line-focused low-frequency transducer.

Besides the dimensions and operating frequency, the basic difference between the probes used in acoustic microscopy (Gilmore et al. 1989, Atalar 1979, Kojima 1989) and the probe designed here is that in the new construction no separate focusing lens is needed. The ultrasonic beam is focused to the required depth by using, as an active element, a rectangular-shaped piece of polyvinylidene fluoride (PVDF) film that has been glued on the cylindrical convex surface of the probe body. The flexibility of the PVDF film allows bending to the curvature needed for required focusing. The radius of the curvature was 20 mm and the aperture angle of the probe 120°. Kushibiki & Chubachi (1985) have used a sapphire lens with a cylindrical concave surface to create a line-focus beam. In the present work a narrow-line-focus was created by bending the rectangular piece of film also in its width direction (Fig. 22). The curvature was adjusted to focus the beam in this direction at a distance 5 mm shorter than in the other direction. Thus the focus of the probe was a narrow line after defocusing the probe by 5 mm. The probe body was manufactured from bulk PVDF material that was machined to the shape of the final probe. By using the PVDF body as backing material, the matching problems between the film and the body could mainly be avoided. In order to further improve the match a copper-acrylate coating was glued on both sides of the PVDF element. Figure 23 shows schematically a cross-section of the matching layers used in the first prototype transducers. No electrical matching was used.

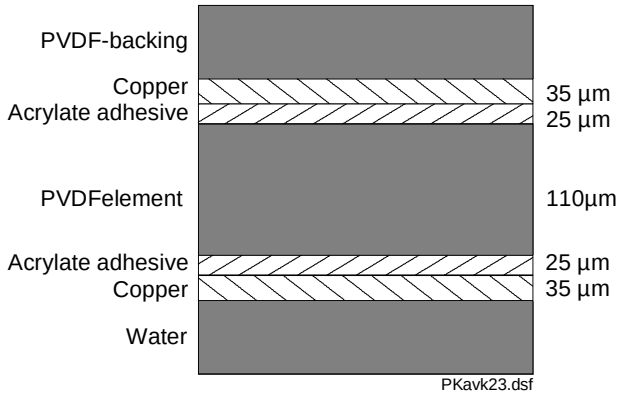

Figure 23. Schematic cross-section of the prototype transducer.

In order to optimize the transducer and to increase the central frequency from the original 6 MHz to 10–15 MHz, a theoretical study and necessary calculations were made. The impedance and insertion loss curves were calculated for a case where the transmitted sound is reflected back to the transducer. The calculations showed that in the optimal construction, no copper layers should be used for matching. Figures 24 and 25 show the 2-way insertion loss curve and the impedance curve of a transducer where copper layers are not used for matching.

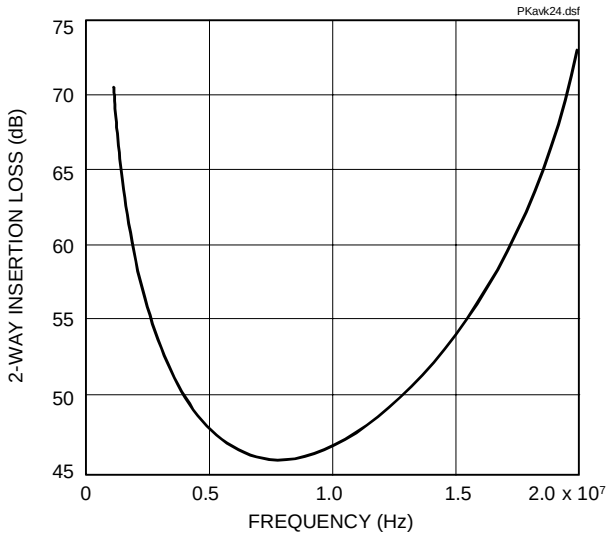

Figure 24. The 2-way insertion loss curve for a transducer having no matching layers.

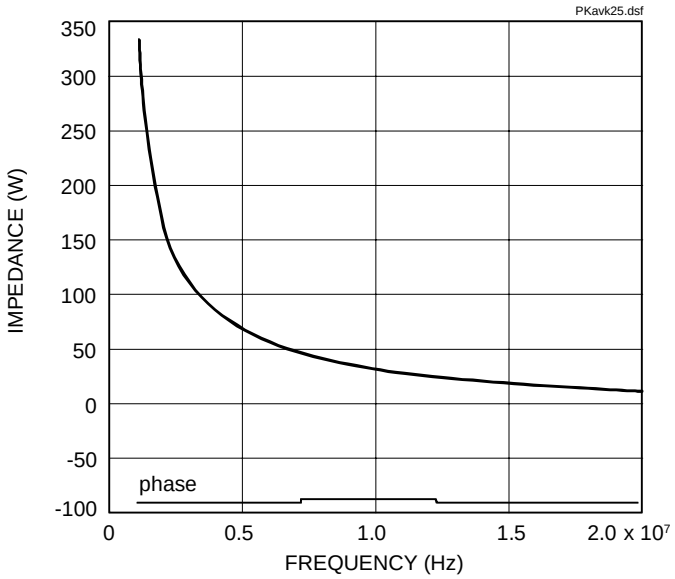

Figure 25. The impedance curve for a transducer having no matching layers.

One of the surfaces of the body was machined to the curvature necessary to focusing of the beam. Small holes were drilled in the body for the thin electrical wires connecting the PVDF film to the cable socket. The wires were fixed on the upper and lower surfaces of the film using electrically conductive adhesives and tapes. Finally, the whole probe assembly was covered with a watertight housing made of stainless steel or aluminum. The probe housing contained a watertight UHF socket from where there cables were connected to the ultrasonic unit of the measurement system. The piezoelectric films used in the experimental probes were SOLEF P(VDF-TrFE) 75/25 copolymer films manufactured by SOLVAY & Cie S.A. The effective sizes of the rectangular films were 40 mm × 10 mm and 25 mm × 10 mm. The thickness of the film having 700 Å thick metallized Au layers on both surfaces was 110 μm. The nominal frequencies of the films used were 10 MHz and 32 MHz. The adhesive used in electrical contacts was a two-component silver epoxy ELECOLIT 325.

The final experimental probes constructed are shown in Fig. 26.

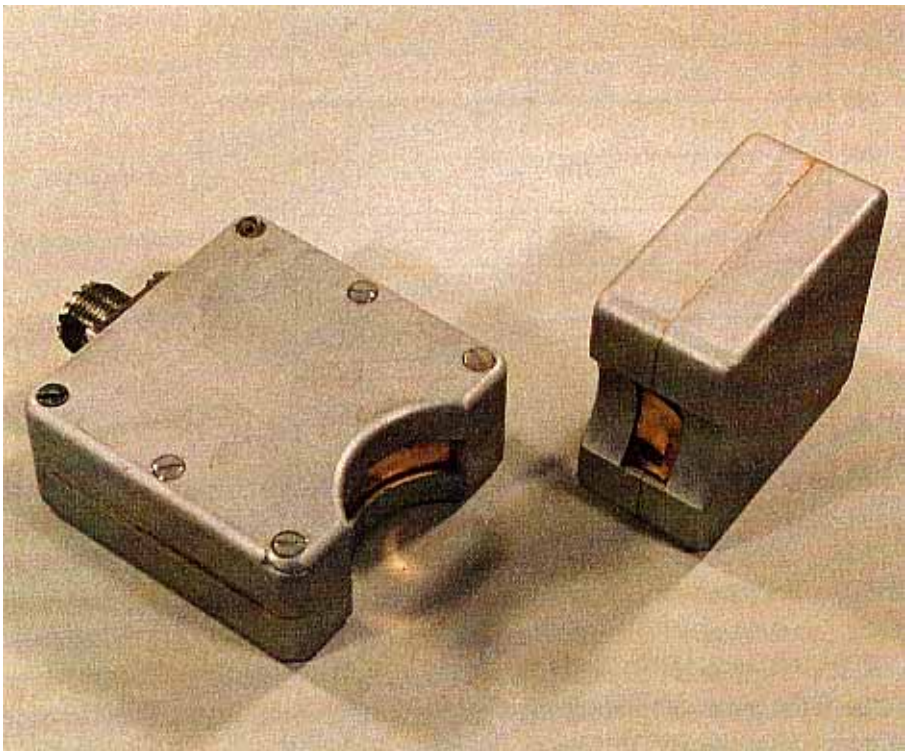

Figure 26. The experimental probes used in the measurements.

2.5.3 Determination of sound velocities using a wide-aperture transducer

The ray paths of a defocused wide-aperture probe are schematically shown in Fig. 27.

A common approach to surface wave velocity measurement with acoustic microscopy is to monitor the difference in arrival times of pulses propagating along ray paths a - b - d - e and f - c - f in Fig. 27. Similar approach has been used by Gilmore et al. (1989). The time difference is calculated by a simple consideration of difference in path lengths and wave velocities.

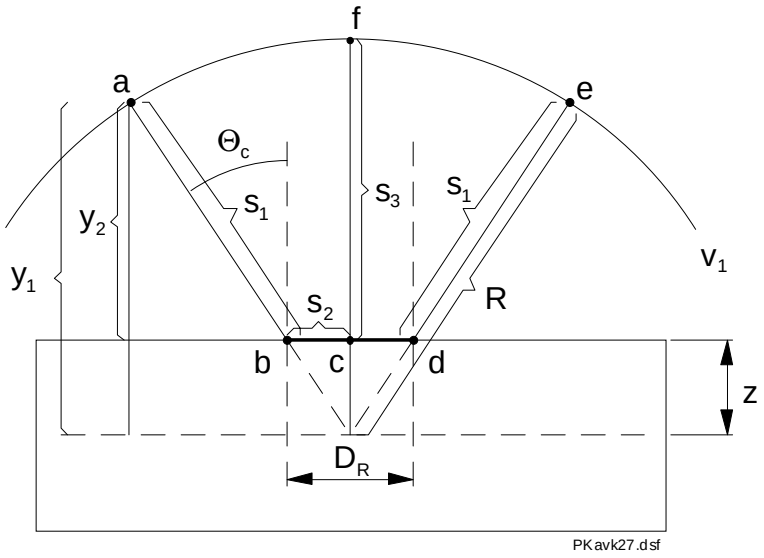

Figure 27. Ray paths of a defocused wide aperture PVDF probe.

Let the velocity of longitudinal waves propagating from transducer to the test material through the contact liquid be V_1 and the propagation velocity in the test material V_2. In Fig. 27 the ultrasonic beam hits the surface of the material at the critical angle θ_c of Rayleigh waves. The diameter of the entry circle (D_R) where the incident pulse is mode converted into a leaky Rayleigh wave is:

$$D_R = 2z \tan\theta_c \,. \tag{67}$$

Then according to Snell's law:

$$\theta_C = \arcsin\left(\frac{V_1}{V_2}\right). \tag{68}$$

We consider the ultrasonic ray propagating from the transducer to the material following the path a - b - c - d (Fig. 27). Thus we neglect the mode conversions from surface wave to longitudinal waves in all other areas except at point r. On the central axis of the transducer (f - c), a direct reflection from the surface of the material occurs. The focus point of the transducer is assumed to be at depth z in the material (Fig. 27).

The difference in the time-of-flights between the ultrasonic rays propagating along paths f - c - f and a -b - c - d can be determined by the following trigonometric consideration:

From Fig. 27 we get

$$y_1 = R\cos\theta_C \tag{69}$$

and

$$y_2 = R\cos\theta_C - z\,. \tag{70}$$

Thus sound path S_1 is equal to:

$$S_1 = \frac{R\cos\theta_C - z}{\cos\theta_C} \tag{71}$$

and sound path S_2 equals to:

$$S_2 = z\tan\theta_C\ . \tag{72}$$

The direct sound path S_3 is:

$$S_3 = R - z\,. \tag{73}$$

The time-of-flight (t_1) of the sound beams following the path a - b - c - d is

$$t_1 = \frac{2S_1}{V_1} + \frac{2S_2}{V_2} \tag{74}$$

and

$$t_1 = \frac{2R\cos\theta_C - z}{V_1\cos\theta_C} + \frac{2z\sin\theta_C}{V_2\cos\theta_C}\ . \tag{75}$$

From Formula (31) we get

$$t_1 = \frac{2R}{V_1} - \frac{2z}{\sqrt{1-\left(\frac{V_1}{V_2}\right)^2}}\left(\frac{1}{V_1} - \frac{V_1}{V_2^{\,2}}\right). \qquad (76)$$

The time-of-flight (t_2) of the sound beams following the route f - c - f is

$$t_2 = \frac{2(R-z)}{V_1}\ . \qquad (77)$$

Thus, the time difference $\Delta t = t_1 - t_2$ is equal to

$$\Delta t = \frac{2z}{V_1} - \frac{2z}{\sqrt{1-\left(\frac{V_1}{V_2}\right)^2}}\left(\frac{1}{V_1} - \frac{V_1}{V_2^{\,2}}\right). \qquad (78)$$

2.5.4 Characterization of the experimental transducers

After construction, the pulse shapes and central frequencies of the transducers were measured. The results of one of the probes are shown in Fig. 28. As can be seen, the probe transmits a relatively short broadband pulse having a central frequency from 2 to 5 MHz. Thus the central frequency of the probe is essentially lower than the nominal frequency of the PVDF film used as active element.

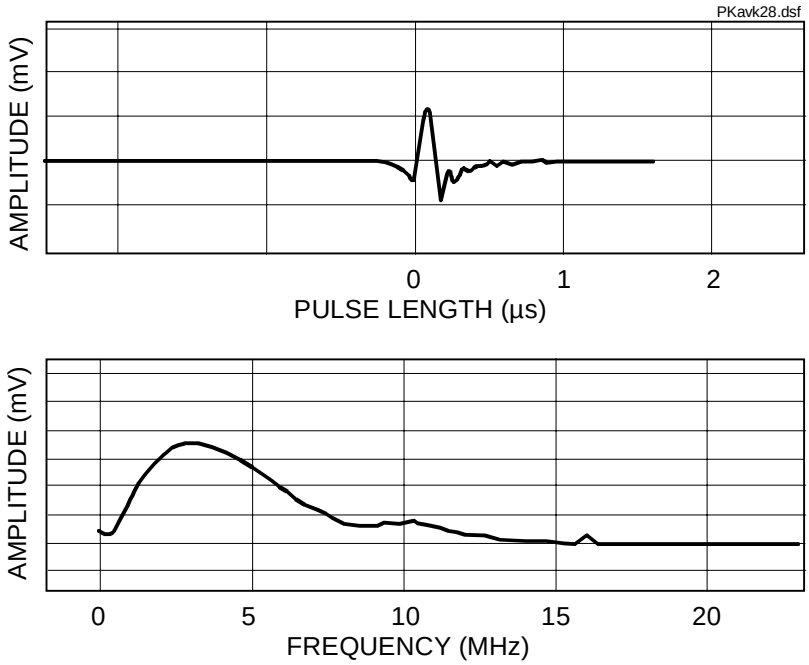

Figure 28. Pulse shape of the 10 MHz transducer: (a) Pulse in time domain. (b) Pulse in frequency domain.

The proper operation of the probes was studied by performing measurements with materials for which the sound velocities are known. The test materials were: carbon steel, stainless steel and copper. The sound velocities were measured by using the application of V(z) technique presented by Gilmore et al. (1989). The results are very close to the values given in the literature. Only in the case of stainless steel a remarkable difference was noticed. This is presumably caused by different microstructures of the materials compared. The detailed specification of the material is not given in the literature. The results are shown in Table 2.

Additionally, the sound velocity in perspex was measured. Because the Rayleigh wave could not be created on a water-perspex interface, the velocity of lateral (longitudinal) wave was measured. The measured velocity (2686 m/s) corresponds to the value given in literature (2700 m/s).

Based on the experimental characterization of the prototype probes it could be concluded that the probes can be used for the measurement of Rayleigh wave velocities using V(z) technique. In materials where the sound velocity is very low, the propagation velocity of skimming longitudinal (lateral) waves can be measured. In layered materials, different modes of surface acoustic waves can be excited. This will be discussed in connection of experimental measurements.

Table 2. The propagation velocities of Rayleigh waves in various known materials. The measured velocities and velocities given in the literature (Briggs 1985).

Material	**V_R (measured) m/s**	**V_R (literature) m/s**
carbon steel	2977-3027	2996
stainless steel	2819	3048
copper	2173	2171

2.6 Evaluation of porosity of bulk ceramics

2.6.1 Measurement technique

The validity of the experimental correlation Formulas (79)–(80) presented by Roth et al. (1990) were tested by measuring the sound velocities in bulk ceramic specimens specified in Table 3. The measurement of shear (V_S) longitudinal (V_L) wave velocities was performed using ultrasonic contact probes and Krautkrämer USIP12 ultrasonic equipment. In the measurement the pulse-echo technique and echo overlap method (Hull et al. 1985) was used. From the sound velocities the porosity was calculated by using the following formulas (Roth et al. 1990):

$$V_L = -0.018xP(\%) + 1.11 \tag{79}$$

and

$$V_S = -0.011xP(\%) + 0.703\,. \tag{80}$$

The sound velocities V_L and V_S in formulas (79) and (80) are expressed in 10^4 m/s.

2.6.2 Results

The results are summarized in Table 3.

Table 3. Details of the bulk ceramic specimens. Sound velocities, calculated porosities (P_C), porosities determined from weight and dimensional measurement (P_M).

Specimen	Dimensions [mm]	V_L [m/s]	V_S [m/s]	P_C [%]	P_M [%]
1	$41.5 \times 41.5 \times 7.8$	2583	1982	45.9 - 47.3	46.3
2	$51.9 \times 30.4 \times 2.4$	10950	-	2.8	3.2

As can be seen from the table, the porosity values determined from the propagation velocities of ultrasonic waves are very close to the values determined from the weight and dimensional measurements of the samples.

2.7 Integrity of thick ceramic coatings under bending loads

2.7.1 Measurement technique

The integrity of thick (> 3000 μm) ceramic coatings sprayed on thick (> 5 mm) steel substrates was examined after different levels of bending loads.

The bending of specimen 185 × 50 mm was made with 4-point bending. The distance between the outer supporting rolls was 120 mm and those of inner rolls 80 mm. The bending test was conducted at a cross-head speed of 1 mm/min in the bending fixture. Freely tilting rolls were used as specimen supports, and the deflection of the central part of the specimen was measured during bending by means of a riding fixture with LVDT (Linear Variable Difference Transformer).

The longitudinal surface strains were also measured by two strain gauges on the central part, one gauge on the steel side and one on the coating side of the specimen.

The specimens were examined both before bending and after bending by using the through-transmission technique and the C-SAM equipment. For comparison of the techniques, some of the damaged specimens were also measured by the pulse-echo technique. In the through-transmission technique separate transmitter and receiver transducers are placed on opposite sides of the sample and the ultrasonic energy passing through the sample is monitored (Krautkrämer & Krautkrämer, 1983). The probes were mounted on a fixed frame in order to assure parallel movement of probes on different sides of the specimen. The scanning was made automatically and the amplitudes measured in each point of the scanning area were presented in a C-scan image combining the position data of the probes and the corresponding amplitude data. The amplitude data is presented in colors that correspond to a certain height of amplitude. In the images, the structural discontinuities can be clearly seen due to the local change in amplitude (color) in the image. The sizes of the discontinuities can not be directly measured from the images because their sizes are strongly overestimated due to the beam opening of the transducer and other transducer parameters. The probes used in the measurements were a flat (not focused) 5 MHz probe type Panametrics V309 and a similar focused probe Panametrics V309F2". The water path between the probe and specimen was 50 mm.

For the evaluation of the elastic properties of the coating, the velocity of both longitudinal and transversal ultrasonic waves in the coating was measured by using the first-arrival-time method. The experiment was made with specimen of 5 mm thick thermally sprayed alumina-based coating on 19 mm ferritic steel provided by Osaka University, Laboratory of Mechanics on Materials/ Structures, Japan (Auerkari et al. 1991).

2.7.2 Results

In the baseline examination, relatively large differences in the ultrasonic attenuation of different specimens were recorded. Even in each specimen the local variations of attenuation were large, which is presumably caused by the inhomogeneous structure of the coating and differences in the bonding between

the coating and substrate. Also the unfavorable preparation of samples caused spurious indications, e.g., due to some grinding scratches on the back surface of the substrate plate.

In the following the results of ultrasonic examinations after various levels of bending are analysed. The results of all samples are not presented, but the most representative ones have been selected. In some of the samples the coating was totally damaged already in the first bending experiment and ultrasonic examination was therefore of no interest.

In Figure 29 the C-scan images of sample A12 before bending and after various levels of bending are presented. The bending forces in this case are 2 kN, 3 kN and 3.5 kN. In the baseline image (A) the structure of the sample looks relatively homogeneous although a couple of minor discontinuities (1 and 2) can be seen in the image. The discontinuity (3) in the image is caused by a grinding defect on the back wall of the sample. After bending with 2 kN (image B) some minor changes in these discontinuities can be noticed, and especially the echo amplitude from discontinuity (2) has strongly decreased. Image C has been made after 3 kN bending, but here a slightly different transducer has been used and therefore direct comparison with images A and B is not possible. However, in image C the discontinuities (2) and (3) can be clearly seen. The bending load of 3.5 kN has caused cracking in the sample, as can be seen in image (D). Based on the analysis of images A, B and D it can be confirmed that the crack (4) is exactly at the location of discontinuity (2) in images A and B. This result shows that the initiation of a critical crack is caused by structural discontinuity (fabrication defect) in the coating.

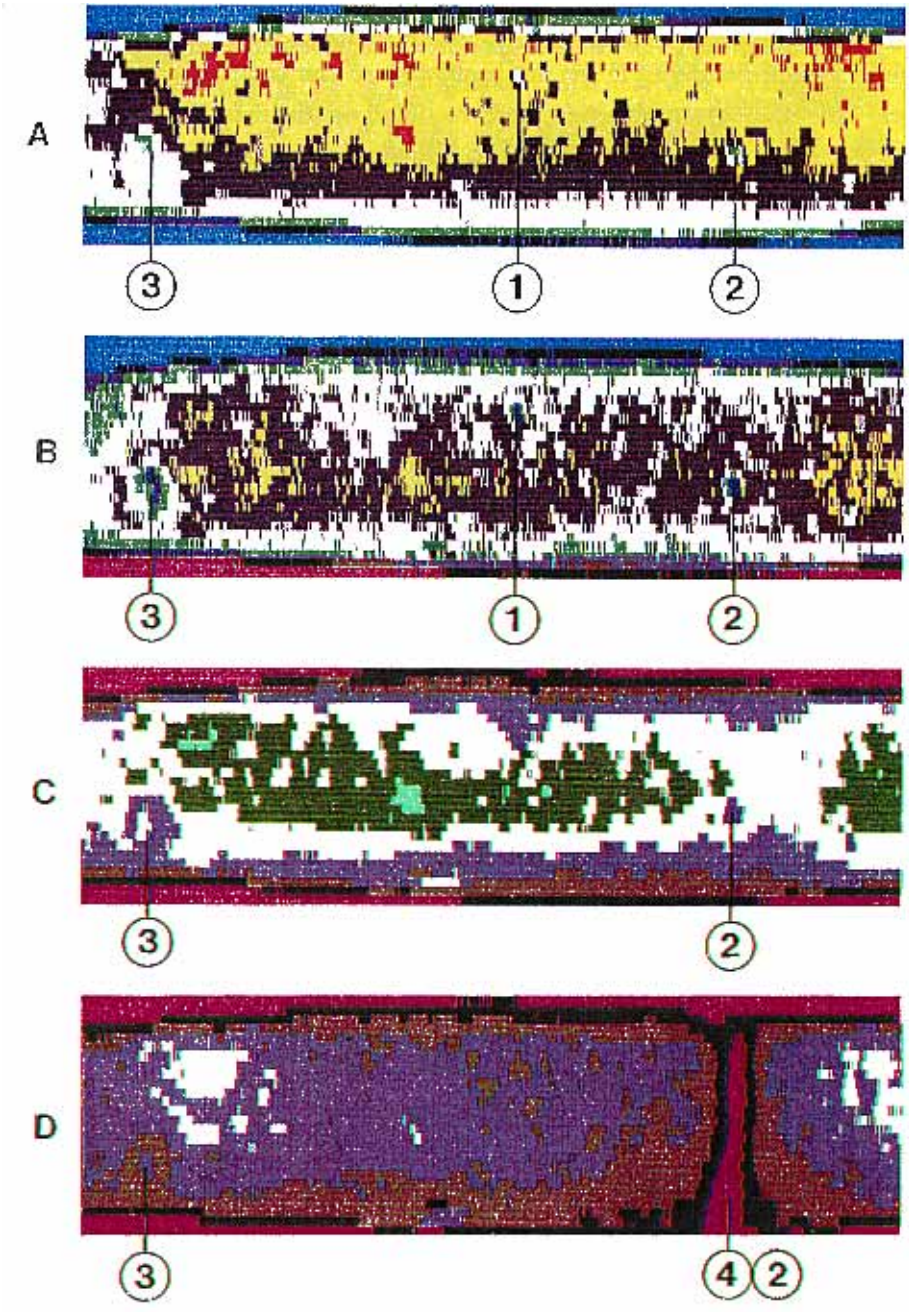

29. C-SAM images of sample A12 after various levels of bending.

In Figure 30 the C-scan images of sample A13 have been presented. In this sample a grinding defect (1) on the back wall of the sample is visible in all images. No other discontinuities were recorded in the baseline examination (image A). After bending with 3 kN the initiation of cracks (2, 3, 4) from the edges of the sample has occurred (image B). After increasing the force up to 3.5 kN the cracks have propagated towards the middle of the sample (image C). Additionally, two new cracks (5 and 6) are formed. Bending with 4 kN finally causes the growth of cracks (3) and (4) together across the width of the sample and totally damages the coating (image D). Looking carefully the images A and D it can be assumed that the minor discontinuities acting as starting points for cracks 2, 3 and 4 were already existing before the bending. It is, however, not possible to analyse the edges of the sample in image A for very small discontinuities, due to the random scattering of ultrasonic waves from the edges of the sample.

In Figure 31 the ultrasonic images of sample B3 are presented. In image (A) which shows the sample before bending, no discontinuities are visible and the structure of the sample looks homogeneous. After bending with 3 kN no damages can yet be seen in image (B). The cracking (1, 2, 3) has started from the edges of the sample after bending with 4 kN as can be seen in image (C). Increasing the bending load to 4.5 kN causes the growth of cracks (1, 2, 3) and the formation of a new crack (4). It is interesting to notice that in this case the cracks propagating from different edges of the sample (e.g. 2 and 3) do not grow together in the middle of the sample, but grow parallel to each other (image D). As in sample A13, also here the first two cracks are starting from locations where a small discontinuity is visible already in the image (A), but the edge area of the sample can not be reliably analysed.

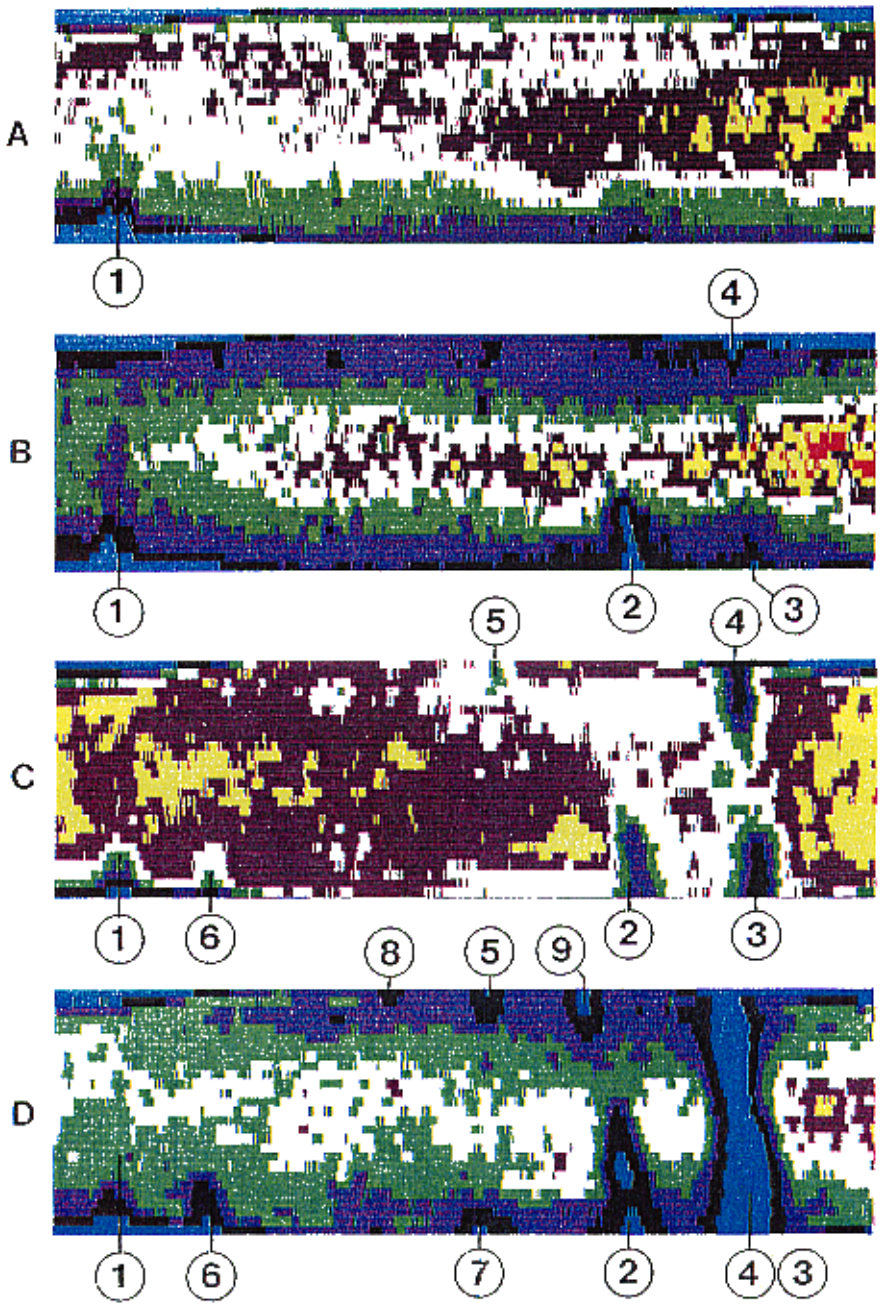

30. C -scan images of sample A13 after various levels of bending.

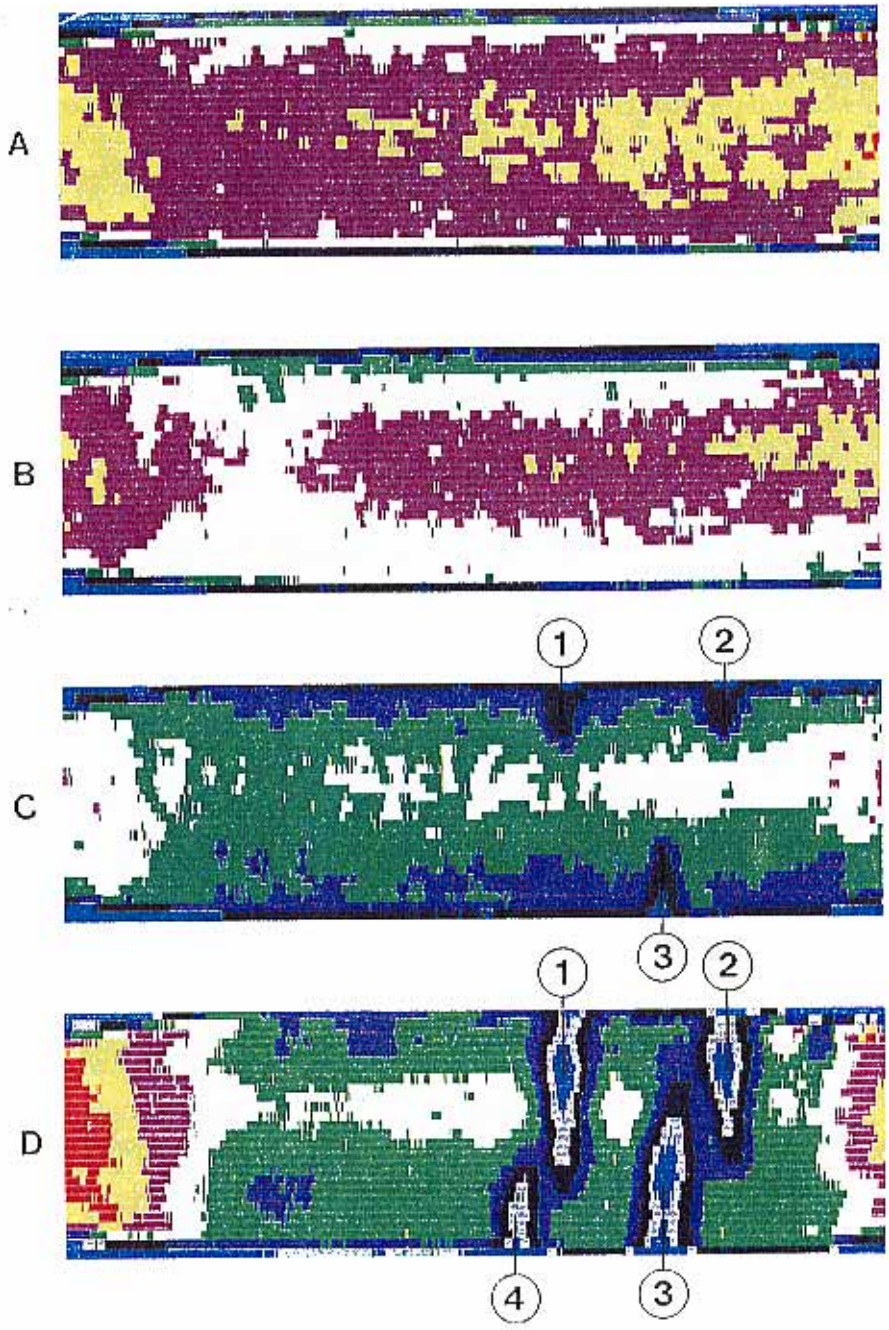

Figure 31. C -scan images of sample B3 after various levels of bending.

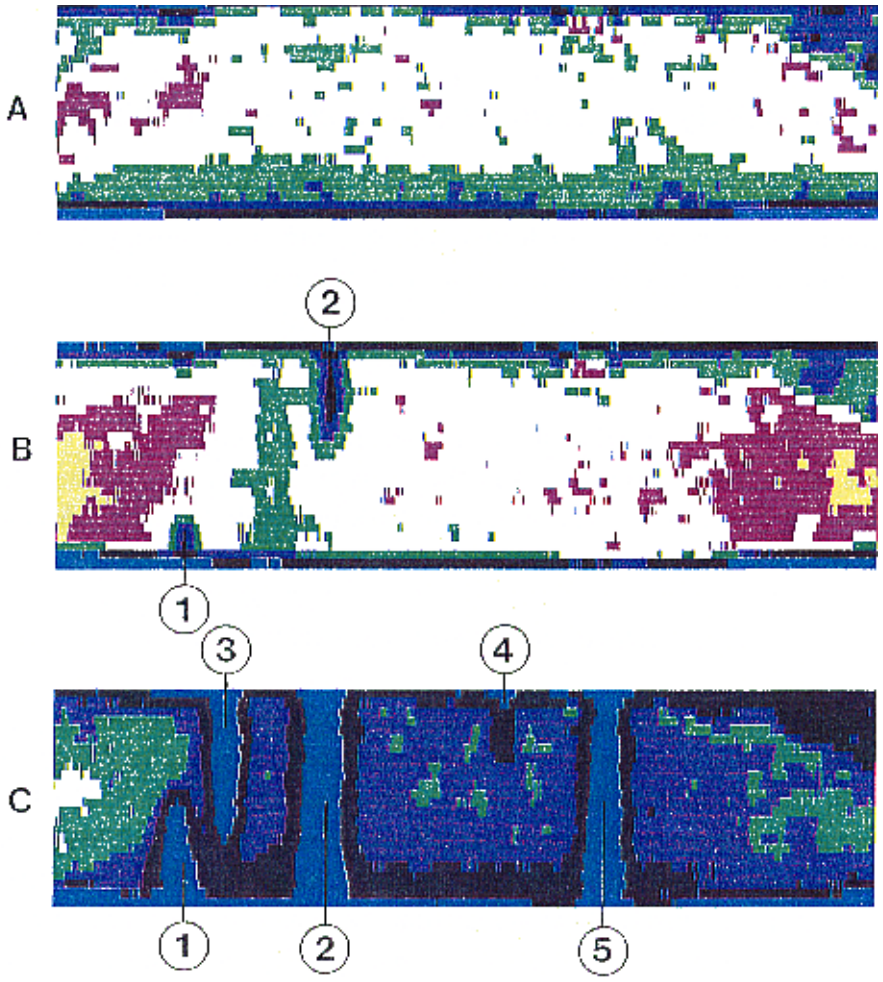

Figure 32. C -scan images of sample B4 after various levels of bending.

The ultrasonic images of sample B4 are presented in Figure 32. In the baseline image (A) no remarkable discontinuities are seen. In image (B) two cracks (1, 2) starting from the edges of the sample after bending with 4 kN are detected. Total damage of the coating has occurred in bending with 4.5 kN (image C). Crack (2) has grown across the sample and three new cracks (3, 4, 5) are formed. Crack (5) has rapidly grown across the sample because no indication was detected at this location in image (B). Even in the post-analysis of images (A) and (C) no

discontinuity can be seen at the position where the cracks start from the edges of the sample.

2.8 Elasticity and porosity of thin ceramic coatings

The main target of this part of experimental work was to study the possibility to use acoustic microscopy to evaluation of elasticity and porosity of thin (< 1000 μm) ceramic coatings. The material of all thin coatings was alumina.

2.8.1 Microstructure of samples

Optical microscopy was primarily performed for the determination of the thickness of different coatings. From the cross-sections of the coating the microstructure can also be seen. In order to have more information, SEM and EDS analysis was performed to selected samples.

2.8.2 Ultrasonic measurement technique

The evaluation of elasticity and porosity of coatings was based on the measurement of the propagation velocity of surface acoustic waves (SAW) in the coating. Based on this velocity, both parameters were evaluated. The first measurements were made by using the scanning acoustic microscope described in 2.3.2. The samples studied were 11 alumina coatings having various thickness varying from approximately 50 μm to 600 μm. The coatings were manufactured from practically identical powders by plasma spraying, detonation and the HVOF technique. The measurements were made by using the V(z) technique described in 1.4.4. Due to the very low thickness of the samples, the other techniques for measurement of sound velocity were considered to be unreliable and were not used. The frequency used in the measurements was 1 GHz. Because the wavelength of the Rayleigh waves in alumina at this frequency is only about 5 μm, which is also the penetration depth of effective Rayleigh waves, even the thinnest coatings could be measured without the influence of substrate. The drawback of using a very high frequency is that the surface of the sample had to be carefully polished and was therefore not in the normal ”as manufactured” condition. Also the use of a strongly focused acoustical lens restricts the area covered in one measurement. The focus diameter of the lens

used was about 30 μm and thus each measurement result represents only a very small local area on the sample surface. The behavior of ultrasonic waves in the material examined and in the water drop creating the acoustic contact between the lens and the material is schematically illustrated in Figure 33.

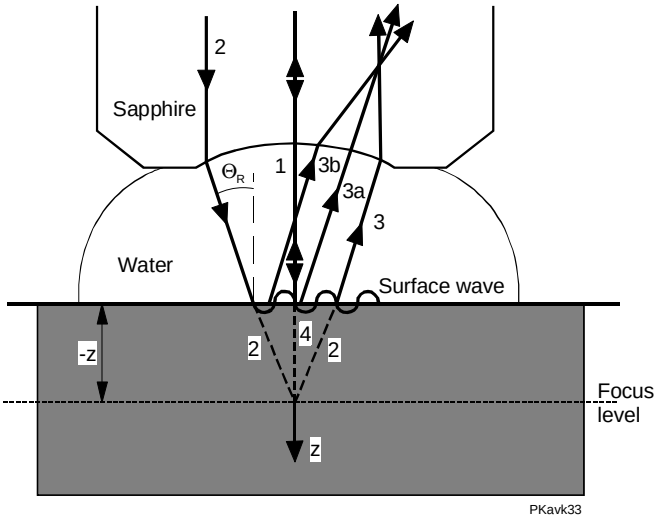

Figure 33. Reflection of ultrasonic waves and formation of surface waves in acoustic microscopy.

In order to have more representative results for each sample, the measurement was made at 3 points randomly selected and the measurement was made 3 times at each point. In several cases, additional samples were prepared from the original material in order to have more representative results for each coating. The software of the measurement system produced the V(z) curve from each measurement, and based on the distance between two minima of the curve, the software calculated the velocity of the Rayleigh wave using Formula (53). Originally the intention was to measure also the velocity of skimming longitudinal waves. It turned out, however, that this was not possible with the equipment used. When the distance between two minima in the V(z) curve for Rayleigh waves was about 25 μm, the same for skimming longitudinal waves was theoretically about 40 μm. Because the vertical movement (Δz) of the lens could only be 53.5 μm it was not possible to have two minima caused by skimming longitudinal waves in the V(z) curve.

2.8.3 Results

The optical microscopy showed that the thickness of the coating varied strongly even with one sample, and therefore no unique thickness value could be determined for all samples. For this reason, in Table 4 giving the thicknesses only the minimum and maximum values measured in some samples are presented. The surface of the substrate was in most samples sandblasted before spraying, in order to improve the adhesion between the coating and substrate. In the samples having a thin coating, the roughness of the substrate surface was too large and has probably influenced the measurement. Figure 34 shows a typical cross-sectional view of the samples. In this case the interface between the coating and substrate does not significantly affect the measurement, due to the slight roughness.

Due to the very inhomogenous surface condition in several samples (porosity, surface roughness), the surface waves were strongly scattered and their propagation along the surface disturbed. This could be seen in the V(z) curves that showed large variations both in the height of the maxima and in the distance between two maxima. An example of a typical V(z) curve measured is presented in Figure 35. Here the minima and maxima can be clearly identified and the determination of sound velocity is reliable. In general, the velocities of Rayleigh waves measured at different points of each sample varied strongly and a remarkable scatter was also recorded for velocities measured at each measurement point. The coatings, their thicknesses, maximum and minimum velocities measured and the average values in each sample are presented in Table 4.

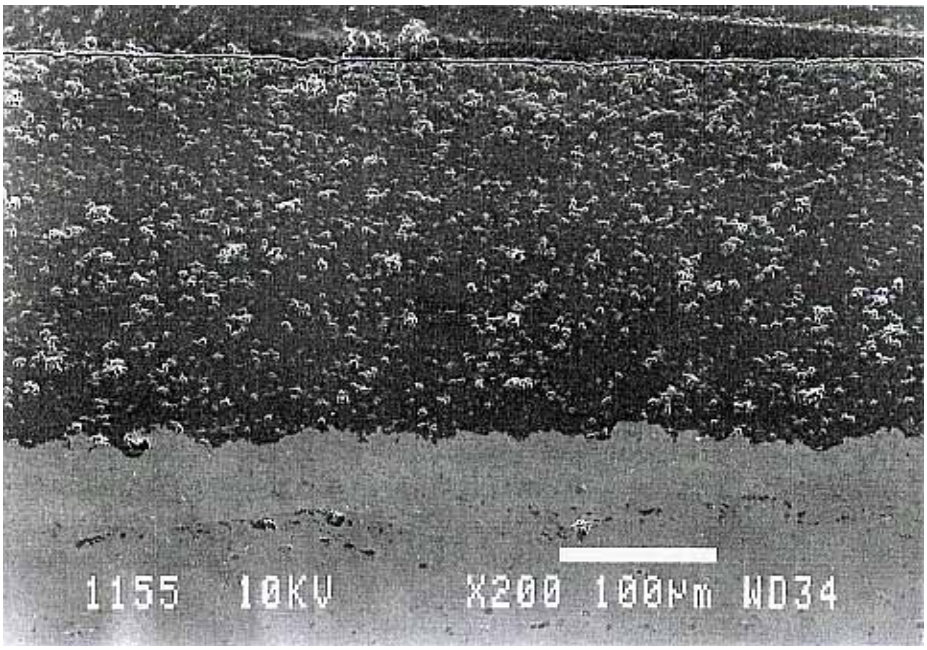

Figure 34. Cross-section of sample H6 (X 200).

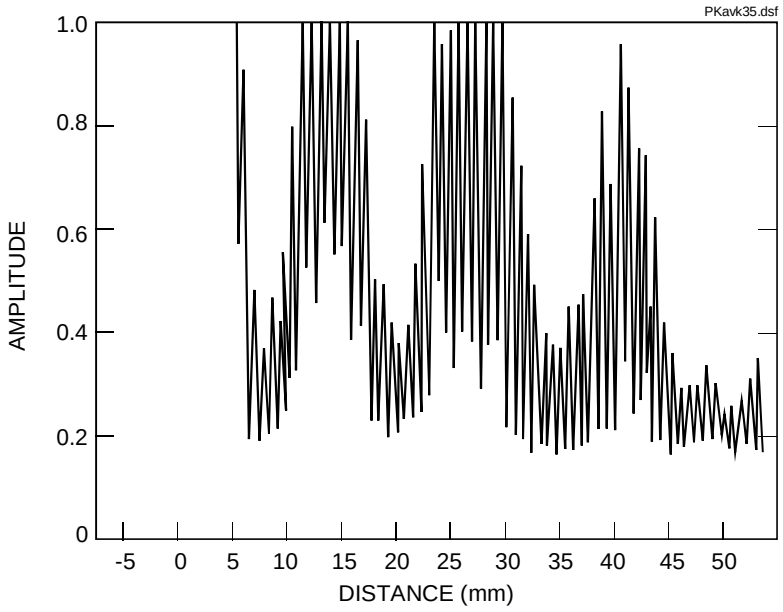

Figure 35. The V(z) curve measured from sample H6.

Table 4. Samples, coating thickness, coating technique and velocities of surface acoustic waves (Rayleigh waves).

Sample	Thickness [μm]	Coating technique	V_{min} [m/s]	V_{max} [m/s]	V_{ave} [m/s]
1	5-40	plasma	3411	4002	3743
2	50-200	plasma	3178	3879	3622
3	200	plasma	3603	4101	4074
4	50	plasma	3185	4007	3688
5	500	plasma	3032	4260	3807
6	30-60	plasma	3440	4388	3916
7	630	plasma	3302	4371	3889
10	430	plasma	3979	4101	3979
H6	280	HVOF	3412	4410	3823
H9	400	HVOF	3810	4562	4065
D	500	detonation	3388	4214	3737

As can be seen from the values in Table 4, the variation of the sound velocity was in some samples about 30%. Therefore the differences between samples manufactured with different coating processes can not be considered remarkable. In general, the sound velocities are very low compared to the values measured for pure non-porous alumina (V_L =10822 m/s, Briggs 1985).

Based on the velocities presented in the table Young's modulus for the samples can be calculated. In the calculations, the value ρ = 3200 kg/m^3 has been used for density and ν = 0.25 for the Poisson ratio. By substituting these in Formula (12) the E values presented in Table 5 have been achieved.

Table 5. The E values of coatings based on the Rayleigh wave velocities measured.

	1	2	3	4	5	6	7	10	H6	H9	D
E [GPa]	132	124	157	129	137	145	143	150	138	156	132

The value 3200 kg/m^3 for density has been used, assuming that the porosity of coating surface is about 20%. This density value for plasma-sprayed alumina coating has also been used by Tietz et al. (1992). The influence of the Poisson ratio on the results is relatively marginal. A reduction of the Poisson ratio to 0.2 causes a decrease in Young's modulus of only about 2%.

The measured velocities of the Rayleigh waves can also be used for the evaluation of the porosity. The correlation formulas given in the literature are based on experimental measurements with practically pure ceramic materials. The wave modes used in these measurements have been the conventional shear and longitudinal waves. In order to be able to use the velocities of Rayleigh waves, approximate shear wave velocities have to be calculated using Formula (13), giving the relation of velocities V_R and V_S. The substitution of the Poisson ratio $\nu = 0.25$ in Formula (13) gives for the relation $V_R / V_S = 0.92$. The use of shear wave velocities calculated based on this relation in the correlation formula presented in Figure 18 (Roth et al. 1990), results in the approximate porosity values given in Table 6.

Table 6. The calculated shear wave velocities V_S [m/s] and porosities P [%] of samples.

	1	2	3	4	5	6	7	10	H6	H9	D
V_S	4068	3937	4428	4009	4138	4257	4227	4325	4155	4418	4062
P	27	28	24	28	26	25	26	25	26	24	27

As can be seen from the table, the porosity values are higher than expected and the variation of porosity between different samples is relatively small.

2.9 Elasticity and porosity of thick ceramic coatings

2.9.1 Measurement of sound velocities with the new transducer

The measurements of the surface wave velocities in the coated specimens were performed by using the C-SAM equipment and transducers described in 2.5. In order to assess the anisotropy of the coating, the measurement was, if possible due to geometrical restrictions, performed both in the direction of thermal spraying and perpendicular to this direction. A practical method for performing the measurement in a short time and with a reasonable accuracy for industrial applications was developed. The measurement was performed using the following steps:

(1) First the probe was adjusted at a distance from the specimen giving the maximum signal from the directly reflected beam (the focus of the probe on the surface of the specimen). The Z coordinate of the scanning system was reset to 0.

(2) The probe was moved in the Z direction, closer to the surface of the specimen (defocused). The probe was stopped at the position where the distance (time difference t) between the signal from the directly reflected beam and from the beam travelling the route a-b-d-e (Fig. 27) could be accurately measured on the CRT screen.

(3) The displacement (z) of the scanner in the Z direction was recorded.

(4) Based on the measured values of z [mm] and t [ns] the sound velocity can be determined from Formula (78). An approximate value can also be seen from the curves calculated from the same formula. An example of curves valid for measurements performed in water is in Fig. 36.

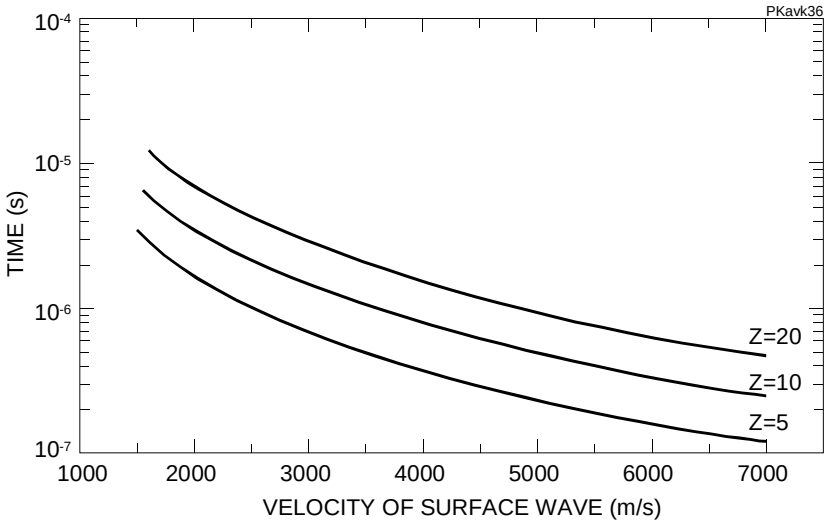

Figure 36. Curves for determination of surface-wave velocities based on the measurement of defocus distance (Z) and time difference (t) between a directly reflected and mode-converted leaky Rayleigh wave signal.

2.9.2 Mechanical testing of coated specimen

As a reference method, three-point bending of stripped coatings was used for the assessment of the elastic modulus of the chromium carbide coating. For this purpose, the coatings made on aluminum profiles were used, with the aluminum substrate stripped by boiling in an NaOH solution. Three coating specimens of this type were prepared and tested as $0.5 \times 40 \times 200$ mm strips.

A loading fixture for three-point bending of the strip specimens was constructed to use full-width free rolling support rolls with a spacing of 120 mm and a radius of 5 mm, and a similar central loading roll. Stepwise loading was performed up to a central bending deflection of about 7 to 8 mm and then reversed in unloading. Because of the specimen curvature, the loading procedure was repeated from both specimen sides for all specimens. The estimation of elastic modulus has been described in details by Auerkari et al. (1997).

Because the bending tests are relatively unreliable for estimating the value of E as a function of strain, the strain dependence of E was evaluated from the results of instrumented tensile testing of coated bars.

The samples used in this experiment were CHR-V1, CHR-V2 and CHR-V3. The experimental set-up for instrumented coated bar tensile testing for combined measurement of in-plane elastic modulus and tensile strength is shown in Figure 37. Multiple instrumentation was used by application of

- longitudinal strain gauges (type Micro-Measurements CEA-06-062WT-120), attached on two (flat) sides or three (one flat) sides of the specimen;

- Instron extensometer, measurement length 25 mm, on one of the short sides;

- acoustic emission sensors attached on both ends of the gauge length; and

- ultrasonic equipment with the new large aperture transducer, immersed into a water-filled testing chamber built over the specimen (Figure 38).

Tensile testing was performed by a stepwise increase of the loading level at the testing head displacement rates of 0.2 or 0.5 mm/min, interrupting for ultrasonic testing at predefined 5 to 10 loading levels, and continuing until extensive acoustic emission signals were recorded from the gauge length region. Liquid penetrant testing was used to confirm cracking of the coating. Testing was continued intermittently until several cracks were observed across the flat side of the specimen in liquid penetrant testing (Auerkari et al. 1997).

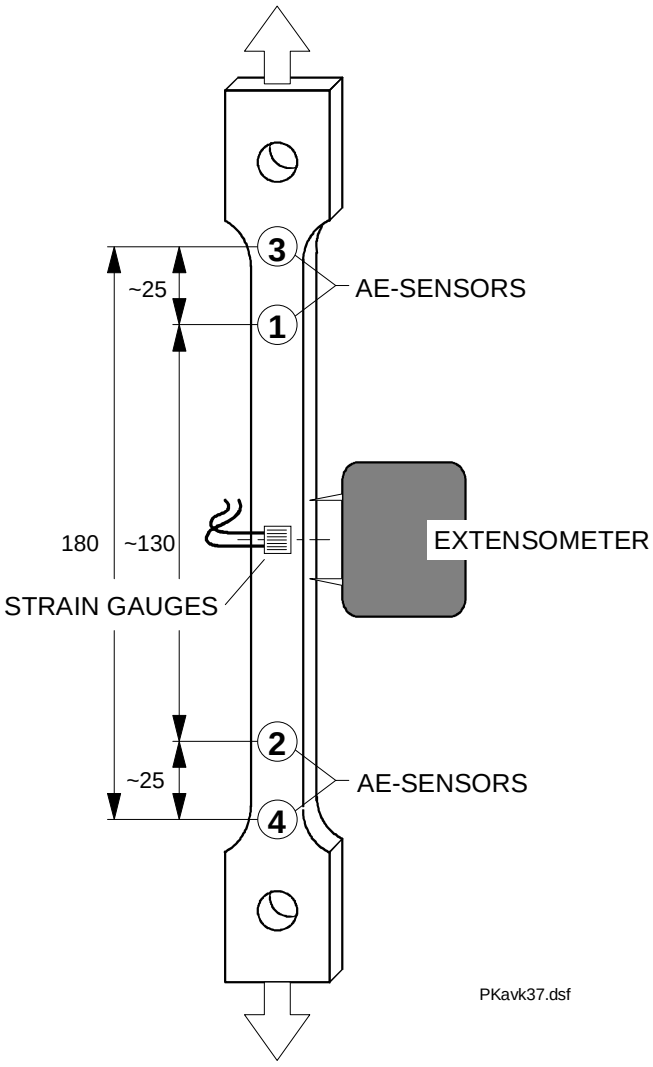

Figure 37. The experimental arrangement for instrumented coated bar testing of thermal spray coatings for combined elastic properties and in-plane tensile strength.

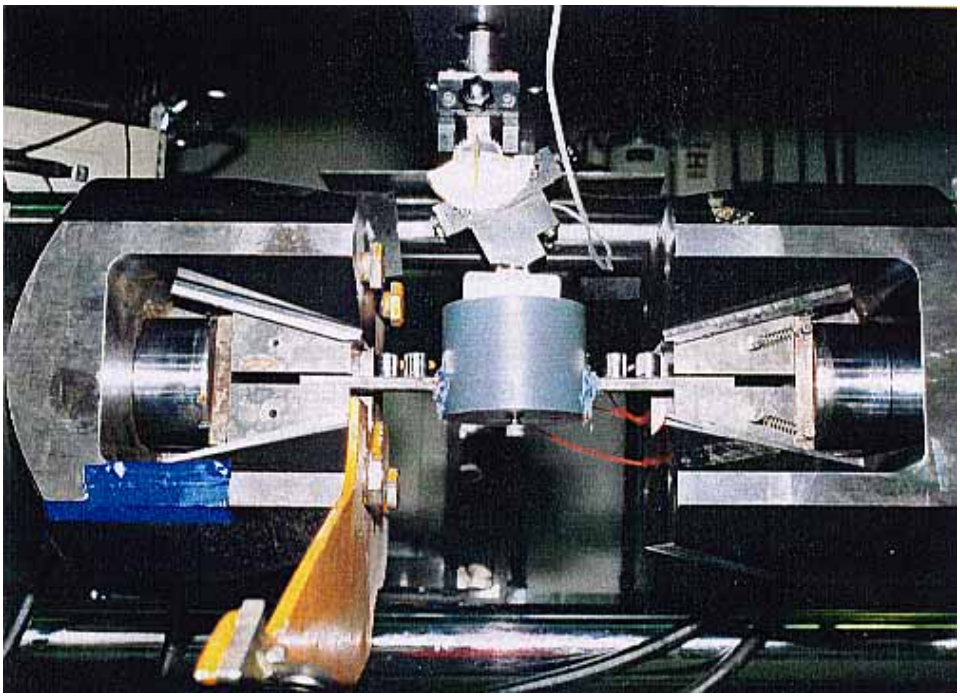

Figure 38. The arrangement used for the measurement of the sound velocity with the new transducer immersed into a water-filled testing chamber built over the specimen.

2.9.3 Results

The velocities of surface acoustic waves (V_{SAW}) measured by using the technique and probe described in 2.5 are shown in Tables 7–10.

Table 7. Velocities of surface acoustic waves in alumina coatings. The velocities are measured in the direction of spraying (0°) and perpendicular to the spraying direction (90°).

Specimen	**V_{SAW} (0°) [m/s]**	**V_{SAW} (90°) [m/s]**
AL4500	3168-3257	3211-3406
AL500	2670	2690
AL1000	2420	2430
AL1500	2430	2400
AL2000	2335	2290

Table 8. Velocities of surface acoustic waves in chromium carbide coatings. The velocities are measured in the direction of spraying (0°) and perpendicular to the spraying direction (90°).

Specimen	**V_{SAW} (0°) [m/s]**	**V_{SAW} (90°) [m/s]**
Cr-1	3120-3310	3220
Cr-2	3110	3315
Cr-3	2455	2470
Cr-4	2410-2640	2470
Cr-5	2855	3020-3130
Cr-6	-	2880
Cr-7	2800	2780
P-1-55	2900	2810
P-1-60	2830	2750
P-1-120	2760	2690
P-1-180	2680	2610
P-1-270	2560	2500
P-1-330	2500	2380
P-1-370	2470	2360
P-1-400	2450	2350
P-1-470	2440	2320
CHR-V1	2690	2680
CHR-V2	2710	2720
CHR-V3	2660	2640

Table 9. Velocities of surface acoustic waves in chromium carbide coatings measured at various levels of strain.

CHR-V1		**CHR-V2**		**CHR-V3**	
ε [μm/m]	**V_R [m/s]**	**ε [μm/m]**	**V_R [m/s]**	**ε [μm/m]**	**V_R [m/s]**
472	2808	135	2852	29	2678
687	2806	336	2848	167	2677
872	2804	498	2848	313	2675
1087	2800	678	2843	449	2673
1294	2798	854	2844	585	2671
1327	2798	1045	2840	722	2666
1365	2794	1160	2839	870	2663
				1001	2660
				1122	2657

Table 10. Velocities of surface acoustic waves in tungsten carbide coatings. The velocities are measured in the direction of spraying (0°) and perpendicular to the spraying direction (90°).

Specimen	**V_{SAW} (0°) [m/s]**	**V_{SAW} (90°) [m/s]**
WC36-1	2130	2120
WC36-2	1845	1880
WC36-3	2010	1990
WC36-4	2310	2330

3. Discussion of results

3.1 Porosity of bulk ceramics

As can be seen from Table 3, the porosity values determined from the propagation velocities of ultrasonic waves are very close to the values determined from the weight and dimensional measurements of the samples. This result is not surprising, because the method for the determination of the porosity based on the propagation velocity of ultrasonic bulk waves has been widely applied to various materials (Roth et al. 1990).

3.2 Integrity of thick ceramic coatings

The results of the ultrasonic measurements carried out between various levels of 4-point bending of coated steel specimens show clearly that the ultrasonic through-transmission technique can reliably reveal cracks and other damages caused by bending stresses in thick ceramic coatings. The growth of cracks can be monitored, although it is clear that the sizes of cracks are strongly overestimated by this measurement technique. In particular the actual crack opening to the surface is an order of magnitude smaller than in the images. This was verified in some samples, by performing a liquid penetrant test to the cracked areas. The length of the cracks is estimated relatively well by the ultrasonic technique and it corresponds to the estimation based on liquid penetrant testing. From the C-scan images it is not possible to evaluate the depth of the cracks in the through-wall direction, or, in general, the location of a discontinuity in this direction.

The major drawback of the through-transmission technique in industrial applications is the need to access both sides of the area of interest. Furthermore, both surfaces used for measurement should be parallel. In industrial applications these preconditions are not always fulfilled and parallel scanning with separate transmitter and receiver probes is not practical or possible. Therefore the pulse-echo technique, where access only to one side of the inspection object is necessary, is highly preferred. The applicability of this technique was also examined with some of the specimens. In these measurements a focused 5 MHz

immersion transducer (Panametrics V309 F2") was used. The echo amplitudes received from the coating/substrate interface were monitored in C-scan images. The cracks opening to the surface caused a strong scatter of the ultrasonic beam and therefore a significant decrease in the amplitude recorded. The cracks can be detected from this loss of amplitude. The results of using the pulse-echo technique were encouraging and this technique can be further optimized for industrial applications. For the evaluation of the adhesion of sprayed coatings, the pulse-echo technique has been successfully used by Suga et al. (1993) and Namba et al. (1993). In both these studies, the coating material has been metallic and the main interest has been to evaluate the adhesion between the substrate and coating, based on the measurement of the echo amplitude reflected from the interface. The measurements performed here show that besides for detecting laminations or disbonds, the same technique can be used for the detection of surface-opening cracks in ceramic coatings.

Ultrasonic velocity measurements with the Japanese specimen gave a through-thickness longitudinal wave velocity of V_L = 1920 m/s and an axial transverse wave velocity V_{TA} = 1554 m/s. Then, using Formulas (49) and (50), taking ρ = 3200 kg/m^3 and ν = 0.3 yields E_L = 15.8 GPa and E_{TA} = 20.1 GPa. These can be regarded as comparable to the value E = 18 GPa obtained by Toyoda (1989) from mechanical testing of nominally the same alumina coating without the substrate.

The good agreement of Young's modulus values obtained by mechanical loading and ultrasonic testing may indicate that corrections for the coating porosity would not often be required. In fact, the porosity affects the sound velocity and thus the modulus calculated from the results of ultrasonic measurements. However, the data is very limited and Young's modulus values are not measured in equivalent directions. The agreement of the directly measured strains from the strain gauges and the calculated strains from the displacements seems to support the validity of ultrasonic determination of Young's modulus (Auerkari et al. 1991). The Young's modulus value measured for the alumina coating is more than one order of magnitude lower than the value measured on compact samples of non-porous alumina (344 GPa, Kauppinen 1991). In similar measurements for estimation of Young's modulus of ZrO_2 coatings performed by Schneider et al. 1993, modulus values that were only 6% of that of a compact material were reported. The reason for this is

assumed to be the presence of a large number of defects which significantly reduces the stiffness of the material.

3.3 Elasticity and porosity of ceramic coatings

3.3.1 Alumina coatings

Measurements with acoustic microscope

The Young's modulus values (Table 4) calculated from the sound velocities measured in thin alumina coatings by using the acoustic microscope operating at 1 GHz frequency are remarkably lower than the values given in literature for bulk alumina (380 GPa, Richersson 1982). The results are similar to the results measured with ZrO_2 coatings by Schneider et al. (1993). The highest value of Young's modulus measured by Schneider was 38% of the value given for non-porous ZrO_2. For alumina this would mean E = 152 GPa, which is very close to values measured here. In some samples measured by Schneider, Young's modulus was only 6% of that in compact ZrO_2. Tietz et al. (1994) have measured Young's modulus of thermally sprayed alumina coatings both by bending tests and by the resonance method. The values for Young's modulus were 32 GPa and 38 GPa, respectively. Thus the modulus was only about 10% of that of solid alumina. Compared to these values, the modulus measured here is very high.

The porosity values determined from the sound velocities measured are higher than expected and the variation of porosity between various samples is relatively small. Based on the information given by the manufacturer of the samples, the porosity of coatings is less than 10%. It is, however, very difficult to evaluate the porosity precisely and most techniques available measure only the open porosity. In order to have some porosity values for comparison, optical microscopy was performed to a few samples. To improve the accuracy of the porosity an estimation image analysis technique was used. The surface of the coating was sprayed with liquid penetrant before the analysis in order to improve the contrast of pores. With this technique the porosities of samples 7 and 10 were 18% and 22%, respectively. Figure 39 presents the surface of sample 10 that has been treated with liquid penetrant. Excess penetrant has been

carefully removed and the dark areas in the picture are thus caused by pores, voids and cracks where penetrant has remained. The image analysis was performed in 4 areas (30 × 30 mm each) and the average value was regarded as the porosity of the sample.

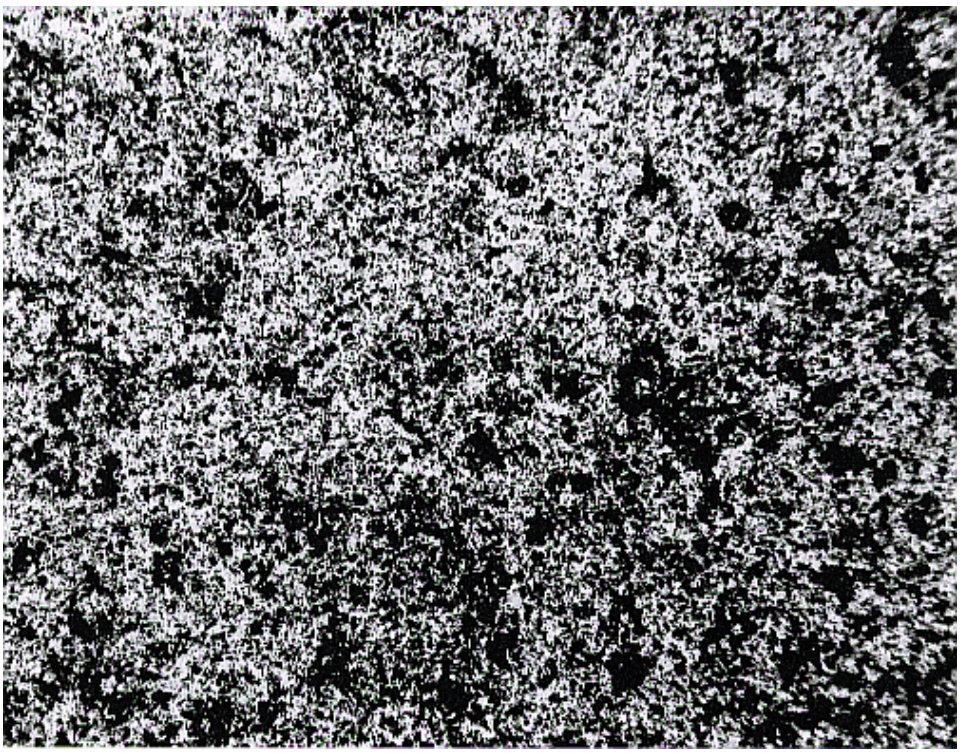

Figure 39. Surface of sample 10 after liquid penetrant treatment (X 100).

The porosity of plasma-sprayed alumina coatings has been studied by Tietz et al. (1992). The porosities reported by Tietz vary between 12 and 23% and are thus in agreement with the results measured in this study.

The measurements performed showed that acoustic microscopy using a very high frequency can be used to characterise porous anisotropic ceramic coatings. The scatter in the propagation velocities measured by the V(Z) technique is, however, very large and therefore leads to a large scatter in values of Young's modulus and porosity calculated from the velocities measured. One of the

reasons to a large dispersion in results is certainly the very small diameter of the focal area of the acoustical lens used. In the ELSAM equipment used the surface wave propagates only 20–30 μm along the surface and the leaky Rayleigh wave affecting the output of the lens is created from this surface wave. Thus the velocity measured represents only a very small area of the surface of the sample. It was already noticed during the measurements that the measurement point had to be selected carefully using the optical microscope connected to the system. Several times the measurement point had to be changed due to infavorable surface conditions. The measurements could only be performed in areas where the sample surface was properly polished and the surface was practically free from discontinuities, like cracks and pores. Therefore the measurements carried out with the ELSAM equipment represent the velocity of Rayleigh waves within single particles of the lamellar structure of the coating, and do not represent the coating structure containing cracks and other structural discontinuities between the lamels. These micro-structural discontinuities are, however, the factors improving the elasticity of the coating and are therefore an essential part of the coating structure.

Measurements with the low-frequency large aperture transducer

The velocity of the surface waves was measured with the low-frequency large aperture transducer in two directions perpendicular to each other, in order to detect any possible directional anisotropy of the coating. The results presented in Table 7 show no remarkable differences in the velocities measured in these two directions. The differences are small when taking into account the general scatter of the sound velocity due to the inhomogeneous structure of the coating. Based on these results, no remarkable variation in the porosity exists in directions parallel to the direction of spraying and perpendicular to this direction. However, a clear difference in the sound velocity was measured in the samples delivered by different manufacturers. In the Japanese specimen a clearly higher velocity than that in the samples manufactured by the Tampere University of Technology (TTKK) was measured. Figure 40 shows the surface acoustic wave velocities measured in the two directions in samples AL500–AL2000.

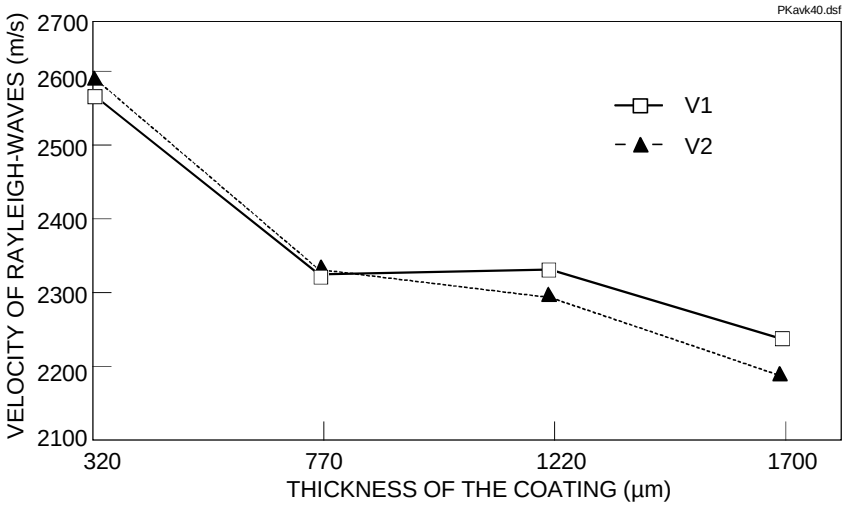

Figure 40. Sound velocities (V_{SAW}) measured in directions parallel to the coating direction (V1) and perpendicular to it (V2) in samples AL500–2000.

It is evident that the velocities measured in samples AL500−AL2000 are affected by the substrate material and do not purely represent the coating. With the frequency of the probe (nominally 10 MHz) used in the measurements, the wavelength is too large, and therefore the surface waves penetrate also into the substrate. In layered specimens the surface acoustic waves are dispersive and the velocity V_{SAW} is a function of both the frequency and the layer's film thickness and elastic parameters (Weglein 1985). Because in most of the samples studied here the thickness of the coating is less than the effective wave length (λ > 2 mm) used in the measurement, the substrate has affected the result. The velocity of the Rayleigh wave in steel is 2996 m/s (Briggs 1992), which is higher than the velocities measured in samples AL500−AL2000. In this case, acoustically slow layers are deposited on fast surfaces. This was also verified by measuring the velocity of the bulk longitudinal waves in the coating. The velocities measured (3200−4100 m/s) are clearly lower than the velocity of the longitudinal waves in steel V_L = 5960 m/s (Briggs 1992). This means that also other modes of surface waves than Rayleigh waves (e.g. Lamb waves) can be formed in the coating. Atalar et al. (1991) have developed a special technique for the evaluation of the elastic parameters of layers supporting Lamb wave modes. This technique was briefly described in 1.7 but was not applied here.

Only in the sample AL4500 was the measured velocity higher than the velocity of the Rayleigh waves in the substrate and the thickness of the coating was clearly higher than the effective wavelength. Thus this velocity can be used to evaluate the porosity and elasticity. By substituting the velocity in Formulas (12)–(13) and in the experimental correlation formula presented in Fig. 17, Young's modulus and the approximate porosity can be calculated. In the calculation the value $\nu = 0.25$ for the Poisson ratio has been used. The results are as follows:

Young's modulus	E = 100 GPa
Porosity	P = 29%

If the same calculations are made using the sound velocities measured in samples AL1000–2000 for comparison, the approximate values E = 54 GPa and P = 37% are achieved. The values of Young's modulus are remarkably higher than the value 18 GPa reported by Toyoda (1989) for the same type of coating. However, the values are closer to the values (32–38 GPa) reported by Tietz (1994) than to the values achieved by using the ELSAM equipment.

In both cases the approximate formulae yield very high values of porosity. There may be several reasons for the high porosity values. Because the velocity of Rayleigh waves in the substrate is in most cases higher than the velocity measured in the coating, the influence of the sound waves on the substrate would increase the sound velocities measured. The correlation formulae for porosity estimation are based on measurements performed with pure samples with different amounts of porosity. The velocity of the longitudinal waves in fully dense alumina has been determined to be approximately 11000 m/s (Roth et al. 1990). From this value, the decrease of the velocity as a function of the porosity is estimated on the basis of the linear dependency between the velocity and porosity up to porosity values of 40–50%. It is clear that the structure of thermally sprayed coating is not similar to pure sintered alumina. The shape and distribution of the pores are different, the coating contains cracks and other structural defects and, finally, the amount of impurities in the coatings is much higher. All these factors decrease the sound velocity and therefore the calculation of porosity, based on the measured sound velocities, leads to over-high porosity. In the literature a propagation velocity of 6163 m/s has been given to shear waves in fully dense alumina. This value is significantly lower

than the velocity originally used in the experimental correlation formula, and using this velocity in the formula leads to lower and more realistic porosity values. In the case of sample AL4500, the porosity value would be 23%. It is also logical that the velocities measured with the ELSAM equipment are higher and the porosities lower than the values measured with a wide aperture low-frequency probe. As already described earlier, the area affected by the sound beam of an acoustical microscope is very small and, in many cases, also the measurement area is especially selected for a successful measurement. Therefore the sound wave propagating on the surface is not affected by structural discontinuities to the same degree as the sound wave transmitted by a probe having a significantly larger focus area. The highest velocity measured for Rayleigh waves in thin alumina coatings was approximately 4500 m/s as presented in Table 4. By using formula (13), the corresponding velocity of shear waves is approximately 4890 m/s. Because this velocity has been measured by using an acoustic lens with an approximate focus diameter of only 30 μm, the result can be assumed to represent the propagation velocity of sound waves inside one lamel of the lamellar structure of the coating. The SEM analysis of sample (7) in Table 4 shows that on the surface of the coating, limited areas of low porosity can be found, even when the sample surface in general looks porous. The pores (voids) are mainly located between the lamels of the coating. The lamellar structure of the coating is clearly seen in the cross-sectional micrograph of the coating. Figures 41–43 show the microstructure of the alumina coating of specimen (7).

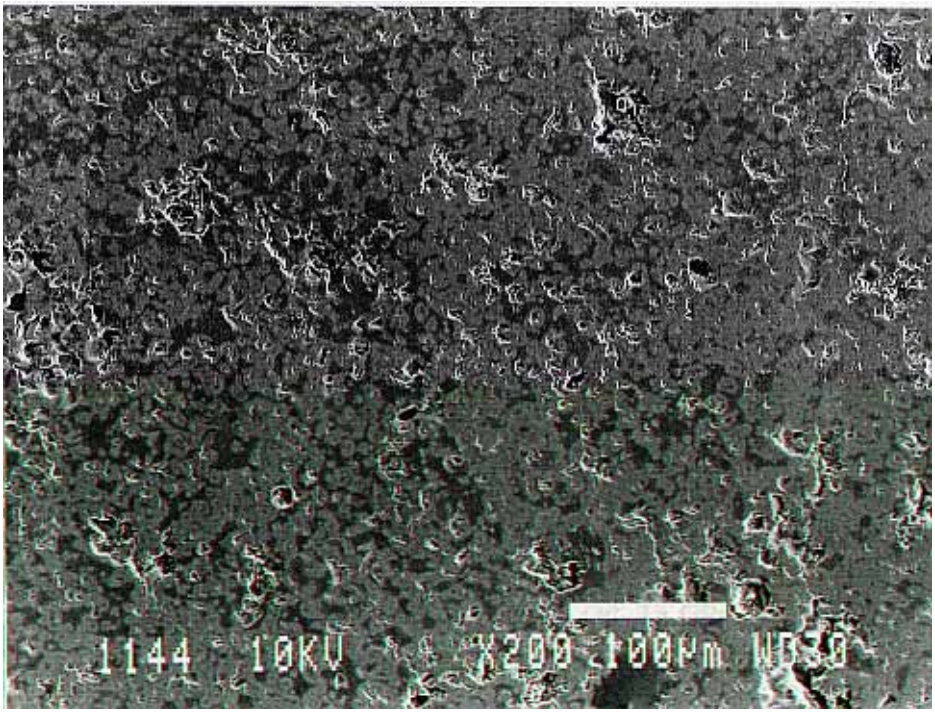

Figure 41. Microstructure of the surface of specimen (7) in Table 4 (X 200).

The EDS analysis also revealed some metallic particles in the coating, but due to their very small amount and random occurrence in the structure, the effect on the sound velocity can be considered negligible.

By assuming that the velocity measured in sample (7) represents the velocity of acoustic surface waves in a sprayed alumina coating containing a locally low amount of porosity, the correlation formula presented in Figure 17 can be slightly modified. By assuming that the porosity of the coating surface inside the focus area of the lens is 5%, the following equation can be achieved by using the same approach as used by Roth et al. (1990).

$$V_S = -0.011xP(\%) + 0.533 \tag{81}$$

When the porosity of sample AL4500 is estimated using this equation and the sound velocity measured, an approximate porosity value of 16% is achieved.

This value is very close to the porosity values (18–22%) measured in similar samples by using liquid penetrants and the image analysis technique.

In the evaluation of Young's modulus with a probe having a wide aperture, the error is theoretically much smaller than in the porosity estimation, because all the structural discontinuities affecting the sound velocity also affect the elasticity. If the density of the coating is based on the porosity calculated above, the value of Young's modulus for sample AL4500 will be E = 110 GPa. This is less than what could be estimated from Figure 18 presented by Wang (1984b) for porous bulk alumina. However, no systematic experimental data about the effect of porosity on Young's modulus of thermally sprayed coatings has been presented in the literature.

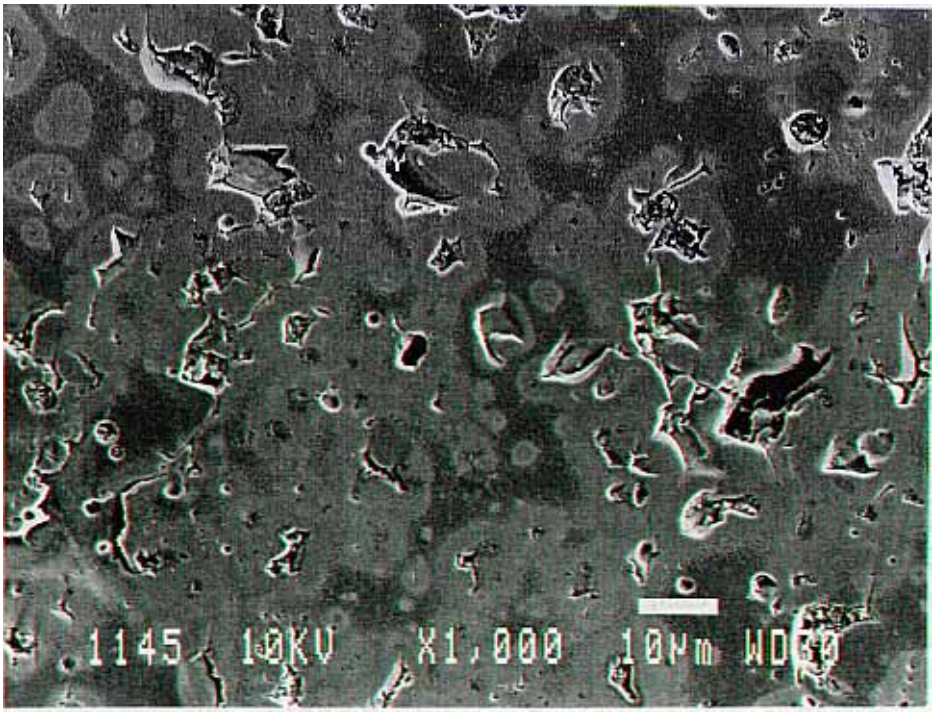

Figure 42. Microstructure of the surface of specimen (7) in Table 4 (X 1000).

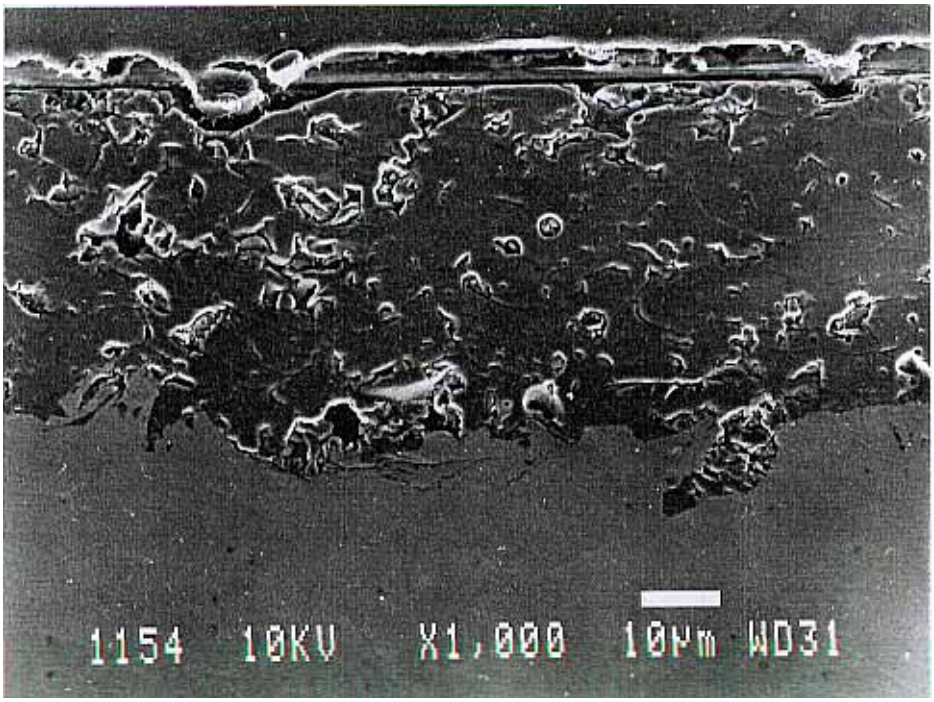

Figure 43. Cross-sectional micrograph of the coating of specimen (7) (X 1000).

3.3.2 Chromium carbide based cermet coatings

The velocity of the surface waves in chromium carbide based cermet coating was measured by using the transducer developed for this work. Due to the strong attenuation of ultrasonic waves in the inhomogeneous coating structure, the use of high (> 100 MHz) ultrasonic frequencies would not have been possible. The velocities measured in samples P-1-55–P-1-470 are presented in Figure 44. As can be seen, the sound velocity decreases with increasing coating thickness. The highest velocity (2900 m/s) has been measured from a coating with a thickness of 55 µm. This velocity is very close to the velocity of the Rayleigh waves in mild steel (2996 m/s) given in literature (Briggs 1992). Thus the result mainly represents the substrate material. With coating thickness higher than 300 µm, the sound velocity no longer changes rapidly. This

indicates that the velocities are less affected by the substrate material. The difference between the sound velocities measured along the direction of spraying and perpendicular to that is approximately 100 m/s. Higher velocities have systematically been measured in the direction of spraying.

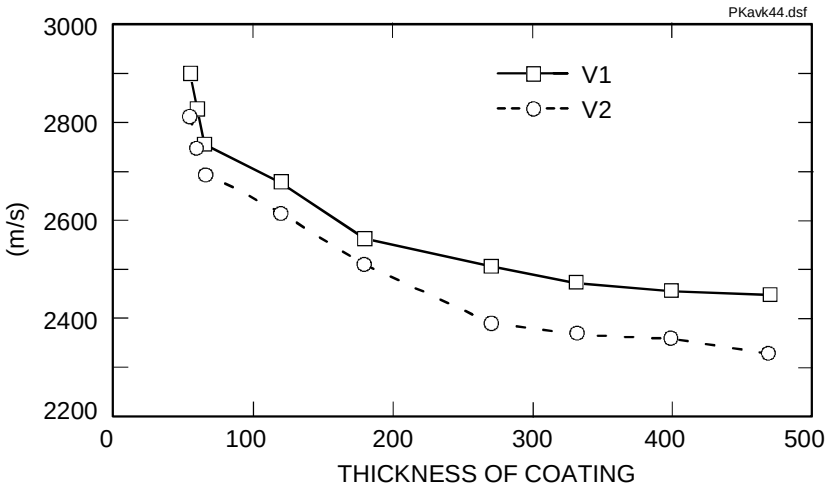

Figure 44. Leaky wave velocities measured in samples P-1-55–P-1-470. The thicknesses of the coatings are from 55 µm to 470 µm.

The decrease of the sound velocity with increasing coating thickness indicates that the velocity of the surface waves in the coating is lower than the velocity of the Rayleigh waves in the substrate. As described in 1.3.3, this means that the leaky waves can be in the form of Lamb waves and for the measurement of elastic parameters of coatings the technique developed by Atalar et al. (1990) has to be used. This technique has been briefly described in 1.7. but was not applied here.

Also the sound velocities measured in samples Cr-3, Cr-4, Cr-5, Cr-6, Cr-7 and CHR-V1, CHR-V2 , CHR-V3 were lower than the velocity of the Rayleigh waves in the substrate material. The difference between the sound velocities measured in the direction of spraying and perpendicular to it was in these samples small and no systematic tendency could be seen. As can be seen in Table 8, the velocities measured are close to the velocities measured in samples of the P-1-series, having similar coating thicknesses.

The sound velocities measured are higher than the velocity of the Rayleigh waves in the substrate only in samples Cr-1 and Cr-2.

Young's modulus of specimens CHR-V1, CHR-V2 and CHR-V3, calculated from the sound velocities measured, is presented in Table 11. The density of the coating was estimated by measuring the weight and dimensions of the three stripped coatings used for the assessment of Young's modulus in three-point bending. The average of the densities measured was $\rho = 4280$ kg/m^3. Based on this, and assuming a porosity fraction of 7%, the density 4500 kg/m^3 has been used in the calculations. In literature the density $\rho = 4600$ kg/m^3 has been given for chromium carbide (Takahashi & Yoshioka, 1992). By using the values $\nu = 0.25$, $\rho = 4500$ kg/m^3 and the sound velocities measured, the values of Young's modulus given in Table 11 are achieved from Formula (12).

Table 11. Young's modulus of samples CHR-V1, CHR-V2 and CHR-V3.

Sample	**E [GPa]**
CHR-V1	96
CHR-V2	98
CHR-V3	94

The values presented in Table 11 are higher than the average value measured in the three-point bending tests of the three stripped coatings (E = 53 GPa). As discussed above, the sound velocities measured are affected by the substrate material when the thickness of the coating is less than a few wavelengths. To correct the results of the ultrasonic measurement, it is assumed that for each test and coating thickness, there is an effectively distinct substrate layer below the interface influencing the testing results. If the thickness of this substrate layer is s_s and the thickness of the coating s_c, a simple weighting by layer thickness would suggest that the measured $E_m(\varepsilon)$

$$E_m(\varepsilon) = \frac{\left(s_c E_c(\varepsilon) + s_s E_s\right)}{s} \quad , \tag{82}$$

where the total effective layer thickness $s = s_c + s_s$, and $E_c(\varepsilon)$ and E_s are the elastic moduli of the coating and the substrate (steel), respectively. Since the elastic modulus of the substrate is a known constant (206 GPa at room temperature) and the value $E_c(0)$ has been measured in the bending tests, the values of s_s for all tested specimens can be calculated from (82). The results are shown in Table 12.

Table 12. The measured coating thickness s_c and the calculated effective substrate thickness s_s in the ultrasonic assessment of the elastic modulus of the coating.

Specimen	**Coating thickness s_c [μm]**	**Effective substrate thickness s_s [μm]**
CHR-V1	300	116
CHR-V2	150	62
CHR-V3	500	181

Using these values of s_s , the desired elastic modulus of the coating is obtained from (82) as

$$E_c(\varepsilon) = E_m(\varepsilon)\left(1+\frac{s_s}{s_c}\right) - E_s\left(\frac{s_s}{s_c}\right), \tag{83}$$

where $E_m(\varepsilon)$ is the elastic modulus calculated from the uncorrected ultrasonic measurements carried out at different strain levels. The results from the mechanical testing of the three specimens and the corresponding results based on ultrasonic measurement are shown in Figure 45. The results of ultrasonic measurements have been corrected as presented above.

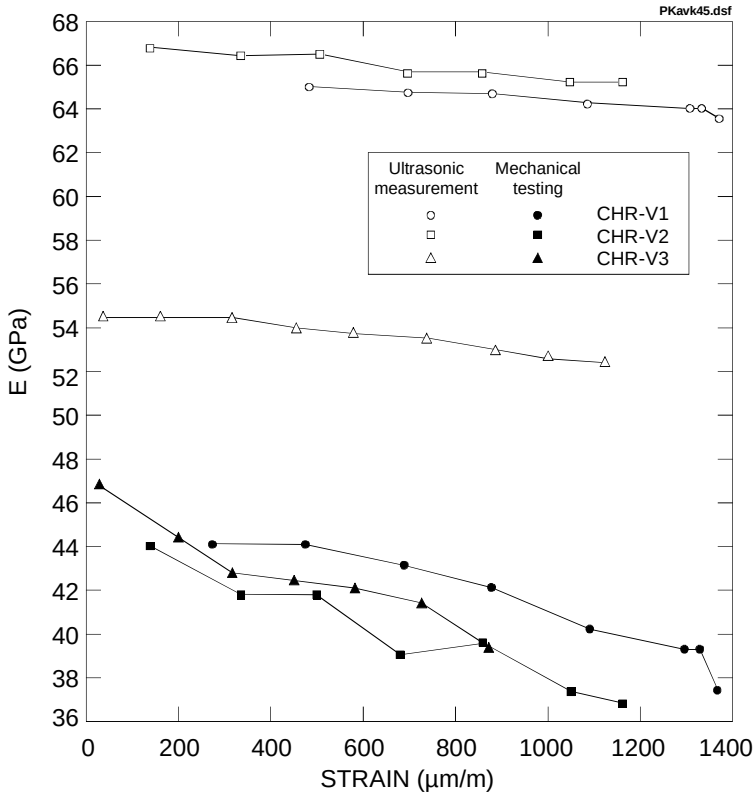

Figure 45. The elastic modulus as a function of measured longitudinal strain for three coated specimens subjected to instrumented tensile testing.

It is seen that the elastic modulus decreases approximately linearly with the measured longitudinal strain ε of the coating surface. The results of the ultrasonic measurement show a lower decrease of elastic modulus with increasing strain than the results of mechanical testing can show. Although the effect of increasing strain on the elastic modulus was relatively weak in the results based on the ultrasonic measurements, the decrease of the sound velocity with increasing strain was consistent. By performing the measurements in immersion, the variations in acoustic coupling could be avoided and therefore the tendency seen in the sound velocities can be considered significant. In general, the values of elastic modulus calculated from the results of the ultrasonic measurement are slightly higher than the values achieved in the mechanical testing. Due to the specific composition of the coating, no relevant results for comparison have been found in literature. This type of experiment,

where the elastic modulus of coating was determined at different strain levels by using the ultrasonic technique, is probably quite unique and no other results are available.

3.3.3 Tungsten carbide coatings

Similar to the alumina coatings, no significant differences between the sound velocities measured in different directions were observed. The velocities were very low, as can be expected from the value given in literature (Briggs 1992) for pure tungsten carbide (V_R = 3643 m/s). Thus it is evident that the surface acoustic wave used in the measurement is in the form of Lamb wave. Therefore the estimation of the porosity can only be very approximate. Furthermore, no correlation formulae for the evaluation of the porosity have been found in the literature. In order to assess at least very roughly the porosity of the samples measured, a similar approach to that presented by Roth et al. (1990) for silicon carbide has been used. Between the velocity of shear waves (V_S) and the percentage of porosity (P) of silicon carbide the following experimental formula has been presented (Roth et al. 1990):

$$V_S = -0.009P + 0.786 \tag{84}$$

Similarily the formula for tungsten carbide can be written as follows:

$$V_S = -0.009P + 0.3984 \tag{85}$$

Here the value 0.3984 is based on the theoretical velocity of shear waves in tungsten carbide (V_S = 3984 m/s) given by Briggs (1992). Furthermore, by using Equation (13) and value $\nu = 0.22$, the shear wave velocities corresponding to the measured surface wave velocities can be calculated. From these the porosity of different specimens can be estimated using Formula (85). The porosity values achieved this way are presented in Table 13.

The theoretical density of tungsten carbide is $\rho = 15000$ kg/m^3 and the Poisson ratio $\nu = 0.22$ (Briggs 1992). These values can be used to calculate Young's modulus from the sound velocities measured. For the velocity, the average value

measured in each specimen has been used. In Table 12, Young's modulus calculated from Equation (12) has been presented.

Table 13. The approximate porosity (P) and values of Young's modulus (E) calculated for tungsten carbide coatings.

Specimen	P [%]	E [GPa]
WC36-1	18.5	197
WC36-2	21.7	151
WC36-3	20.0	175
WC36-4	16.1	235

In literature no values for thermally sprayed tungsten carbide coatings have been found. For bulk tungsten carbide, Young's modulus value 710 GPa has been given (Brown et al. 1968). Kuribayashi et al. (1971) have measured the elastic modulus of bulk tungsten carbide with the ultrasonic technique and have reported values E = 480–636 GPa depending on the Co-content of the material. When considering the results presented here, it is necessary to point out that the approach used is very approximate for several reasons. The sound velocities measured in the coatings are clearly lower than the velocity of the Rayleigh waves in the substrate material. This means that the leaky waves can be in the form of Lamb waves and for a more reliable assessment of elastic parameters of coating, other techniques should be used (Atalar et al. 1991).

3.4 Applicability of the new measurement technique

The design and construction of the new transducer was started in 1992 and the first results were reported in 1994 (Kauppinen et al. 1995). Recently similar experimental constructions have been reported by Kawashima et al. (1996) and Xiang et al. (1996).

The experimental measurements performed with the new large aperture transducers confirm the theoretical advantages of this type of transducer construction. The results measured with known materials show that the

transducer and measurement technique can be used to characterise the elastic properties of materials with an accuracy acceptable in most industrial applications. In connection of this work only a few transducers of the new type were constructed and these first transducers can certainly be optimized further. Especially the operating frequency of the probes should be increased in order to be able to measure also coatings where the sound velocity is high and the coating thickness small.

Measurements performed using the ”local immersion technique” in connection with the tensile testing of specimens show that the technique can also be applied in many industrial conditions, where an acoustic microscope or other laboratory techniques can not be applied.

4. Conclusions

The experimental measurements with different ultrasonic techniques lead to the following main conclusions:

The new probe construction enables to measure the propagation velocities of different wave modes effectively and accurately. PC software can be used for the rapid calculation of velocities and elastic properties. A local immersion arrangement can be used in industrial applications where the object to be measured can not be immersed completely.

The line-focus of the new probe can be used to evaluate the elastic anisotropy of the coating. By turning the probe, the focus can be adjusted in various directions in the plane of the surface and the corresponding elastic properties can be assessed.

By optimising the ultrasonic frequency used in the measurement, coatings with varying thicknesses can be measured without the influence of the substrate material on the results. If necessary, material-specific correction factors can be applied to eliminate the effect of substrate material. The proper selection of the frequency allows to characterise the complete thickness of the coating because the penetration depth of Rayleigh waves depends on the wavelength. Thus the result does not represent only a tiny surface layer of the coating. Also other wave modes, like skimming longitudinal waves or Lamb waves, can be used for the comparative evaluation of elasticity.

Cracking of the coating can be reliably revealed with Rayleigh waves propagating on the surface of the coating. The cracks can also be detected with a transmitter-receiver probe arrangement. Nevertheless, the applicability of this technique to industrial measurements is often limited by restricted access to the component.

The porosity of the coating can be estimated on the basis of the propagation velocity of different wave modes. For most industrial applications, the use of Rayleigh waves offers a practical method for a rough estimation of porosity, because the measurement can be performed also in conditions where access is limited to one side of the specimen.

For the evaluation of in-homogeneous thermally sprayed ceramic coatings, the accuracy of the method presented here is sufficient. The method is not as sensitive to local in-homogeneity as the conventional acoustic microscopy, where very high frequencies are used. The focal area of the low-frequency transducer is larger than the focal area of the lenses used in acoustical microscopy and therefore the result is more representative of the coating structure.

References

Almond, D. P. 1982. An evaluation of the suitability of ultrasonic techniques for the testing of thermally sprayed coatings. Surfacing Journal, Vol. 13, No. 3, pp. 50–55.

Arons, R. M. and Kupperman, D. S. 1982. Use of sound-velocity measurements to evaluate the effect of hot isostatic pressing on the porosity of ceramic solids. Materials Evaluation, Vol. 40, No. 9, pp. 1076–1078.

Atalar, A. 1978. An angular-spectrum approach to contrast in reflection acoustic microscopy. Journal of Applied Physics, Vol. 49, No. 10, pp. 5130–5139.

Atalar, A. 1979. A physical model for acoustic signatures. Journal of Applied Physics, Vol. 50, No. 12, pp. 8237–8239.

Atalar, A. 1985. Penetration depth of the scanning acoustic microscope. IEEE Transactions on Sonics and Ultrasonics, Vol. SU-32, No. 2, pp. 164–167.

Atalar, A., Quate, C.F. and Wickramasinghe, H. K. 1977. Phase imaging in reflection with acoustic microscope. Applied Physics Letters, Vol. 31, No. 12, pp. 791–793.

Atalar, A., Köymen, H. and Yemisciler, O. 1991. Characterization of layered structures by a liquid wedge transducer and a corner reflector. In: Lee, H. & Wade, G. (eds.). Acoustical Imaging, Volume 18. New York, USA: Plenum Press. Pp. 179–188.

Auerkari, P., Kauppinen, P., Santaoja, K. and Uuttu, T. 1991. Strength and integrity of ceramic coatings. Espoo: Technical Research Centre of Finland (VTT). 18 p. (Research Reports 734).

Auerkari, P., Sarkimo, M., Kytö, P., Kauppinen, P., Pankakoski, P. H. and Korpiola, K. 1997. Tensile strength of thermal spray coatings. Espoo: Technical Research Centre of Finland (VTT). 25 p. (VTT Publications). (To be published).

Bergmann, L. 1954. Der Ultraschall. Zürich, Switzerland: S. Hirzel Verlag. 1114 p.

Bertoni, H. L. and Tamir, T. 1973. Unified theory of Rayleigh-angle phenomena for acoustic beams at liquid-solid interfaces. Applied Physics, Vol. 2, No. 4, pp. 157–172.

Briggs, A. 1985. An introduction to scanning acoustic microscopy. Oxford, UK: Oxford University Press. 70 p.

Briggs, A. 1992. Acoustic Microscopy. Oxford, UK: Clarendon Press. 325 p.

Briggs, G. A. D. and Somekh, M. G. 1987. Acoustic microscopy of surface cracks: Theory and practice. Proceedings of the ONR Symposium on Solid Mechanics Research for QNDE. Evanston, USA: Martinus Nijhoff Publishers. Pp. 155–170.

Brown, H. L., Armstrong, P. E., O'Rourke, J. A. and Kempter, C. P. 1968. Directional variations of elastic properties of some transition metal monocarbide cubes. Planseeberichte für Pulvermetallurgie, Vol. 16, No. 2, pp. 114–118.

Bushell, A. C., Edwards, C. and Palmer, S. B. 1991. Laser-generated surface waves on plates of varying thickness. British Journal of NDT, Vol. 33, No. 4, pp. 177–182.

Chubachi, N., Kushibiki J., Sannomiya, T., Naruge, I, Saito, K. and Watanabe, S. 1991. Acoustical images observed by directional PFB microscope. In: Lee, H. & Wade, G. (eds.). Acoustical Imaging, Volume 18. New York, USA: Plenum Press. Pp. 255–260.

Fahr, A., Johar, S., Murthy, M. K. and Sturrock, W. R. 1984. Surface acoustic wave studies of surface cracks in ceramics. Proceedings of the Tenth Annual Review of Progress in Quantitative Nondestructive Evaluation. New York, USA: Plenum Press. Pp. 239–249.

Firestone, F. A. and Frederick, J. R. 1946. Refinements in supersonic reflectoscopy. Polarized sound. The Journal of the Acoustical Society of America, Vol. 18, No. 1, pp. 200–211.

Fountain, L. S. 1967. Experimental evaluation of the total-reflection method of determining ultrasonic velocity. The Journal of the Acoustical Society of America, Vol. 42, No. 1, pp. 242–247.

Gault, C. 1989. Ultrasonic non-destructive evaluation of microstructural changes and degradation of ceramics at high temperature. In: Holbrook, J. and Bussiere, J. (eds.). Nondestructive Monitoring of Materials Properties. Pittsburgh, Pennsylvania, USA: Materials Research Society. Pp. 263–274.

Gilmore, R. S., Hewes, R. A., Thomas, L. J. and Young, J. D. 1989. Broadband acoustic microscopy: scanned images with amplitude and velocity information. In: Shimizu, H., Chubachi, N. and Kushibiki, J. (eds). Acoustical Imaging, Volume 17. New York, USA: Plenum Press. Pp. 97–110.

Hasselman, D. P. H. and Singh, J. P. 1979. Analysis of thermal stress resistance of microcracked brittle ceramics. Ceramic Bulletin, Vol. 58, No. 9, pp. 856–860.

Henneke, E. G. and Jones, G. L. 1976. Critical angle for reflection at a liquid-solid interface in single crystals. Journal of The Acoustical Society of America, Vol. 59, No. 1, pp. 204–205.

Hildebrand, J. A. and Lam, L. K. 1983. Directional acoustic microscopy for observation of elastic anisotropy. Applied Physics Letters, Vol. 42, No. 5, pp. 413–415.

Hull, D. R., Kautz, H. E. and Vary, A. 1985. Measurement of ultrasonic velocity using phase-slope and cross-correlation methods. Materials Evaluation, Vol. 43, No. 10, pp. 1455–1460.

Ilett, C., Somekh, M. G. and Briggs, G. A. D. 1984. Acoustic microscopy of elastic discontinuities. Proceedings of the Royal Society of London, A393. London, UK. Pp. 171–183.

Jagnoux, P. and Vincent, A. 1989. Ultrasonic imaging by leaky Rayleigh waves. NDT International, Vol. 22, No. 6, pp. 339–346.

Jones, M. P., Blessing, G. V. and Robbins, C. R. 1986. Dry-coupled ultrasonic elasticity measurements of sintered ceramics and their green states. Materials Evaluation, Vol. 44, No. 6, pp. 859–862.

Jungman, A., Adler, L. and Quentin, G. 1988. Ultrasonic velocity measurements in porous materials. In: Höller, P. Hauk, V., Dobmann, G., Ruud, C. and Green, R. (Eds.). Nondestructive Characterization of Materials. Berlin, Germany: Springer-Verlag. Pp. 123–130.

Kauppinen, P. 1991. Characterization of ceramics and ceramic-metal joints by ultrasonic techniques. Licentiate Thesis. Espoo: Helsinki University of Technology. 113 p.

Kauppinen, P. and Kivilahti, J. 1991. Evaluation of structural defects in brazed ceramic-to-metal joints with C-mode scanning acoustic microscopy. NDT&E International, Vol. 24, No. 4, pp. 187–190.

Kauppinen, P., Jeskanen, H., Heikinheimo, L., Siren, M. and Auerkari, P. 1995. The evaluation of integrity of ceramic-metal joints and ceramic coatings by C-mode acoustic microscopy. Nondestructive Characterization of Materials VII. Part 2. Bartos, A. L., Green, R. E. and Ruud, C. O. (eds.). Switzerland: Transtech Publications Ltd. Pp. 767–773.

Kawashima, K., Fujii, I., Sato, T. and Okade, M. 1996. A digital signal processing for measuring leaky surface wave velocity with C-scan acoustic microscope. Preprint of the proceedings of the conference Review of Progress in Quantitative NDE. Vol. 14. 6 p.

Kojima, S. 1989. Application of scanning acoustic microscope to ferroelectrics. In: Shimizu, H., Chubachi, N. and Kushibiki, J. (eds). Acoustical Imaging, Volume 17. New York, USA: Plenum Press. Pp. 61–69.

Krautkrämer, J. and Krautkrämer, H. 1983. Ultrasonic Testing of Materials. Berlin, Germany: Springer-Verlag. 667 p.

Kulik, A., Gremaud, G. and Sathish, S. 1989. Continuous wave reflection scanning acoustic microscope (SAMCRUW). In: Shimizu, H., Chubachi, N. and Kushibiki, J. (eds). Acoustical Imaging, Vol. 17. New York, USA: Plenum Press. Pp. 71–78.

Kupperman, D. S. and Karplus, H. B. 1984. Ultrasonic wave propagation characteristics of green ceramics. Ceramic Bulletin, Vol. 63, No. 12, pp. 1505–1509.

Kuribayashi, T. and Watanabe, M. 1971. Measurement of Young's modulus of hard alloys by ultrasonic method. Kanagawa-Ken Kogyo Shikensho Kenkyu Hokoku 32, pp. 31–36 (in Japanese).

Kushibiki, J., Ohkubo, A. and Chubachi, N. 1982. Effect of leaky SAW parameters on V(z) curves obtained by acoustic microscopy. Electronics Letters Vol. 18, No. 15, pp. 668–670.

Kushibiki, J. and Chubachi, N. 1985. Material characterization by line-focus-beam acoustic microscope. IEEE Transactions on Sonics and Ultrasonics, Vol. SU-32, No. 2, pp. 189–212.

Kushibiki, J., Ishikawa, T. and Chubachi, N. 1987. Precise measurement of film thickness by line-focus-beam acoustic microscope. Proceedings of Ultrasonics International 87. Guildford, UK: Butterworth. Pp. 291–296.

Ledbetter, H. M., Lei, M. and Datta, S. K. 1989. Elastic properties of porous ceramics. In: Holbrook, J. and Bussiere, J. (eds.). Nondestructive Monitoring of Materials Properties. Pittsburgh, Pennsylvania, USA: Materials Research Society. Pp. 275–282.

Liang, K., Bennett, S. D., Khuri-Yakub, B. T. and Kino, G. S. 1982. Precision measurement of Rayleigh wave velocity perturbation. Applied Physics Letters Vol. 41, No. 12, pp. 1124–1126.

Mackenzie, J. K. 1950. Elastic constants of a solid containing spherical holes. Proc. Phys. Soc. London, Vol. 63B, No. 1, pp. 2–11.

Mak, D. K. and Steinfl, R. B. 1989. Ultrasonic velocity measurements of Au-W composites. Nondestructive Testing and Evaluation, Vol. 5, pp. 39–48.

Matthaei, E., Vetters, H. and Mayr, P. 1989. Einsatz der akustischen Mikroskopie in der Werkstoffkunde. DGZfP-Jahrestagung, Kiel, Germany, 25–27 September. Deutsche Gesellschaft für Zerstörungsfreie Prüfung e.V. Pp. 231–238.

Mayer, W. G. 1960. Determination of ultrasonic velocities by measurement of angles of total reflection. The Journal of the Acoustical Society of America, Vol. 32, No. 10, pp. 1213–1215.

Morsch, A., Korn, D., Gleiter, H. Hoppe, M. and Arnold, W. 1988. Characterization of the elastic behaviour of nanocrystalline materials by scanning acoustic microscopy. In: Höller, P. Hauk, V., Dobmann, G., Ruud, C. and Green, R. (eds.). Nondestructive Characterization of Materials. Berlin, Germany: Springer-Verlag. Pp. 384–390.

Nagarajan, A. 1971. Ultrasonic study of elasticity-porosity relationship in polycrystalline alumina. Journal of Applied Physics, Vol. 42, No. 10, pp. 3693–3696.

Namba, Y., Nakazato, H. and Honma, K. 1993. An ultrasonic method to study the adhesion of thermally sprayed coatings. Proceedings of the International Thermal Spray Conference & Exposition, Orlando, Florida, USA, 28 May – 5 June 1992. Pp. 241–245.

Nickerson, R. A. 1973. Wave propagation theory for ultrasonic testing. Proceedings of the Seventh International Conference on Nondestructive Testing. Warszawa, Poland: Institut Podstawowych Problemow Techniki Polskiej Akademii Nauk. Pp. 321–337.

Nielsen, L. F. 1982. Elastic properties of two-phase materials. Materials Science and Engineering, Vol. 52, pp. 39–62.

Nikoonahad, M. 1984. Reflection acoustic microscopy for industrial NDE. In: Sharpe, R. (ed.). Research Techniques in NDT, Vol. 7. London, UK: Academic Press. Pp. 217–257.

Nomura, T., Mizuno, S. and Yasuda, T. 1989. Measurement of SAW velocity by focusing system using Fresnel phase plate IDT. In: Shimizu, H., Chubachi, N. and Kushibiki, J. (eds). Acoustical Imaging, Volume 17. New York, USA: Plenum Press. Pp. 443–451.

Okano, K. 1960. Rep. Prog. Polym. Phys. Jpn., 3(1960), 69 (other details not known).

Pangraz, S., Quinten, A., Simon, H. and Arnold, W. 1989. Akustische Rastermikroskopie und HF-Ultraschallabbildungsverfahren im Einsatz zur Materialprüfung und -charakterisierung, insbesondere in keramischen Werkstoffen. DGZfP-Jahrestagung, Kiel, Germany, 25–27 September. Deutsche Gesellschaft für Zerstörungsfreie Prüfung e.V. Pp. 239–246.

Papadakis, E. P. 1972. Absolute accuracy of the pulse-echo overlap method and the pulse-superposition method for ultrasonic velocity. The Journal of the Acoustical Society of America, Vol. 52, No. 3, pp. 843–846.

Papadakis, E. P., Patton, T., Tsai, Y.-M., Thompson, D. O. and Thompson, R. B. 1991. The elastic moduli of a thick composite as measured by ultrasonic bulk wave pulse velocity. Journal of the Acoustical Society of America, Vol. 89, No. 6, pp. 2753–2757.

Phani, K. K., Niyogi, S. K., Maitra, A. K. and Roychaudhury, M. 1986. Strength and elastic modulus of a porous brittle solid: an acousto-ultrasonic study. Journal of Materials Science, Vol. 21, No. 12, pp. 4335–4341.

Pilarski, A. 1986. Leaking interface waves in ultrasonic NDE. In: Jones, L., Kasel, J., Risinger, B., Strawn, T. & Thalheimer, M. (eds.). Proceedings of the 11th World Conference on Nondestructive Testing. Dallas, TX, USA: Taylor Publishing Co. Pp. 768–775.

Plona, T. J., Behravesh, M. and Mayer, W. G. 1975. Rayleigh and Lamb waves at liquid-solid boundaries. Ultrasonics, Vol. 13, No. 4, pp. 171–175.

Quinten, A. and Arnold, W. 1989. Observation of stable crack growth in Al_2O_3 ceramics using a scanning acoustic microscope. Materials Science and Engineering, Vol. A122, pp. 15–19.

Ranachowski, J. 1975. Propagation of ultrasonic waves in porous ceramics. Ultrasonics, Vol. 13, pp. 203–207.

Rayleigh, J. W. S. 1885. On waves propagated along the plane surface of an elastic solid. Proceedings of The London Mathematical Society, Vol. 17, pp. 4–11.

Richerson, D. W. 1982. Modern ceramic engineering: Properties, processing, and use in design. Phoenix, USA: Marcel Dekker Inc. 399 p.

Roberts, R. A. 1989. Local measurement of material properties by use of acoustic microscopy. Proceedings of the 1989 SEM Spring Conference on Experimental Mechanics. Boston, USA: The Society for Experimental Mechanics. Pp. 943–953.

Rokhlin, S. I. and Wang, W. 1989. Critical angle measurement of elastic constants in composite material. Journal of The Acoustical Society of America, Vol. 86, No. 5, pp. 1876–1882.

Roth, D. J., Stang, D. B., Swickard, S. M. and DeGuire, R. M. 1990. Review and statistical analysis of the ultrasonic velocity method for estimating the porosity fraction in polycrystalline materials. NASA Technical Memorandum 102501. Cleveland, Ohio, USA: Lewis Research Center. 44 p.

Saurel, J., Alami, K. and Chaffaut, C. 1989. Mechanical characterization by acoustic techniques of SiC chemical-vapour-deposited thin films. Materials Science and Engineering, A122, pp. 27–31.

Sayers, C. M. and Smith, R. L. 1982. The propagation of ultrasound in porous media. Ultrasonics, Vol. 20, No. 5, pp. 201–205.

Schneider, D., Schwarz, T., Buchkremer, H.-P. and Stöver, D. 1993. Non-destructive characterization of plasma-sprayed ZrO_2 coatings by ultrasonic surface waves. Thin Solid Films, Vol. 224, pp. 177–183.

Schreiber, E., Anderson, O. L. and Soga, N. 1973. Elastic constants and their measurement. New York, USA: McGraw–Hill Book Company. 196 p.

Shin, F. G., Tsui, W. L., Yeung, Y. Y. and Au, W. M. 1993. Elastic properties of a solid with a dispersion of soft inclusions or voids. Journal of Materials Science Letters, Vol. 12, pp. 1632–1644.

Simpson, W. A. and McClung, R. W. 1989. Ultrasonic characterization of ceramic joints. Ceramic Engineering Science Proceedings, Vol. 10, No. 11–12, pp. 1879–1892.

Sinclair, D. A., Smith, I. R., and Bennett, S. D. 1984. Elastic constants measurement with a digital acoustic microscope. IEEE Transactions on Sonics and Ultrasonics, Vol. SU-31, No. 4, pp. 271–277.

Spriggs, R. M., 1961. Expression for effect of porosity on elastic modulus of polycrystalline refractory materials, particularly aluminum oxide. Journal of The American Ceramic Society, Vol. 44, pp. 628–629.

Suga, Y., Harjanto and Takahashi, J. 1993. Study of the ultrasonic test for evaluating the adhesion of sprayed coatings to a substrate. Proceedings of the International Thermal Spray Conference & Exposition, Orlando, Florida, USA, 28 May – 5 June 1992. Pp. 247–252.

Takahashi, I. and Yoshioka, T. 1992. Young's modulus of ceramics at elevated temperatures. Journal of The Ceramic Society of Japan 100, pp. 153–157.

Tietz, H.-D., Liesaus, R., Winterfeld, J. and Bühling, L. 1992. Nondestructive testing of ceramic layers for quality assurance. Non-Destructive Testing 92. Elsevier Science Publishers B.V. Pp. 214–218.

Tietz, H.-D., Mack, B. and Böhm, St. 1994. Residual stresses in plasma-sprayed ceramic coatings. Proceedings of the Fourth International Conference on Residual Stresses. Baltimore, Maryland, USA, 8–10 June, 1994. Pp. 654–661.

Toyoda, M. 1989. Performance of alumina coated rolls. Osaka, Japan. Osaka University, Laboratory of Mechanics on Materials/Structures. 60 p. (In Japanese.)

Vetters, H., Matthaei, E., Schulz, A. and Mayer, P. 1989. Scanning acoustic microprobe analysis for testing solid state materials. Materials Science and Engineering, Vol. A122, pp. 9–14.

Viktorov, I. A. 1967. Rayleigh and Lamb Waves. New York, USA: Plenum Press. 154 p.

Wang, J. C. 1984a. Young's modulus of porous materials, Part 1: Theoretical derivation of modulus-porosity correlation. Journal of Materials Science, Vol. 19, No. 3, pp. 801–808.

Wang, J. C. 1984b. Young's modulus of porous materials, Part 2: Young's modulus of porous alumina with changing pore structure. Journal of Materials Science, Vol. 19, No. 3, pp. 809–814.

Weaver, J. M. R., Somekh, M. G., Briggs, A. D., Peck, S. D. and Ilett, C. 1985. Applications of the scanning acoustic microscope to the study of materials science. IEEE Transactions on Sonics and Ultrasonics, Vol. SU-32, No. 2, pp. 302–312.

Weglein, R. D. 1979. A model for predicting acoustic material signatures. Applied Physics Letters, Vol. 34, No. 3, pp. 179–181.

Weglein, R. D. 1985. Acoustic Micro-Metrology. IEEE Transactions on Sonics and Ultrasonics, Vol. SU-32, No. 2, pp. 225–234.

Weglein, R. D. and Wilson, R. G. 1977. Image resolution of the scanning acoustic microscope. Applied Physics Letters, Vol. 31, No. 12, pp. 793–796.

Xiang, D. Hsu, N. N. and Blessing, G. V. 1996. The design, construction and application of a large aperture lens-less line-focus PVDF-transducer. Ultrasonics, 34, pp. 641–647.

Yamanaka, K. 1983. Surface acoustic wave measurements using an impulsive converging beam. Journal of Applied Physics, Vol. 54, No. 8, pp. 4323–4329.

Yamanaka, K. Enomoto, Y. and Tsuya, Y. 1985. Acoustic microscopy of ceramic surfaces. IEEE Transactions on Sonics and Ultrasonics, Vol. SU-32, No. 2, pp. 313–319.